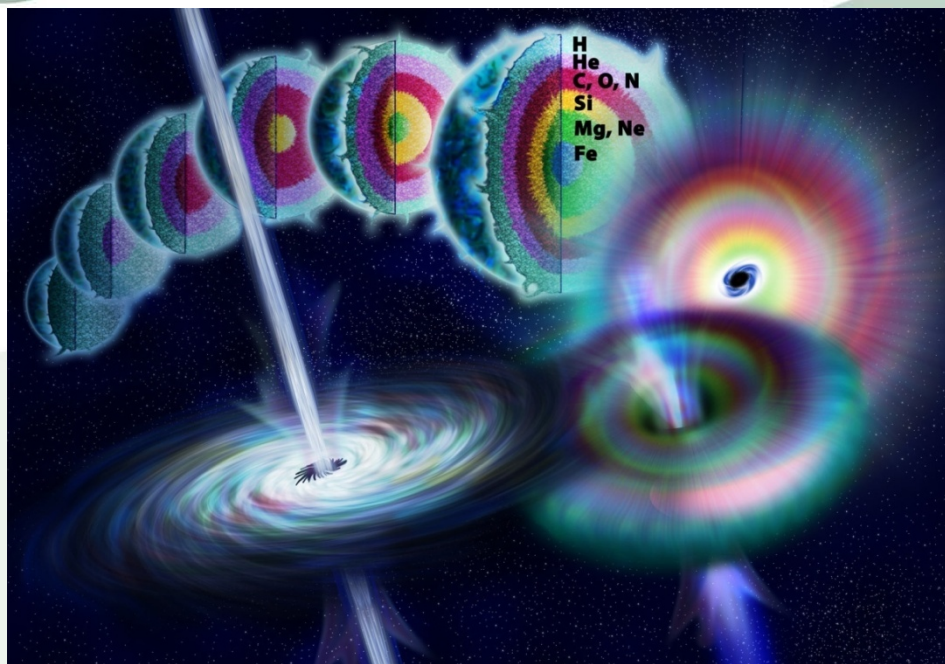# Dark Cosmology Centre

Gamma-Ray Bursts:
afterglow modelling, origin, and implications

A thesis submitted for the degree of
Doctor of Philosophy (PhD)
on March 1st, 2009.
Defended in Copenhagen, May 6, 2009.

Dong Xu

Supervisor: Johan P. U. Fynbo

Co-supervisor: Jesper Sollerman

Dark Cosmology Centre, Niels Bohr Institute

Faculty of Science, University of Copenhagen

Abstract

The topic of this PhD-thesis is Gamma-ray bursts (GRBs). GRBs are short, energetic bursts of gamma-rays. They, and their softer cousins the X-ray flashes (XRFs), are the manifestations of the most violent,cataclysmic explosions in the Universe. GRBs are followed by so-called afterglow emission detected in lower energy bands and on longer timescales, e.g. X-ray, UV, optical, near-infrared, radio emissions from a few hundred seconds to a few months. The first chapter of the thesis introduces the fundamental properties in the GRB prompt and afterglow phases and the most promising progenitor models for GRBs. A brief history on GRB research is also given in this chapter. The second chapter introduces the GRB afterglow temporal and spectral evolution within the jetted internal-external shock model. This is the main foundation on which interpretation of all observed GRB afterglows rest. The third chapter presents the detailed study of the multi-wavelength afterglow of XRF 060218 associated with the energetic supernova SN 2006aj. Through this study, we can clearly see that the X-ray and optical afterglow emission of XRF 060218 must originate from different physical processes. This is in contrast with the standard afterglow model and indicates that the X-ray afterglow could be attributed to a continued activity of the central engine that within the collapsar scenario could arise from fall-back accretion. The fourth chapter focusses on the short GRB 051221A. The afterglow of this burst provides strong evidence for energy injection from the central engine. This interesting phenomenon suggests that the post-merger object for some short GRBs could be magnetars. The fifth chapter addresses the famous SN-less GRB 060505 and GRB 060614. These two events thereby challenge the conventional GRB-SN connection for long GRBs. By investigating the two afterglows, we find that both afterglows can be well interpreted within the framework of the jetted standard external shock-wave model, and that the afterglow parameters for both bursts fall well within the range observed for other GRBs. Hence, from the properties of the afterglows there is nothing to suggest that these bursts should have another progenitor than other GRBs. Recently, GRB 080503 also had the spike + tail structure during its prompt gamma-ray emission seemingly similar to GRB 060614. We also analyse the prompt emission of this burst and find that this GRB is a hard-spike + hard-tail burst with a spectral lag of 0.8 ± 0.4 s during its tail emission. Thus, the properties of the prompt emission of GRB 060614 and GRB 080503 are clearly different, showing that further thinking of the criteria for GRB classification is required. We also note that, whereas the progenitor of the two SN-less bursts remains uncertain, the core-collapse origin for the SN-less bursts would be quite certain if a wind-like environment can be observationally established, e.g, from an optical decay faster than

the X-ray decay in the afterglows slow cooling phase. The sixth chapter deals with the X-ray transient 080109 associated with SN 2008D. This serendipitous discovery may bring important new insight into both GRBs, XRFs and their link to Type Ibc supernovae (SNe). We propose that such X-ray transient, besides being caused by the shock breakout, might be caused by the interaction between a mildly relativistic jet and the surrounding wind medium, thus bridges the gap between energetic hypernovae and ordinary Type Ibc SNe. The thesis ends with an conclusion and outlook.

Contents

Acknowledgments

Many people have contributed to make my PhD years a wonderful experience.

I am certainly most indebted to my supervisor, Dr. Johan P. U. Fynbo, for his guidance, teaching, assistance, encouragement throughout my time at Dark Cosmology Centre. He has influenced me significantly both in research and in daily life. Throughout my PhD he never criticized me even I have postponed my tasks again and again. Instead, he always made new deadlines and asked me what kind of help I needed. This is quite different from the style in Chinese institutes, where many bosses think criticisms may bring higher productivity. Johan focuses on his research of interest and works with high efficiency, which set an excellent example for me. Johan also generously invited me to his home. My sincere thanks go to all his family members: Charlotte, Clara, and Rasmus. Rassmus now already has an oriental name and I wish he can visit his oriental big brother as early as possible.

My thanks also go to my co-supervisor, Dr. Jesper Sollerman. He normally thinks very fast and is able to quickly get the points of a new work and raise the key questions. To work with him, I have to maintain a high standard. And it turns out that most of my works are related to his research of SN-GRB connection and cosmology.

Although at the time of writing I'm not sure whether my family would be able to attend my PhD defense. But what I'm sure is that they are much concerned about my work and life abroad. They would feel very happy if I tell them I have successfully gotten my PhD degree; but they wouldn't be reluctant to still give their love and praise to me if I tell them I fail on my PhD. My thank definitely must go to my girlfriend Shuyu Wu, a kind and the most beautiful girl. I feel so lucky to get to know her here in Copenhagen and to share every happiness and unhappiness together with her. Shuyu makes every day a joy.

I would also like to thank all my officemates and friends/collaborators at DARK: Anja C. Andersen, Jin Hyeok An, José María Castro Cerón, Tamara Davis, Árdís Elíasdóttir, Chloé Feron, Desiree D. M. Ferreira, Christa Gall, Julie Meier Hansen, Steen H. Hansen, Jens Hjorth, Pall

Chapter 1
GRB research during the past four decades

Gamma-ray bursts (GRBs) are fascinating celestial objects. These short, energetic bursts of gamma-rays mark the most violent, cataclysmic explosions in the Universe, likely associated with the births of stellar-size black holes or rapidly spinning, highly magnetized neutron stars.

Like in every other research field, the road leading to understanding the nature of GRBs has been bumpy, mainly due to the limited information contained in the brief gamma-ray radiation and relatively poor localization of GRBs on the sky. The road is far from complete. Fortunately, during the past decade thanks to the significant technological progress in quick, precise localization of these gamma-ray or hard X-ray transients, progress has been rapid both observationally and theoretically.

In this chapter I will review the main properties in the GRB prompt and afterglow emissions collected during the past four decades, addressing how GRB and afterglows manifest themselves, and scetch the history of GRB research, highlighting some important events/models in the development of the understanding of GRBs. I focus on developments that are most directly related to my work and hence do not attempt to be complete in any way. At the end of the chapter, I will make a brief description of the GRB fireball evolution, which will be followed by a description of the afterglow evolution in chapter 2.

Throughout this thesis the convention $Q_x = Q/10^x$ has been adopted in cgs. If not specified, we consider a standard cosmology model with $H_0 = 70$ km s^{-1} Mpc^{-1}, $\Omega_M = 0.3$, and $\Omega_\Lambda = 0.7$.

1.1 Properties of GRB prompt emission

In this section the main properties of the GRB prompt emission are presented.

1.1.1 Temporal properties

Generally speaking, the durations of GRBs are shorter than the timescale for most other astrophysical objects. The GRB duration definition of T_{90} or T_{50} is the time interval within which 90% or 50% of the burst fluence is detected. These durations span 5 orders of magnitude in range, i.e. from $\sim 10^{-2}$ s to $\sim 10^3$ s, typical values: $\sim 20 - 40$ s for long bursts and $\sim 0.2 - 1.3$ s for short
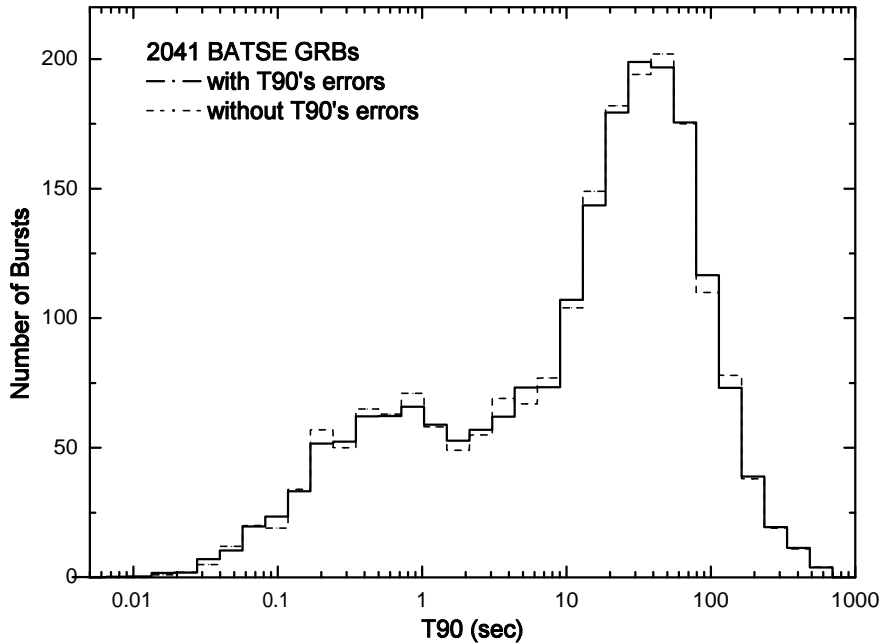
Figure 1.1: Duration (T_{90}) distribution of GRBs in the BATSE Current Catalog. Data are from `http://www.batse.msfc.nasa.gov/batse/grb/`.

bursts. Two categories of GRBs, "long" ($T_{90} \gtrsim 2$ s) and "short", ($T_{90} \lesssim 2$ s) have been identified (Kouveliotou et al. 1993). Also see Fig. 1.1 of my own statistics. As can be seen from the duration distribution, there is no sharp border between the two populations. More importantly, the duration definition has become complicated for the present *Swift* detected GRBs because several short-spike (1-5 s) + long-tail (~ 100 s) GRBs have been observed. Throughout this thesis the notions "long-duration GRB" or "long GRB" can be abbreviated as LGRB and "short-duration GRB" or "short GRB" as SGRB. Special bursts will be clearly introduced in case of any confusion concerning classification.

The GRB lightcurves often consist of irregular pulses. Some bursts consist of very erratic, spiky components, while others are smooth with one or a few components. Some bursts contain distinct, well-separated emission episodes whereas others do not. A table of different types of burst profiles can be found at `http://www.batse.msfc.nasa.gov/batse/grb/lightcurve/` for BATSE bursts. Fig. 1.2 depicts typical GRB prompt lightcurves from the BeppoSAX sample. The widths of individual pulses (δt) vary over a wide range. The shortest spikes have millisecond widths, and $\delta t/T$ reach as low as $10^{-3} - 10^{-4}$, and as high as ~ 1 (See Fig. 1.2). The vast majority of individual pulses are asymmetric, with leading edges steeper than the trailing edges. Smooth
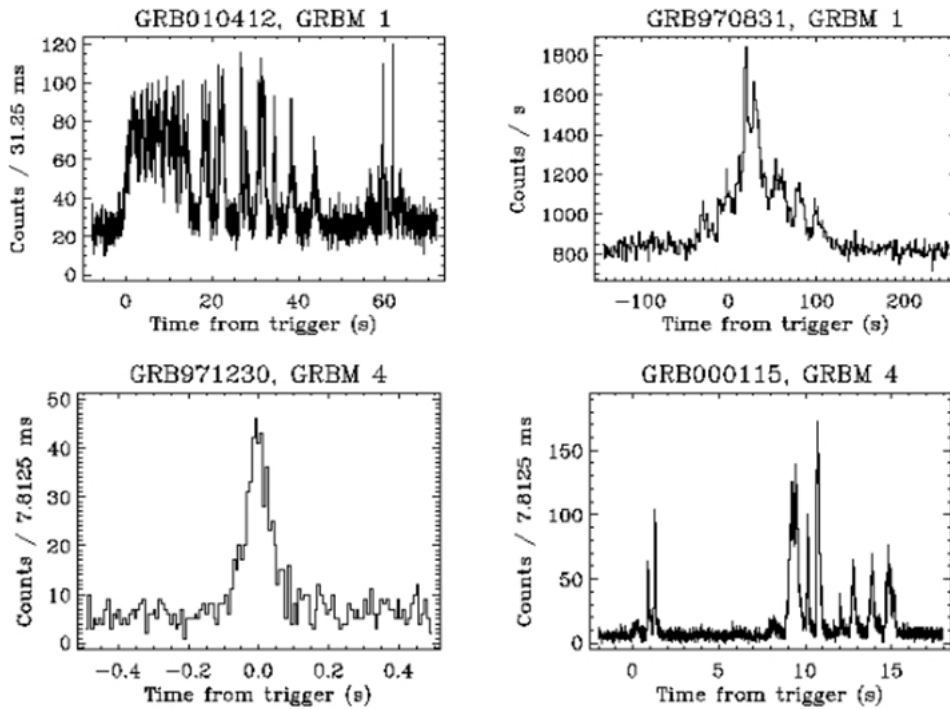
Figure 1.2: Demonstration of different kinds of GRB prompt lightcurves from the *BeppoSAX*/GRBM sample. Data are from `http://www.asdc.asi.it/bepposax/`.

single peak bursts typically have a fast-rise-exponential-decay (FRED)-type lightcurve. In fact all pulses within the prompt emission can be fitted with this phenomenological FRED function (Bhat et al. 1994), revealing the asymmetric temporal character. We are still not very clear about the physical origin for this functional form.

1.1.2 Spatial properties

The angular distributions of all BATSE GRBs is shown in Fig. 1.3. The distribution is isotropic for both long and short bursts. This property strongly supports an cosmological origin or, at least, from an extended dark halo surrounding our Galaxy. After the detection of GRB afterglows in 1997 the cosmological origin was quickly established for long GRBs (Metzger et al. 1997). After the launch of the *Swift* mission the cosmological origin of the short GRBs was also established.

1.1.3 Spectral properties

As a whole, the γ-ray/hard X-ray spectrum is non-thermal. A single thermal (Planck-like) spectral shape is ruled out for almost all the bursts with sufficient spectral information. For most bursts, the spectrum is well described by a smoothly-joining broken power law, known as a "Band-function" (Band et al. 1993; see Fig. 1.4). Three independent spectral parameters are involved, i.e., a low

2704 BATSE Gamma-Ray Bursts
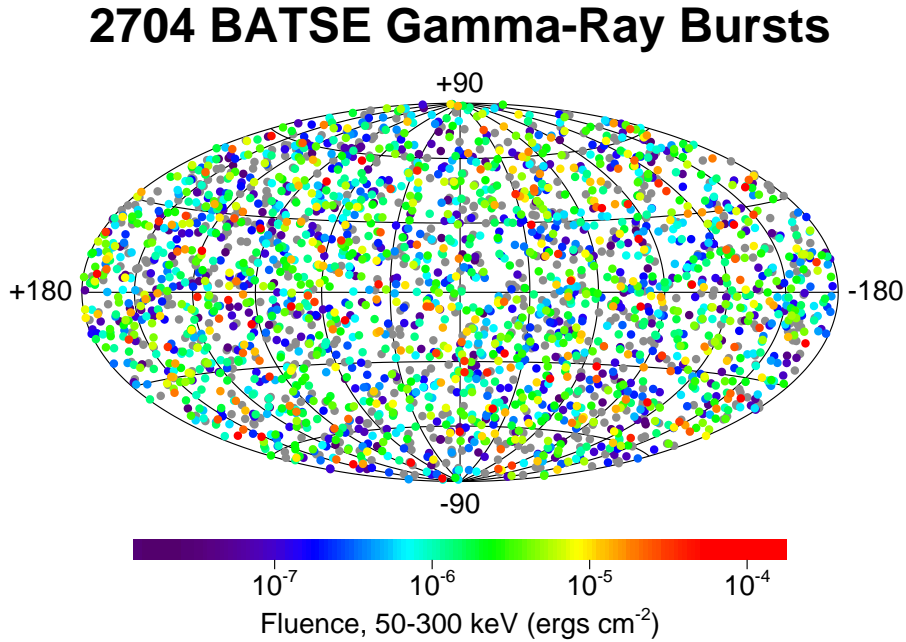
Figure 1.3: Angular distribution of 2704 GRBs recorded with BATSE during the nine-year mission. The projection is in galactic coordinates; the plane of the Milky Way Galaxy is along the horizontal line at the middle of the figure. The burst locations are color-coded based on the fluence. Long duration, bright bursts appear in red, and short duration, weak bursts appear in purple. Grey is used for bursts for which the fluence cannot be calculated due to incomplete data. Figure from `http://www.batse.msfc.nasa.gov/batse/grb/skymap/`.

energy photon spectral index (α), a high energy photon spectral index (β), and the transition energy (E_0) or peak of the energy spectrum for $\beta < -2$ (E_p). This spectral shape is valid both for the integrated emission over the whole burst duration, and for the emission during a certain temporal segment of the burst. Note that the model of a power-law plus a thermal component has also been suggested and it seems that this model can also work for some bursts (e.g., Ryde & Pe'er 2008). In some cases the spectrum fitted with a cuttoff power-law (because the high energy component has fewer photons with larger error bars) or even with a single power-law if the energy band is relatively narrow.

In particular, in Fig. 1.5 and Fig. 1.6 there is some evidence for a anti-correlation between spectral hardnesses and durations. Here the spectral hardness ratio is defined as the fluence ratio between the *BATSE* channel 3 (100-300 keV) and channel 2 (50-100 keV) or between channel 2 and channel 1 (20-50 keV), while the duration is measured in terms of T_{90}. This is the empirical foundation for the terms short-hard and long-soft. Also plotted is the hardness V.S. duration for
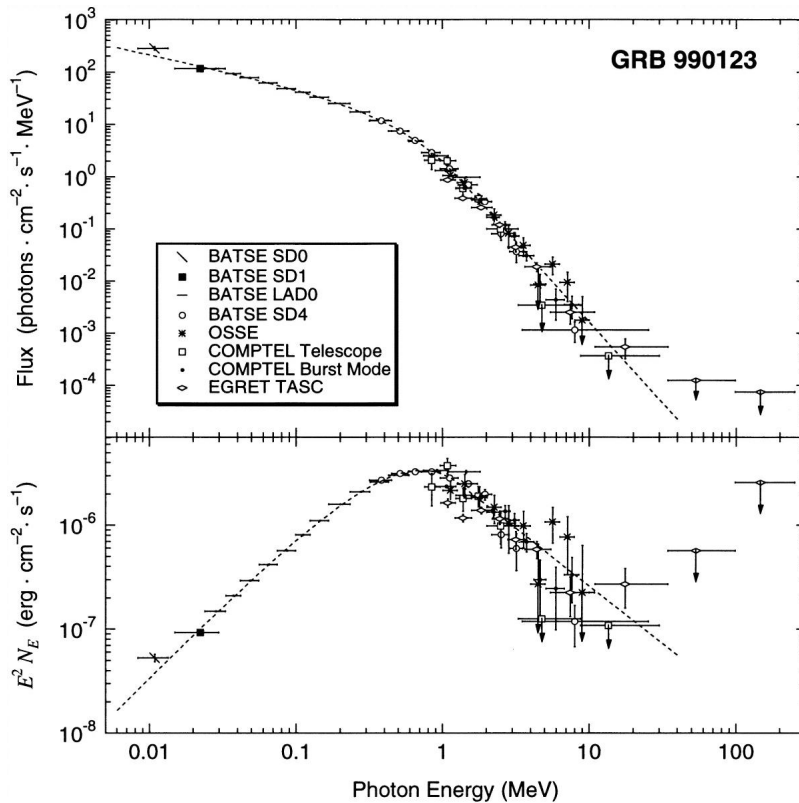
Figure 1.4: Examples for the GRB prompt emission spectrum (GRB 990123; Briggs et al. 1999). The typical spectral form is the "Band" function. Sometimes it can also be fitted with a cuttoff power-law (because the high energy component has fewer photons with larger error bars) or even with a power-law if the energy band is relatively narrow.

Swift GRBs for comparison. As can be seen, the border line for LGRBs and SGRBs is not sharp. Also, most of the *Swift* bursts are softer than for pre-*Swift* bursts (a selection bias set by the BAT sensitivity).

Using the BATSE GRB sample, Preece et al. (2000) found that the α, β, and E_p distributions are roughly *lognormal*, centered around ~ -1.0, ~ -2.3, and ~ 250 keV, respectively. The distributions of α and β are also generally suitable for describing fainter and softer bursts. The relatively narrow E_p distribution among different BATSE bursts is likely to be influenced by selection effects. The lack of high E_p bursts is likely intrinsic (Harris & Share 1998). However, as can be seen at the moment, in the low energy regime the narrowness of the distribution function is due to the "bright" flux-truncation in the BATSE sample, because after the BASTE era a group of X-ray transient events, the so-called "X-ray flashes" (XRFs), resemble classical GRBs in many aspects but with E_p around or below 40 keV (Heise et al. 2001; Kippen et al. 2002). XRFs are typically fainter than classical GRBs. It is worth to point out that all bursts tend to become softer during their prompt emission (Norris et al. 1986). Furthermore, the discovery of the X-ray transient 080109 associated with the Type Ib SN 2008D may reveal that there could
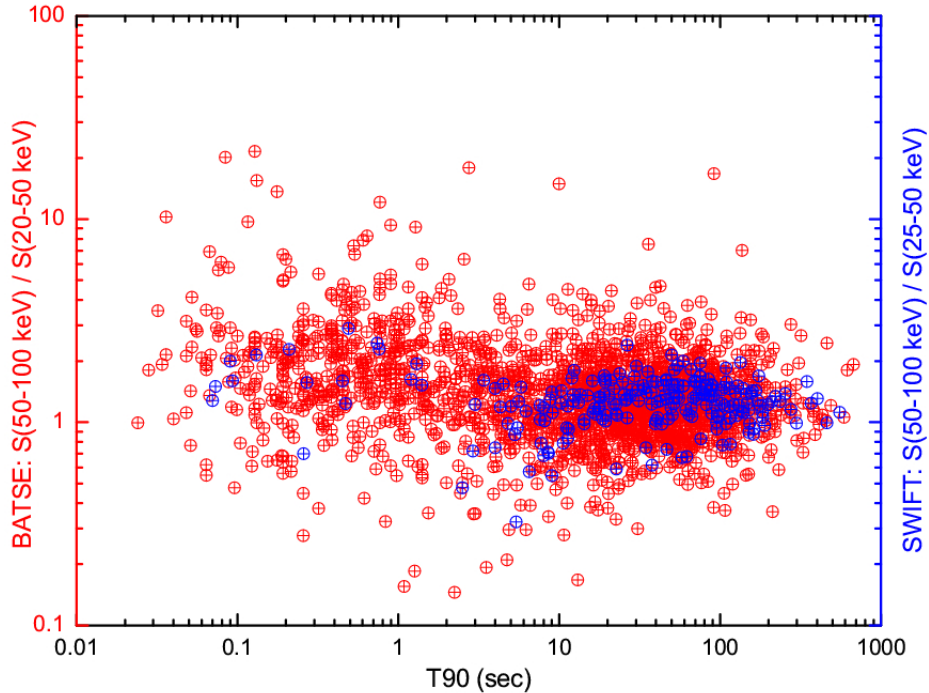
Figure 1.5: Hardness V.S. duration for BATSE GRBs (red circles) and Swift GRBs (blue circles). Hardness is the ratio of fluence in 50-100 keV and in 20-50 keV. Swift population and BATSE population have significant overlap.

exist a population of events which are even softer and fainter than XRFs, bridging energetic SNe Ibc (sometimes called hypernovae, HN) associated with GRBs/XRFs and ordinary SNe Ibc presumably without accompanying quasi-jet bursts, see chapter 6 for more detail.

1.1.4 Empirical correlations

Several empirical correlations have been found among the properties of GRBs or even within a single GRB. These correlations are helpful to understand the underlying GRB physics and predict the possible redshifts for new GRBs to a certain degree. One or two of them even shed light on constraining cosmological parameters with GRBs, populating the high-z region in the Hubble diagram.

Among all, the most important one is the correlation between the rest-frame νF_ν peak energy, E_p and the isotropic energy release, E_{iso} (Amati et al. 2002 and follow-up works on this correlation). In general this correlation is written as $E_{iso,52} \propto E_{p,2}^2$. So far all short GRBs are outliers of this correlation because of their relatively higher E_p values while all long GRBs are consistent with this correlation within 3σ confidence level (C.L.) except the peculiar GRB 980425. The physics for this correlation is somewhat plausible and it seems that it would be expected if the radiation mechanism for the internal shocks is synchrotron radiation. Fig. 1.7 shows a latest version of this
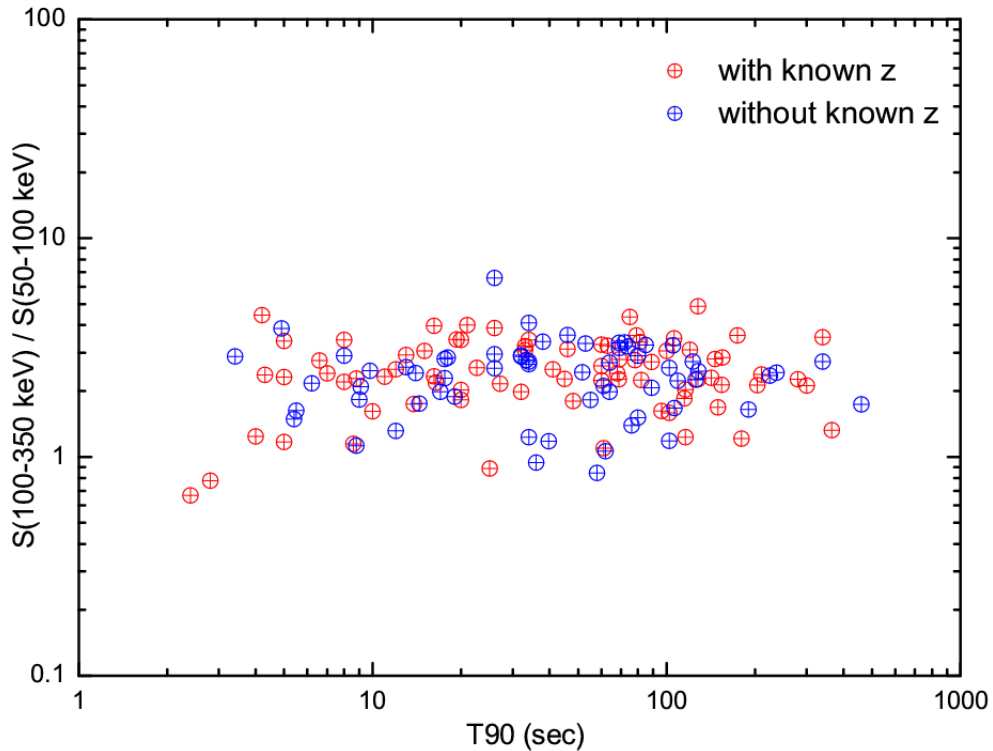
Figure 1.6: Hardness V.S. duration for Swift GRBs with measured redshifts (red circles) and Swift GRBs without measured redshifts (blue circles). Hardness is the ratio of fluence in 100-350 keV and in 50-100 keV. The two populations have significant overlap (Fynbo et al., in prep.)

correlation. As seen, the scatter around the correlation is quite large, especially for cosmography utility.

Another important one is the correlation between the rest-frame νF_ν peak energy, E_p and the collimation-corrected energy release, E_g, where $E_g = (1 - \cos\theta_j)E_{iso}$ and θ_j is the half-opening angle for each GRB jet (Ghirlanda, Ghisellini, & Lazzti 2004). Later, this correlation was discussed in the ISM circumburst scenario and the WIND circumburst scenario respectively but the scaling power-law indexes are very similar (Ghirlanda et al. 2006). This correlation invokes the addition of jet break time. Indeed, this correlation is tighter than the Amati correlation, making use of a sample of pre-*Swift* GRBs, and has even been proposed to constrain cosmological parameters (Dai, Liang, & Xu 2004; Ghirlanda et al. 2004; Xu, Dai, & Liang 2005). However, the more recent *Swift* bursts are distinguished by the chromatic breaks in the X-ray and optical afterglow lightcurves. Also because either there are only few data points with relatively large error bars at the expected jet break time (ie.e, usually at a few days) or the afterglow is already quite faint compared with its host galaxy, this correlation has not been confirmed by the large sample of *Swift* bursts. *Swift* bursts are still widely believed to be jet events. It is just simply not easy to reliably decompose different components from the lightcurves of a certain GRB afterglow.
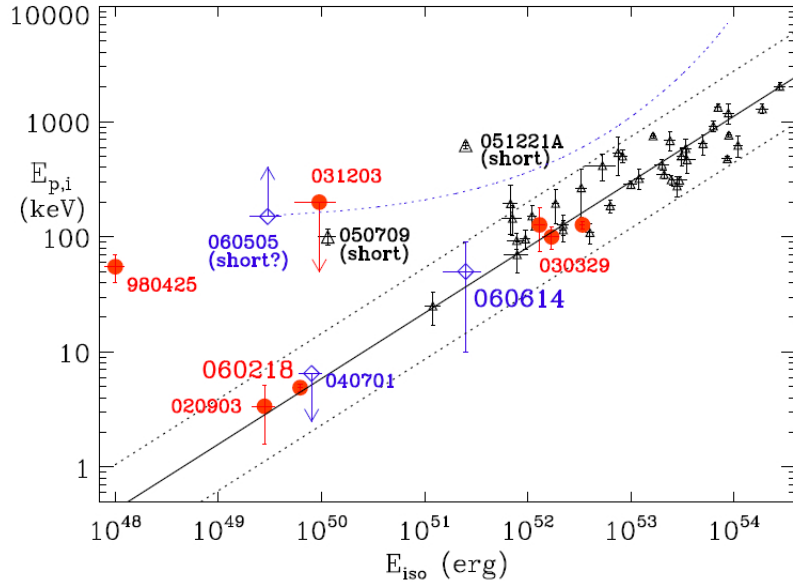
Figure 1.7: Distribution of E_p and E_{iso} values of GRBs and XRFs with firm estimates of z and E_p, including also two short GRBs with known redshift: GRB 050709 and GRB 051221A (from Amati et al. 2007). The GRBs with evidence of association with a SN are marked with big dots. The location in the $E_p - E_{iso}$ plane of GRB 060614 and other the two events with deep limits to the magnitude of the associated SN, XRF 040701 and GRB 060505, are shown as big diamonds. The curved dotted line shows how the GRB 060505 point moves in the $E_p - E_{iso}$ plane as a function of redshift.

1.2 Properties of GRB afterglow emission

The GRB afterglows have been intensively observed and reviewed in the pre-*Swift* and *Swift* eras. Generally, they can be interpreted in the jetted external shock wave model.

1.2.1 X-ray Afterglows

Swift brings revolutionary information in the GRB X-ray afterglow, distinguished as the so-called "canonical X-ray afterglow lightcurve" (Nousek et al. 2006; Zhang et al. 2006; O'Brien et al. 2006; Chincarini et al. 2005). Fig. 1.8 shows this lightcurve, consisting of five segments, besides the prompt emission phase (denoted as '0') already known for about four decades. Of course not every burst has all the five segments and their lightcurves do differ from one another. But as a general case, their afterglow lightcurves could be fit into this generic picture.

In this chapter we use the notation $F(\nu, t) \propto t^{-\alpha} \nu^{-\beta}$ for the afterglow monochromatic flux as a function of time, where ν represents the observed frequency, α is the temporal index, and β is the energy spectrum index.

Steep decay phase (I): The steep decay phase has been identified as a common feature of the early X-ray afterglows shortly after the launch of *Swift* (Tagliferri et al. 2005; Barthelmy et al.
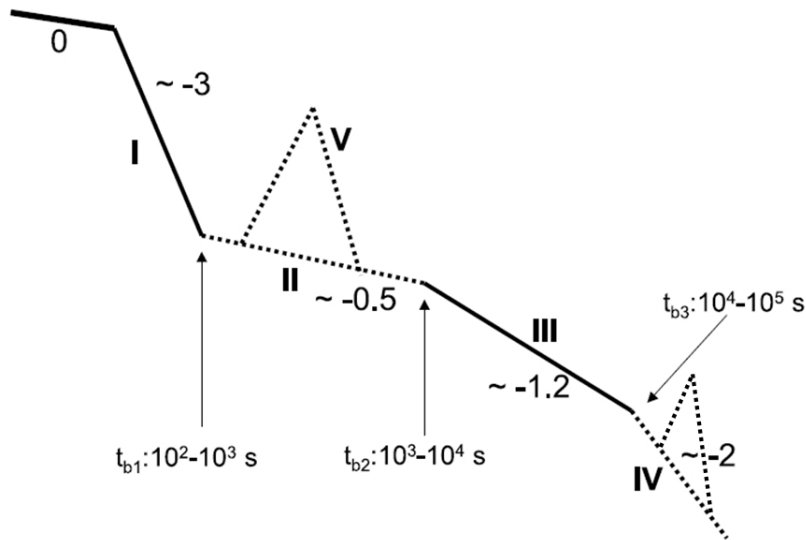
Figure 1.8: The so-called canonical X-ray afterglow lightcurve. The phase "0" denotes the prompt emission. Four power-law lightcurve segments together with a flaring segment are identified in the afterglow phase. Segments I, and III are often seen (solid lines). The other three segments are only observed in a fraction of bursts (dashed lines). Typical temporal indexes in the four segments are indicated in the figure. Segment I is considered as the tail attached to the previous prompt emission. The spectral indexes are gradually becoming softer or largely remain unchanged through segments II to III to IV, with a typical value of $\beta_X \sim 1$ ($F_X \propto \nu^{-\beta_X}$).

2005). It is commonly accepted that the prompt GRB emission originates from some processes taking place within the ejecta, the gamma-rays emitted in the internal shocks before the fireball is decelerated by the circumburst medium. The afterglow quantitatively can be considered as starting when the fireball is decelerated already, thus its emission is apparently at a much larger distance from the central engine compared with the distance for the prompt gamma-ray emission. Therefore, the prompt emission and the afterglow emission arise from different sites. Now that the flux level of the prompt emission is much higher than that of the afterglow emission, we expect to see a steep decay lightcurve during the transition of from the prompt phase to the afterglow phase. This is also why sometimes the steep decay phase is called the tail of the prompt GRB emission.

Often the steep decay phase is smoothly connected to the prompt emission, with a temporal decay slope ~ 3 or steeper (sometimes up to ~ -10, e.g. Vaughan et al. 2006) extending to $\sim (10^2 - 10^3)$s. It usually has a different spectral slope than the later afterglow phases.

The leading interpretation of the steep decay phase is the tail emission due to the "curvature effect" (or called "high latitude emission" sometimes) (Fenimore et al. 1996; Kumar & Panaitescu 2000). For a conical GRB jet with an opening angle θ_j, the emission from the radius R but from different viewing latitudes θ would reach the observer with some time delay. Therefore, even if the emission stops abruptly, due to the propagation effect the observer would receive the emitted

photons at an angle with a time delay $t = (1 + z)(R/c)(\theta^2/2)$, where $1 + z$ is to account the cosmological time dilation. As the emission is confined by θ_j, the tail emission will have a duration of $t_{tail} = (1 + z)(R/c)(\theta_j^2)/2$ corresponding the time delay from the emission from $\theta = 0$ to $\theta = \theta_j$. This is based on the consideration that the line of sight is not too close to the jet edge. The comoving emission frequency ν' of the shock-accelerated electrons is transformed to the observed frequency ν through the form of $\nu = D\nu'$, where $D = [\Gamma(1 - v\cos\theta/c)]^{-1}$ is the Doppler factor. Thus, one has $D \sim 2/\Gamma\theta^2$ for $\theta \gg 1/\Gamma$ (this is easily valid at such early stage), and since we have seen that $t \propto \theta^2$ one obtains $D \propto t^{-1}$. The observed flux, F_ν, is related to the comoving surface brightness, $L'_{\nu'}$, via

$$F_\nu \propto L'_{\nu'}D^2 \propto \nu'^{-\beta}D^2 \propto \nu^{-\beta}D^{2+\beta} \propto \nu^{-\beta}t^{-2-\beta}.$$

As seen, the curvature effect introduces a relation between the temporal index α and the spectral index β: $\alpha = \beta + 2$. This relation can be used to verify that the steep decay is due to the curvature effect.

Panaitescu et al. (2006) used a sample of 28 GRBs to check if the above relation holds. The authors found that for more than half of the bursts, the fast decay satisfies the relations whereas a faster fall-off is found for a quarter of the sample and few afterglows exhibit a slower decline. Similar conclusions have been reached by O'Brien et al. (2006) for a sample of 40 GRBs, and by Nousek et al. (2006) for a sample of 27 GRBs.

To produce slopes flatter than $2 + \beta$, the following interpretations have been invoked. An early contribution of the forward shock emission, appearing near the end of the tail emission, can change the temporal slope of the steep decay phase. This happens if the fireball is already decelerated at the end of the tail emission and if the forward shock emission contributions to the emission in the X-ray band. Alternatively, the central engine activity may not die abruptly, or the shocked region may not cool abruptly but decay with time gradually (Fan & Wei 2005).

To produce slopes steeper than $2 + \beta$, Zhang et al. (2006) showed that the solid angle of the emitting region must be comparable to or smaller than $1/\Gamma$. This would correspond to the patchy shell model (Kumar & Piran 2000) or the mini-jet model (Yamazaki, Ioka & Nakamura 2004). Apparently this interpretation assumes a particular choice for the choice of the line of sight.

Shallow decay phase (II): The shallow decay phase often has a temporal decay slope ~ 0.5 or flatter up to $\sim (10^3 - 10^4)$s, at which a temporal break is observed before the pre-jetbreak decay phase (e.g. Campana et al. 2005; De Pasquale et al. 2006). There is no spectral evolution across the break.

This phase is the most intriguing one among all segments, involving quite a few interpretations.

(1) **Energy injection from a long-lived central engine model.** The most straightforward interpretation of the shallow-decay phase is that the total energy in the external shock continuously

increases with time. This requires substantial energy injection into the fireball during the phase, simply invoking a long-lived central engine.

In this shallow phase, the X-ray flux $F_X \propto t^{-\alpha}$, with $0.2 < \alpha < 0.8$, and $tF_X(t)$ increases with time. If we call $\epsilon_X(t)$ the efficiency of the X-ray afterglow emission, $E_{K,iso}(t)$ the isotropic equivalent kinetic energy in the afterglow at time t, and $L_{X,iso}$ the X-ray luminosity at time t, then we have

$$\epsilon_X(t) = tL_{X,iso}(t)/E_{X,iso}(t)$$

Using $L_{X,iso}(t) \propto F_X(t)$, the equation can also be written as

$$\epsilon_X(t)E_{X,iso}(t) \propto tF_X(t).$$

This shows $\epsilon_X(t)E_{X,iso}(t)$ should also increase with time as $tF_X(t)$. Given the expected decrease of $\epsilon_X(t)$ with time for $p > 2$ (see Granot, Königl, & Piran 2006), the increase of $\epsilon_X(t)E_{X,iso}(t)$ has to be attributed to an increase in $E_{X,iso}(t)$ and to some sort of energy injection in the forward shock. Zhang & Mészáros (2001) formulized the injection luminosity behavior as $L \propto t^{-q}$, and found that in order to obtain injection signature of interest, $q < 1$ is required; otherwise the increase of the total energy in the blast wave is too small. The observational data suggest a range of q values with a typical value $q \sim 0.5$. For the scenario of continuous injection, the luminosity of the central engine has to vary smoothly with time, in contrast to the erratic injection of energy observed during the GRB itself. This largely requires two components: a hot fireball that leads to the prompt emission and a (likely) cold Poynting flux that leads to the smooth energy injection. The second component might be due to the initial spin-down from a millisecond pulsar (Dai & Lu 1998a,b), but for such a model $q = 0$ is required. Interestingly, numerical calculations suggest that a millisecond pulsar model even can fit some of the XRT lightcurves (e.g., Fan & Xu 2006, for the short GRB 051221A). If a long-lived black hole-torus system with a slowing down accretion rate is invoked, $q = 5/3$ at later times (MacFadyen, Woosley, & Heger 2001), too steep to give an interesting injection signature. Ghisellini et al. (2009) selected a sample of 33 GRBs detected by *Swift*, with known redshifts and decomposed the whole X-ray lightcurve into two components: one corresponds to emission from the forward shock due to the interaction of a fireball with the circumburst medium and an additional component, treated in a completely phenomenological way. They found that the decay slope of the additional component emission after the shallow phase is remarkably similar to the time profile expected by the accretion rate of fall-back material (i.e. $\propto t^{5/3}$, suggesting that this can be the reason why the central engine can be active for a long time.

(2) **Energy injection from ejecta with a wide Γ distribution model.** In this scenario the central engine activity may be as short as the prompt emission itself, but at the end of the prompt phase the ejecta has a range of Lorentz factors. The amount of ejected mass moving with

Lorentz factors larger than Γ is given by (Rees & Mészáros 1998)

$$M(>\Gamma) \propto \Gamma^{-s}. \qquad (1.1)$$

In this scenario, the activity of the central engine does not need to be long-lived and the material can be ejected rapidly. The continuous energy injection is due to the different velocities of the ejecta. The slower ejecta progressively piles up onto the blastwave as the latter decelerates. A change in the fireball dynamics is expected for $s > 1$ when most of the energy is stored in the slow-moving material. For each value of s one can find an effective value of q that largely mimics the effect of s. For instance, for $q \sim 0.5$ one gets $s \sim 2.6$ for an ISM environment. The temporal break around $10^3 - 10^4$ s suggests a cut-off of the Lorentz factor around several tens, below which s becomes shallower than unity (Granot & Kumar 2006; Zhang et al. 2006). Xu et al. (2008) used this model to interpret the achromatic plateau/bump in the optical-to-Xray afterglow in GRB 060614 (see Chapter 4 for more details).

Granot & Kumar (2006) also noticed that the end of the shallow decay phase marks the beginning of the Blandford-McKee self-similar external shock evolution. They determine the time-dependence of the blastwave Lorentz factors in the framework of this model and they show that the Lorentz factor typically drops by a factor of 2-4 during the shallow decay phase (in the case of a uniform circumburst medium). With their model based on a deviation at early times from the constant energy Blandford-McKee self-similar solution, they predict a roughly similar shallow decay in the optical band over the same time interval as in the X-ray band. In this scenario of energy injection with a wide distribution of Lorentz factors, the reverse shock is typically non-relativistic because the relative Lorentz factor between the injection shell and the blastwave is always low when the former piles up onto the latter.

Within the two models discussed above, it is also necessary to analyze the sudden termination of the injection at the end of the shallow decay phase. In the long-lived central engine model this time corresponds to the end of the injection process (e.g., the magnetar has lost its dipole radiation significantly). In the varying Lorentz factor model this time corresponds to a cut-off of the Lorentz factor distribution at the lower limit, below which the distribution index s is flatter than unity so that they are energetically unimportant.

(3) **Emission from the reverse shock model.** The shallow decay could also be reproduced as synchrotron emission from the reverse external shock if the microphysical parameters ϵ_e and ϵ_B therein are much larger than those in the forward external shock. In this case the ratio of the X-ray flux produced by the reverse and forward shocks would be dominated by the former. Favoring this interpretation, Uhm & Beloborodov (2007) suggested that the X-ray plateau emission is due to the reverse shock running into ejecta of relatively small (and decreasing) Lorentz factors.

(4) **Off-beam jet model.** In this model it is thought that the line of sight that is more favorable for GRB prompt detection is different from the line of sight that is favorable for the detection of early afterglow. Flat early afterglows are produced for viewing angles slightly outside the region that produces bright afterglow emission. These off-beam viewing angles are offset from the prominent early afterglow emission but not from the prompt gamma-ray beam. That is to say, the regions of prominent afterglow emission and of prominent gamma-ray emission do not coincide. Under these conditions a shallow decay phase can be mimicked by the combination of the decaying tail of the prompt emission and the delayed onset of the afterglow emission seen from view angles slightly outside the edge of the jet.

This model would indicate that as the off-beam viewing angle θ_{offset} increases, the shallow decay phase emerges at later time t_{sd} and at lower flux F_{sd}, and it exhibits a flatter decay index α_{sd}. Therefore, there would be a negative correlation between t_{sd} and α_{sd} and a positive correlation between F_{sd} and α_{sd}. Panaitescu (2007) studied a sample of 32 GRBs with well-shaped shallow decay phases and found that the data didn't confirm the above correlations.

(5) **Two-component jet model.** This geometric model invokes two jet components, producing the sum of two component afterglows. Granot, Königl, & Piran (2006) used this model to analyze the early X-ray afterglow lightcurves. The model includes a narrow and ultra-relativistic conocal outflow, which is the source of the prompt emission, a mildly relativistic outflow inside a wider coaxial cone that decelerates at later time. The line of sight is within the solid angle of the narrow component so that the wide component becomes visible after it has been decelerated and only makes contribution to the afterglow emission. In this model, the shallow decay phase corresponds to the emergence of the wide component emission. As seen, this model invokes more free parameters. The shallow decay in the X-ray afterglow lightcurve of GRB 051221A was interpreted with this model by Jin et al. (2007).

(6) **Varying microphysics parameter model.** One could also invoke evolution of the microphysics shock parameters to reproduce the shallow decay phase (e.g., Ioka et al. 2006).

(7) **Dust scattering model.** Shao & Dai (2007) suggested that small angle scattering of X-rays by dust could also give rise to a shallow decay phase under certain conditions. The model predicts a significant change, about $\Delta\beta \sim$ 2-3, in the X-ray spectral index from the beginning of the plateau towards the end of the plateau, while the observed data show close to zero softening during the plateau and the plateau-to-normal transition phase (Shen et al. 2009).

Pre-jetbreak decay phase (III) and Post-jetbreak phase (IV): These two phases were often seen in optical bands in the pre-*Swift* era. It can be regarded as the "canonical" optical lightcurve at that time. Now in some papers these these two phases are called the "normal decay" phase. Phase (III) is usually with a decay slope $\sim$ 1.2, and usually follows the predictions of the standard afterglow model. Phase (IV) is usually with a decay slope $\sim$ 2.0 but only are clearly
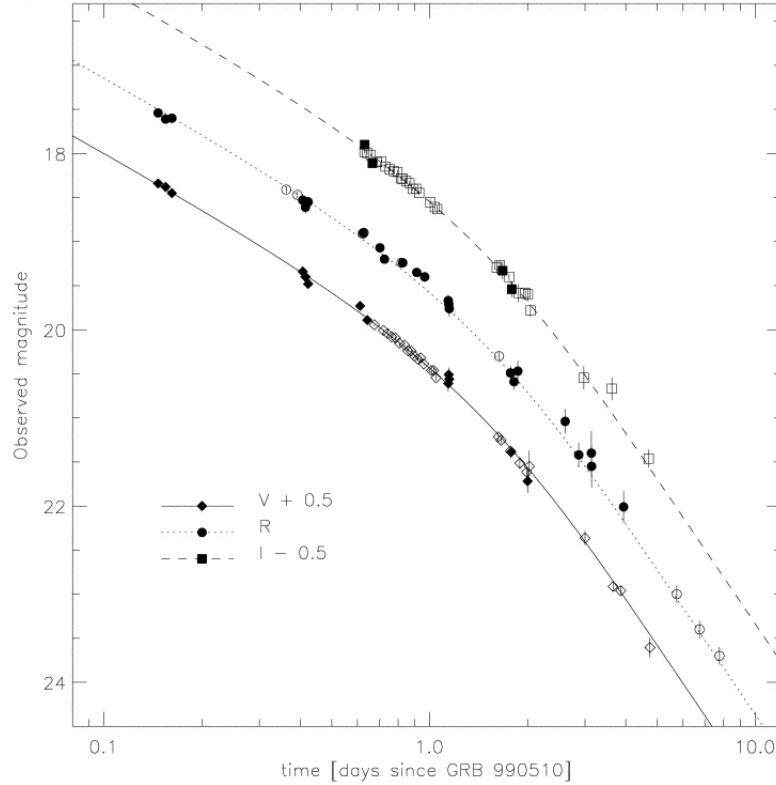
Figure 1.9: A jet-break example in the pre-*Swift* era (from GRB 990510, Harrison et al. 1999). The lightcurves clearly show an achromatic break in several bands. The early-time slope is $\alpha_1 = 0.82$ and the late-time slope is $\alpha_2 = 2.18$, which matches the closure relation from the standard external shock model.

evident in some GRBs. The temporal break between phase (III) and phase (IV) is the so-called *jet break* (Rhoads 1999; Sari, Piran & Halpern 1999).

Following is a straightforward interpretation of the *jet break*. Suppose the GRB ejecta are confined in a jet-like cone, moving towards the observer with a bulk Lorentz factor Γ; the radiation from the shocked ejecta is isotropic in the comoving frame, but the received radiation in the observe frame is primarily from the ejecta along the line of sight, which has a half-opening angle less than $1/\Gamma$ due to the relativity effect. Therefore, at the beginning time the observer cannot judge whether or not the ejecta is radiating isotropically. As times goes, the bulk Lorentz factors decreases, so the observer observes more and more radiating area. But since the edge of the jet-like cone is observed (i.e., $\Gamma \sim 1/\theta_j$), the observer would miss some flux compared with the scenario in which the observer is observing radiation from a spherical surface. Such flux missing would cause a break in both X-ray and optical lightcurves because it's purely a geometric effect. Fig. 1.9 depicts a good example of the jet break.

X-ray flares (V): The X-ray flares have a rapid rise and fall, appearing in both long and short GRBs. Many of them seem to be superimposed on a smoothly decaying afterglow component.

Multiple flares are observed in some bursts. The flux increase is usually large and in a few cases the fluence of the flare can be comparable with that of the prompt emission; flares soften as they progress and later flares are less energetic and broader than early flares. It seems that X-ray flares can be fitted with the FRED profile as for the hard X-ray pulses in the prompt emission.

Interpretation of X-ray flares invokes the re-activity of the GRB central engine, or the upper scattering of the photons by the hot electrons in the forward shock, or due to the environmental significant change, e.g., the density clumps surrounding the GRB progenitor, and some other ideas (see Zhang et al. 2006 and references therein).

1.2.2 Optical and radio afterglows

In the pre-*Swift* era, the afterglow observations were mainly carried out in the optical and radio bands. The late time optical/radio observations were largely used to identify temporal breaks in the lightcurves, which were generally interpreted as the jet break. Broadband modeling was carried out for some well observed afterglows, and the data were generally consistent with the standard external shock afterglow model. In some cases, very early optical flashes have been discovered (e.g. GRB 990123, Akerlof et al. 1999), which are generally interpreted as emission from the reverse shock (e.g., Sari & Piran 1999; Mészáros & Rees 1999). Early radio flares have been detected in some GRBs (Frail et al. 2003), which were also attributed to the reverse shock emission (Sari & Piran 1999).

Meanwhile, optical robotic telescopes such as ROTSE failed to report detections of optical early afterglows for most bursts due to various factors (including technical difficulties), but the general expectation at that time was that the *Swift*/UVOT would collect a large sample of early afterglow lightcurves to allow a detailed study of GRB reverse shock emission. However, now it turns out that in most bursts the reverse shock emission is really not significant simply because most *Siwft* bursts have either dim or undetectable early optical afterglows.

One of the intriguing findings for *Siwft* GRB optical afterglows is that generally speaking, short GRB afterglows may be intrinsically dimmer than those of long GRBs, but with some overlap (e.g., Kann et al. 2007). This finding can be validated if the mean circumburst density for short GRBs is much less than that for long GRBs and/or the mean energetic budget for short GRBs is much less than that for long GRBs. Fig. 1.10 shows such comparisons. Apparently short GRBs trend to have lower isotropic equivalent energy and lower lower optical flux with respect to long GRBs; on the other hand, since isotropic equivalent energy can be approximately regarded as an agent of the kinetic energy of GRB afterglow, the similar ratio of optical flux at 11 hrs after the burst V.S. isotropic equivalent energy for both long and short GRBs would indicate that the difference between the environments for the two GRB classes might be not as big as previously thought.

Since long GRBs are believed to produced by the core-collapse of massive stars (e.g., Woosley
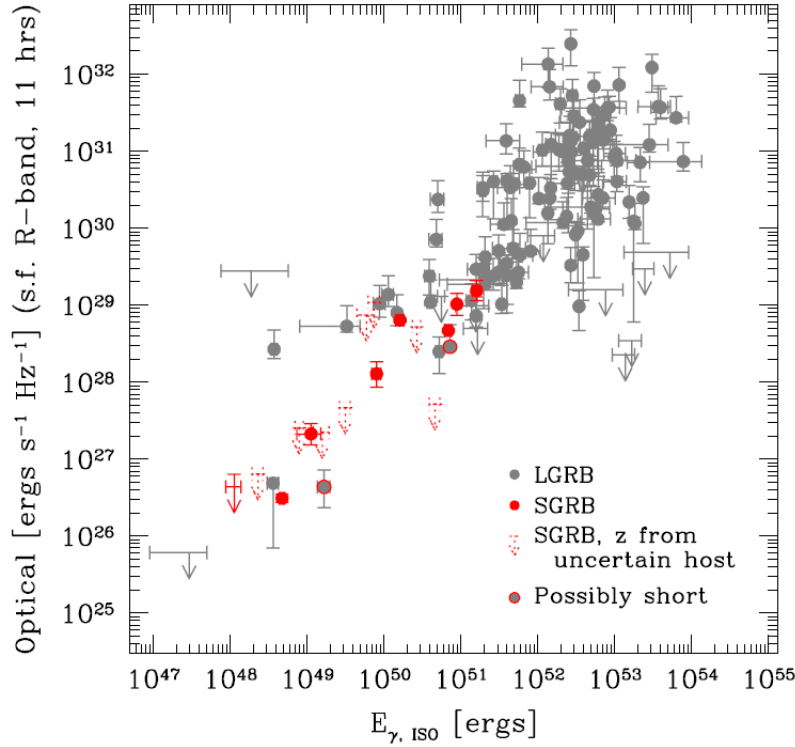
Figure 1.10: A plot of the rest-frame optical R-band (corrected for Galactic extinction) afterglow brightness at eleven hours V.S. E_{iso}, the total prompt emission of the burst in gamma-rays (from Nysewander, Fruchter, & Pe'er 2008). Dashed upper limits represent SGRBs with a host galaxy determined by XRT error circle only. GRB 060614 and GRB 060505 are labeled as "Possibly short" by the authors.

1993), they are naturally expected by be accompanied by SN Ibc. The first (likely) LGRB-SN association was discovered in GRB 980425/SN 1998bw because their positions in the sky appear to overlap (Galama et al. 1998; Kulkarni et al. 1998b). Late, this association was secured in GRB 030329/SN 2003dh: the unambiguous supernova lightcurve and spectra of SN 2003dh accompanying GRB 030329's optical afterglow (Hjorth et al. 2003; Stanek et al. 2003). See Fig. 1.11. Since then, more and more associations have been confirmed in nearby long GRB/XRF events, e.g. XRF 060218/SN 2006aj. However, surprise came on the *Swift*-discovered two nearby long GRBs 060505 and 060614. Their afterglows have been found not to be accompanied by supernovae down to very strict limits hundreds of times fainter than the archetypal supernova SN 1998bw that accompanied GRB 980425, and fainter than any Type Ic supernova ever observed (Fynbo et al. 2006; Della Valle et al. 2006; Gal-Yam et al. 2006). Multi-band observations of the early afterglows, as well as spectroscopy of the host galaxies, exclude the possibility of significant dust obscuration and show that both bursts originated in actively star-forming regions. The origin of such SN-less GRBs is currently under debate, i.e., either origin of the merger of two compact objects or origin of a collapsar but without associated bright SN. Fig. 1.12 shows the optical
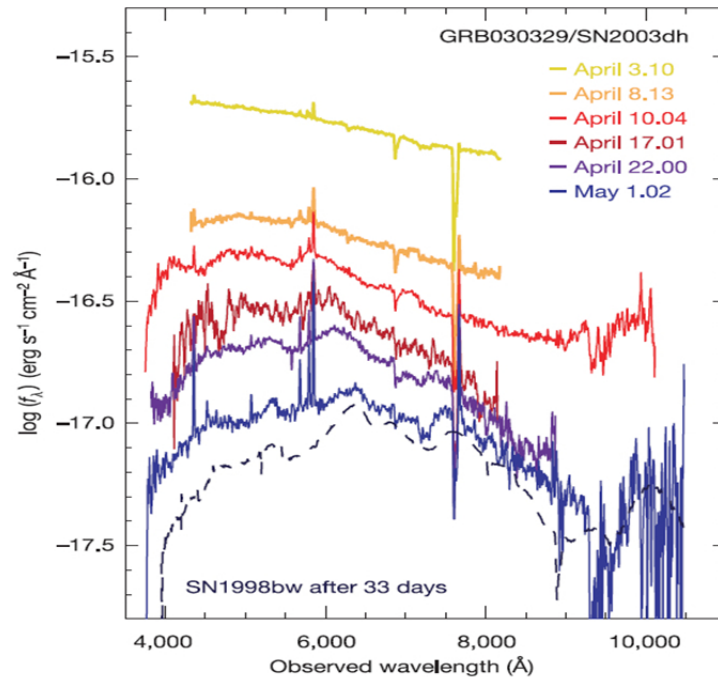
Figure 1.11: Spectral evolution for the afterglow of GRB 030329. The high similarity between GRB 030329 afterglow's spectra and that of SN 1998bw confirms the GRB-SN connection.

lightcurves of these two afterglows with respect to the expected lightcurves (i.e., after redshift and spectrum corrections) from archetypal SN 1998bw, SN 2002ap, SN 2006aj, respectively.

Near-infrared and radio follow-ups have been performed for some afterglows. Currently their utility is not as much as optical due to the restrictions of the available instruments and the observational environment. The radio follow-ups are sometimes limited by the relatively high redshifts of *Swift* bursts, while they have been playing an important role for all nearby GRBs. As a general trend, follow-ups in infrared and radio have been increasing and hopefully will bring richer and richer information.

1.3 Properties of GRB host galaxies

Host galaxies for long GRBs

Besides directly focusing on the GRB outflow and its afterglow, another way is to study the GRB's host galaxy or the GRB site within the host galaxy for some local events. The emission lines of GRB host galaxies can be observed when the afterglow has faded. In contrast, in QSO-DLA the host galaxy is always illuminated by the background quasar.

On average GRB host galaxies have a small size and a low luminosity. They are generally blue with strong emission lines and with active star formation (Sokolov et al. 2001; Le Floc'h et
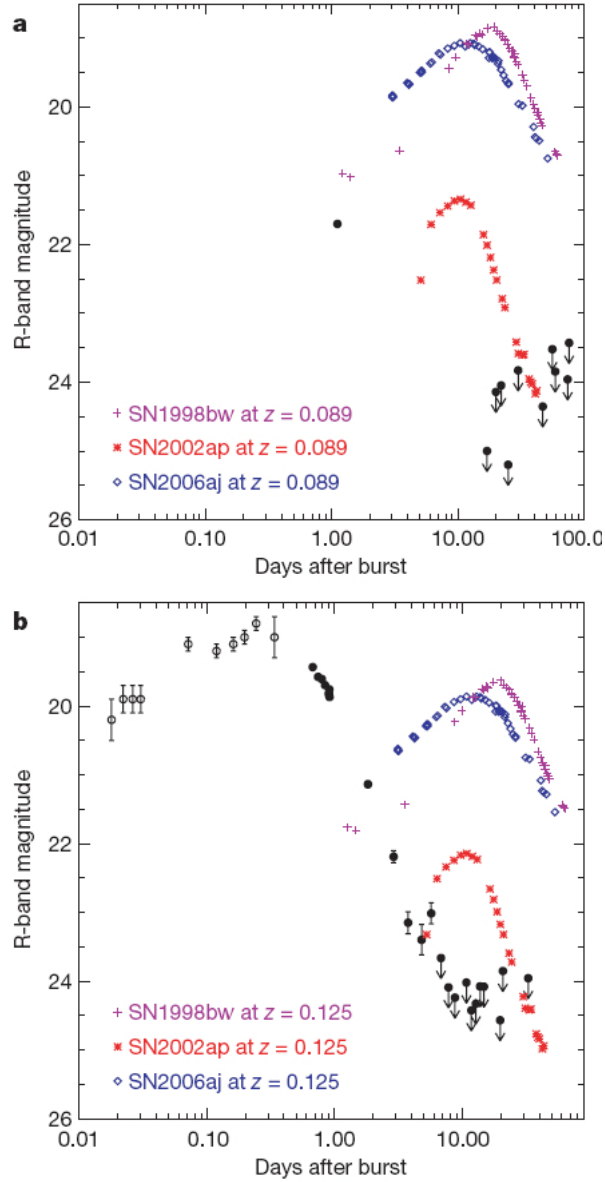
Figure 1.12: No visible supernovae associated with nearby long GRBs 060505 and 060614 (from Fynbo et al. 2006).

al. 2001; Christensen, Hjorth, & Gorosabel 2004; Fynbo et al. 2005; Sollerman et al. 2005). GRBs appear to trace the blue light of their host galaxies. They are more concentrated in the very brightest regions of their host galaxies than are core-collapse SNe, indicating that GRBs are formed from massive stars. Moreover GRB host galaxies are fainter and smaller than SN hosts. Fruchter et al. (2006) found intriguing differences between these two galaxy groups. Out of 42 long GRB hosts, 41 appear to be small star-forming galaxies with size typically like those of the Magellanic clouds[1]. The morphology of GRB hosts is therefore consistent with the idea that long

---

[1]Large Magellanic Cloud (LMC) and Small Magellanic Cloud (SMC) are with metallicities 0.3 $Z_\odot$ and 0.2 $Z_\odot$,

GRBs occur at lower metallicities than normal core-collapse SNe. Wolf & Podsiadlowski (2007) used the sample of Fruchter et al. (2006) and showed that the mean GRB host galaxy is a galaxy with the mass of LMC and half-solar metallicity. Moreover, a majority of GRBs are associated with irregular galaxies. This is another difference compared with core-collapse SNe, which are almost equally distributed between spiral and irregular galaxies (Fruchter et al. 2006). Fruchter et al. (2006) suggested that GRBs could be associated with the most massive stars and restricted to galaxies of limited chemical evolution. Modjaz et al. (2008) reached similar conclusions that broad-lined SNe Ic without GRBs tend to inhabit luminous and more metal-rich galaxies than GRB-SN, consistent with the hypothesis that low metal abundance is the cause of very massive stars becoming SN-GRBs (also see Stanek et al. 2006). Fruchter et al. (2006) reported the observations of seven GRB hosts with measurements or limits on their metallicity which are all less than 1/3 solar. They argued that low metallicity seems to play a decisive role in the GRB phenomenon and even suggested an upper limit to the metallicity of $Z \sim 0.15 Z\odot$ for cosmological GRBs.

Savaglio (2006) summarized the metallicities of 11 GRB hosts and found that for a redshift range between 0.01 and 1 the average value of the metallicity was 0.70 $Z\odot$. To estimate the star formation rate (SFR) of 19 GRB host galaxies, Savaglio, Glazebrook, & Le Borgne (2006) employed the [O II] emission line and found a median dust-corrected SFR of 12 $M_\odot \, yr^{-1}$. The range spanned by the 19 GRB hosts is between 1 and 100 $M_\odot \, yr^{-1}$. Given the generally low stellar masses of the GRB hosts, they concluded that a large fraction of them are undergoing a burst of star formation.

In short, the (long) GRB environment is characterized by large neutral gas column density, often with low metallicity and low dust content.

Host galaxies for short GRBs

After the launch of *Swift*, short GRBs have been found to be associated with both elliptical galaxies and star forming galaxies (e.g., GRB 050509B: Bloom et al. 2006; GRB 050709: Hjorth et al. 2005a; GRB 050724: Berger et al. 2005; GRB 051221A: Soderberg et al. 2006a; GRB 060801, GRB 061006, GRB 061210 and GRB 061217: Berger et al. 2007; GRB 070429B and GRB 070741B: Cenko et al. 2008; GRB 070724: Berger 2009). So far GRBs 050509B, 050813, 051210, 061201, 081211B have been found occurring within a galaxy cluster. Note that GRB 081211 consists of a short spike and a long extended emission, as well as for GRB 080503. These two GRBs are found not be associated with any galaxy down to a deep limit of R$\sim 25 - 28$ mag. The association with elliptical galaxies demonstrates unambiguously that the progenitors of at least some short GRBs are related to an old stellar population, consistent with the popular model of compact object mergers. Note that so far for short GRBs no redshift is obtained directly form their afterglows.

---

respectively.
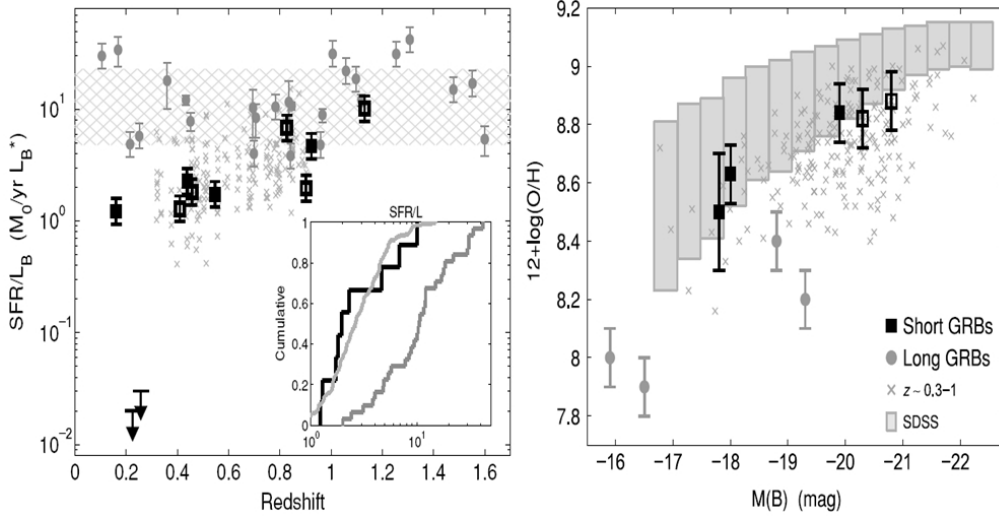
Figure 1.13: *left panel*: Specific SFRs as a function of redshift for the host galaxies of short (black) and long (gray) GRBs, as well as field galaxies from the GOODS-N survey (crosses). The cross-hatched region marks the median and standard deviation for the long GRB host sample. The inset shows the cumulative distributions for the three samples. *right panel*: Metallicity as a function of B-band absolute magnitude for the host galaxies of short (black) and long (gray) GRBs. The gray bars mark the 14C86 percentile range for galaxies at z∼0.1 from the Sloan Digital Sky Survey, while the crosses designate the same field galaxies at z∼0.3C1. Both field samples exhibit a clear luminosity−metallicity relation. The long GRB hosts tend to exhibit lower than expected metallicities, while the hosts of short GRBs have higher metallicities by about 0.6 dex and are, moreover, in excellent agreement with the luminosityCmetallicity relation. Both *left* and *right* panels from Berger (2009).

Recently, Berger (2009) presented a few optical spectra of short GRB host galaxies, and compiled a sample of 23 short bursts with *Swift*/XRT positions. About one half of the sample has spectroscopically identified host galaxies, with $z \sim 0.1 - 1.1$, and the ratio of star forming to elliptical galaxies in this spectroscopic sample is 5:1 while the maximum allowed fraction of elliptical galaxies in the *Swift*/XRT sample is 55%. Despite the fact that most short GRBs occur in star forming galaxies, their properties are strongly distinct from those of long GRB hosts. The rest-frame B-band luminosity distribution of the short GRB hosts is systematically brighter than for long GRB hosts in the same redshift range. An even stronger difference is apparent in the specific SFRs, with a median value for short GRB hosts that is nearly an order of magnitude lower than for long GRB hosts. Similarly, the metallicities of the short GRB hosts are about 0.6 dex higher than those of long GRB hosts, and unlike the long GRB hosts they follow the luminosity−metallicity relation of field galaxies. These differences indicates that the progenitors of long and short GRBs are themselves distinct, supporting additional lines of evidence such as the lack of supernova associations in short GRBs. Interestingly, Berger (2009) found that a comparison to a large sample of star forming field galaxies in a similar redshift range reveals excellent agreement in terms of specific SFRs and the luminosity-metallicity relation (see Fig. 1.13).

Thus, short GRBs select galaxies that are representative of the average stellar populations at least to z∼1. These comparisons, along with the presence of some short GRBs in elliptical galaxies, indicate that the progenitor ages span a wide range of ∼0.1-10 Gyr (the lower limit actually is not clear yet).

1.4   Notes on GRB observation and progenitor

This section is intended to give some notes of GRB research both in observation and progenitor.

GRBs were discovered in 1960s by the U.S. spy satellites *Vela* and this finding was made public in early 1770s (Klebesadel, Strong, & Olson 1973; Mazets et al. 1974). Due to limited information at that time, the proposed GRB models were more than the number of found GRBs.

A breakthrough came in early 1990s when the *Compton Gamma-ray Observatory* (*CGRO*) was launched, with the *Burst and Transient Experiment* (BATSE) and the *Energetic Gamma Ray Experiment Telescope* (EGRET) on board. *CGRO* was out of service in June 2000. One of the main goals of *CGRO* was to detect GRBs, with BASTE covering 25-50, 50-100, 100-300, 300-2000 keV, and EGRET covering 20 MeV to 30 GeV. BATSE data brought evidence for an isotropic spatial distribution of GRBs (Meegan et al. 1992), the conventional long-soft and short-hard GRB classes (Kouveliotou et al. 1993), and the widely adopted "Band function" for GRB spectra (Band et al. 1993). On the other hand, EGRET found the high-energy GeV emission of GRBs (Hurley et al. 1994).

The launch of the Italian-Dutch satellite *Beppo-SAX* in April 1996 brought GRB research into another era. *Beppo-SAX* covers 0.1-200 keV, being suitable to detect the X-ray afterglow of GRBs. In 1997, *Beppo-SAX* pinpointed the first GRB afterglow for GRB 970228 in the X-ray band (Costa et al. 1997), bringing optical and radio follow-ups into reality. Shortly afterwards, GRB redshift measurements were obtained for GRB 970508 (Metzger et al. 1997) and GRB 971214 (Kulkarni et al. 1998a), giving solid evidence that GRBs are of cosmological origin. By around 2000, the (likely) LGRB-SN association (Galama et al. 1998; Kulkarni et al. 1998b), prompt optical flash (Akerlof et al. 1999), achromatic steepening break in the afterglow lightcurves (e.g., Harrison et al. 1999) had been observed, solidifying the jetted GRB fireball interpretation. In Oct. 2000, the *High Energy Transient Explorer II* (*HETE-II*) joined in the hunting of GRBs. Tow years later, the *International Gamma-Ray Astrophysics Laboratory* satellite, (*INTEGRAL*) also joined in the game. In 2001-2002, XRFs were identified (Heise et al. 2001; Kippen et al. 2002). Later, more and more XRFs were found to be the downward extension of classical GRBs in the energy domain. GRB energy budget covers a few orders of magnitude even after their collimation corrected, indicating that is is not easy to develop GRBs into standard candles. It was *HETE-II* that found GRB 030329 and enabled the solid evidence of the LGRB-SN association.
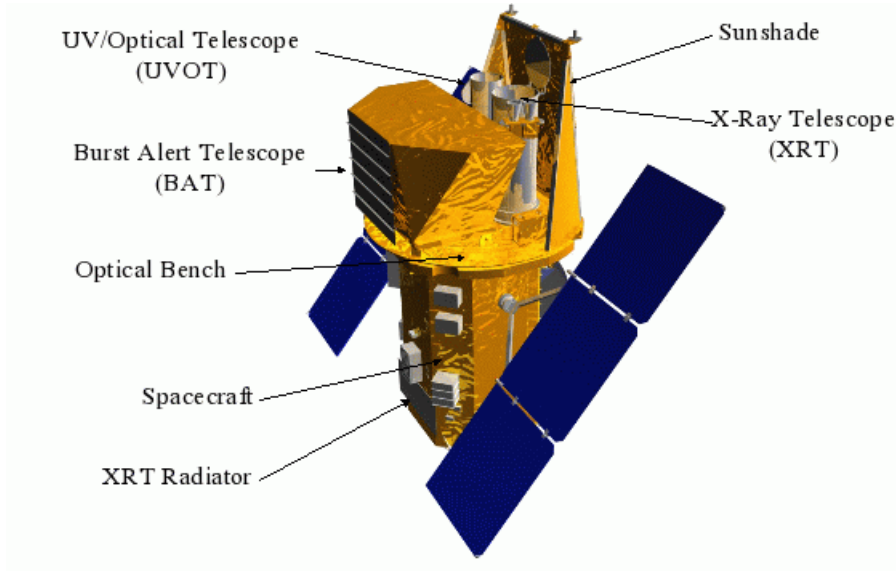
Figure 1.14: Sketch of the *Swift* Gamma-Ray Burst mission, including the Burst Alert Telescope (BAT), the X-ray Telescope (XRT), and the UV/Optical Telescope (UVOT). From Gehrels et al. (2004).

Finally we entered the *Swift* era since late 2004. *Swift* is the current leading space-based GRB mission. *Swift* is distinguished for its work mode as follows: (1). *Swift*/BAT triggers on GRB and calculates position to within 4 arcmin; (2). Spacecraft autonomously slews to the GRB position in 20-70 seconds; (3). *Swift*/XRT determines position to within $\sim$5 arcsec; (4) *Swift*/UVOT images the field and transmits finding chart to ground. This work mode has enabled the most comprehensive study of GRBs and their host galaxies to date. So far *Swift* has enabled the statistical finding of the "canonical" GRB X-ray afterglow lightcurve which involves the prompt tail emission, the mysterious shallow decay, and the weird X-ray flares. Interestingly, the previously expected jet break is seldom shown in *Swift* bursts; the conventional LGRB-SN interpretation is challenged in the case of GRBs 060505 and 060614. The most distant GRB 080913 ($z = 6.7$, Fynbo et al. 2008) has broken the record of QSO ($z = 6.43$), making the study of the early universe into reality. The discovery of nearby XRF 060218 and X-ray transient 080109 brought the plausible shock breakout under debate. *Swift* even detected a naked-eye burst with a uniquely bright peak visual magnitude of 5.3 at z=0.937 (Racusin et al. 2008). This is the optically brightest burst to date. Last but not least, the afterglow and host study of short GRBs began in this era and now it has been widely believed that short GRBs are diverse and probably contain sub-classes.

Accordingly, some notes closely related to GRB progenitor interpretations are also presented here (for review works see Woosley & Bloom 2006 and Lee & Ramirez-Ruiz 2007).

Firstly, Ruderman (1975) raised the "compactness problem" on the GRB fireball model. One year later, Blandford & McKee (1976) found a self-similar solution of the relativistic blast

waves. It is the mathematical foundation for the relativistic GRB blastwave model, and has been extensively applied since the discovery of GRB afterglows. Although most people thought GRBs were of galactic origin, Paczyǹski (1986) proposed a cosmological model of GRBs, involving neutron star−neutron star (NS-NS) mergers as the power source. A pure photon-electron pair fireball was found to expand relativistically. Shemi & Piran (1990) found that the fireball thermal energy is essentially converted into kinetic energy of the expanding ejecta by including only a small amount of baryon contamination. The GRB fireball evolution was thus unveiled.

For the short GRB progenitor model(s), the NS-NS merger model was further studied (Eichler et al. 1989; Narayan et al. 1992). The BH - NS merger model was proposed (Paczyǹski 1991) and further studied (Lee & Kluźniak 1995, 1999a,b; Perna & Belczynski 2002; Davies, Levan, & King 2005; Rosswog 2005; Belczynski et al. 2006). The millisecond magnetar (neutron stars with surface magnetic field of order 10^{14-15} G) model was proposed (Usov 1992). A white dwarf (WD) may also merger with a black hole. The formation scenario parallels those of BH-NS binaries (Fryer et al. 1999).

For the long GRB progenitor model(s), the "failed" supernova model was proposed (Woosley 1993), which is now known as the "collapsar" model. As a push, Paczyński (1998) suggested that GRBs were likely to originate from "hypernovae", and were associated with star forming regions. Since 1990s, the GRB progenitor models involving collapses of massive stars have been further developed. On the one hand, the "collapsar model" was extensively studied numerically and analytically; Some simulations have shown that core-collapse could produce dim SN explosion due to relatively less Ni is generated (e.g., Nagataki et al. 2003; Fryer et al. 2006). On the other hand, a variant of the massive-star-collapse model, invoking a delayed GRB with respect to the SN explosion, was proposed (Vietri & Stella 1998), known as the "(delayed) supranova" model. But this model is not well supported by observations of GRB-SN connection events so far, i.e., the observational association events do not support a long delay.

After the discovery of SN-less long GRB 060614, King, Olsson, & Davies (2007) proposed explaining such bursts by the WD-NS merger. GRBs due to NS-WD mergers must be associated with star-forming regions and lie within their host galaxies which can be of any type. Davies, Ritter, & King (2002) estimated the formation rate of such systems in the Galaxy and showed that half of them merger within 10^8 yr. Therefore, it seems that NS-WD mergers should not be neglected, even though the favorite models are the collapsar model for long bursts.

1.5 Fireball + internal shock model for GRBs

The leading GRB fireball model tells us that the GRB central engine would spurt out some ultra-relativistic shells with different Lorentz factors, likely due to rapidly variable mass accretion rate

onto the central object after the launch of the GRB jet (e.g., Nagataki 2009). These shells will be will collide with one another, accelerating electrons and amplifying the magnetic field. The resulting synchrotron radiation and inverse Compton scattering by electrons and photons give rise to the observed multi-peak, irregular gamma-ray pulses within a GRB. This is the so-called standard fireball model (e.g., Mészáros 2002; Piran 1999, 2005).

1.5.1 Initial conditions for the fireball

The duration of a GRB can be as short as $\Delta T = 1$ ms, therefore the size for the GRB fireball is

$$R_0 \sim c\Delta T \sim 3 \times 10^7 \Delta T_{-3} \text{ cm.} \tag{1.2}$$

If one requires an energy as high as $E = 10^{51}$ erg to be released in such a short timescale and particular within the above mentioned size, then an optically thick, extremely hot fireball is inevitable. The optical depth is estimated as $\tau \simeq \sigma_T n R_0 \sim \sigma_T(\frac{E}{R_0^3 m_e c^2})R_0 \sim 10^{17} E_{51} R_{0,8}$, where σ_T is the Thompson scattering section, n is the particle density, m_e is the rest mass of an electron, c is the speed of light. This is the so-called "compactness problem" mentioned in the last section.

Such high optical depth indicates that the fireball would be adiabatically expanding until most of the internal energy (or thermal energy) in the fireball ejecta is converted to the kinetic energy of the baryons within the GRB ejecta.

Suppose the fireball is composed of photons and electron-positron pairs. The energy density is $\rho_\gamma = aT^4$, where $a = 7.57 \times 10^{-15} \text{ erg K}^{-4} \text{ cm}^{-3}$ is the Boltzmann constant for energy density and T is the temperature. For the pairs, their energy density can written as

$$\rho_e = \frac{8\pi}{h^3} \int_0^\infty \frac{\sqrt{m_e^2 c^4 + p^2 c^2} p^2 \mathrm{d}p}{\mathrm{e}^{\sqrt{m_e^2 c^4 + p^2 c^2}/kT} + 1} \simeq \frac{8\pi}{h^3} \int_0^\infty \frac{p^3 c \mathrm{d}p}{\mathrm{e}^{pc/kT} + 1} = \frac{7}{8} aT^4, \tag{1.3}$$

where k is the Boltzmann constant, p is the momentum of the electron or positron. Because the temperature is very high, one has $pc \gg m_e c^2$. Then the total energy, including photons and pairs, of the fireball is given by

$$E = \frac{11}{4} aT^4 (\frac{4}{3}\pi R_0^3). \tag{1.4}$$

We here directly obtain $T \simeq 1.03 \times 10^{10} E_{51}^{1/4} R_{0,8}^{-3/4}$ K, about 0.9 MeV, larger than the rest-mass energy for an electron (i.e., 0.511 MeV). This result indicates that photons would generate pairs during the fireball expansion even if there are no input pairs at all. So our assumption above is reasonable.

Baryons play an important role here, because too little baryons will lead to that most initial energy in this fireball is radiated out instead of being converted to kinetic energy of baryon ejecta. On the other hand, baryons should not be too abundant, otherwise the energy from radiation

during the expansion of the fireball cannot accelerate the baryons to relativistic status–this largely corresponds to the supernova explosion case.

1.5.2 Evolution of the fireball

Since the initial energy of the fireball is mostly converted to the kinetic energy of baryons within the ejecta, we now consider an adiabatic expansion of the baryon-dominated outflow ($m_p = 1$, $c = 1$, $p = e/3$):

$$\begin{cases} \frac{\partial}{\partial t}(n\gamma) + \frac{1}{r^2}\frac{\partial}{\partial r}(r^2 nu) = 0, \\ \frac{\partial}{\partial t}(e^{3/4}\gamma) + \frac{1}{r^2}\frac{\partial}{\partial r}(r^2 e^{3/4}u) = 0, \\ \frac{\partial}{\partial t}[(n + \frac{4}{3}e)\gamma u] + \frac{1}{r^2}\frac{\partial}{\partial r}[r^2(n + \frac{4}{3}e)u^2] = 0, \end{cases} \tag{1.5}$$

where $u = \sqrt{\gamma^2 - 1} \sim \gamma$, e represents the internal energy.

We now derive the scaling relations between r, γ, n, e. Take the first one of the above set of equations as an example: multiply the left and right hand sides with r^2 and then expand the left hand side, one obtains

$$\begin{aligned} &\frac{\partial}{\partial t}(n\gamma) + \frac{1}{r^2}\frac{\partial}{\partial r}(r^2 n\gamma) = 0 \\ \Rightarrow\ & r^2 \frac{\partial}{\partial t}(n\gamma) + \frac{\partial}{\partial r}(r^2 n\gamma) = 0 \\ \Rightarrow\ & r^2 n\frac{\partial\gamma}{\partial t} + r^2\gamma\frac{\partial n}{\partial t} + n\gamma\frac{\partial r^2}{\partial r} + r^2\gamma\frac{\partial n}{\partial r} + r^2 n\frac{\partial\gamma}{\partial r} = 0 \\ \Rightarrow\ & r^2 n\frac{\partial\gamma}{\partial t}dt + r^2\gamma\frac{\partial n}{\partial t}dt + n\gamma\frac{\partial r^2}{\partial r}dr + r^2\gamma\frac{\partial n}{\partial r}dr + r^2 n\frac{\partial\gamma}{\partial r}dr = 0 \\ \Rightarrow\ & r^2 n(\frac{\partial\gamma}{\partial t}dt + \frac{\partial\gamma}{\partial r}dr) + r^2\gamma(\frac{\partial n}{\partial t}dt + \frac{\partial n}{\partial r}dr) + n\gamma\frac{\partial r^2}{\partial r}dr = 0 \\ \Rightarrow\ & r^2 nd\gamma + r^2\gamma dn + n\gamma dr^2 = 0 \\ \Rightarrow\ & d(r^2 n\gamma) = 0 \end{aligned} \tag{1.6}$$

where we have used $dr = cdt = dt$ (in the radial direction). We thus have

$$r^2 n\gamma = const. \tag{1.7}$$

Treating the second and third equations in a similar fashion, we find

$$r^2 e^{3/4}\gamma = const, \tag{1.8}$$

$$r^2(n + \tfrac{4}{3}e)\gamma^2 = const. \tag{1.9}$$

Combing the above three forms, it's straightforward to see

(1) for the radiation-dominated phase when $e \gg n$,

$$\gamma \propto r, n \propto r^{-3}, e \propto r^{-4}, \tag{1.10}$$

$$T_{obs} = \gamma T_{co} \propto \gamma e^{-1/4} \sim const. \tag{1.11}$$

During this phase, the Lorentz factor increases as the radius increases. This period is sometimes called *acceleration phase*;

(2) for the matter(baryon)-dominated phase when $e \ll n$,

$$\gamma \sim const., n \propto r^{-2}, e \propto r^{-8/3}, \tag{1.12}$$

$$T_{obs} \propto r^{-2/3}. \tag{1.13}$$

During this phase, the Lorentz factor remains unchanged. This period is sometimes called *coasting phase*.

The prompt gamma-ray emission is widely believed to originate from the collision of the shells when the fireball enters the coasting phase. For comparison, the afterglow emission phase is believed to start when the shock-accelerated (kinetic) energy of the circumburst medium is comparable to that of the fireball just when it enters the coasting phase. Fig. 1.15 is an illustration of the fireball model, marked with some typical radii and timescales.

Since the gamma-ray radiation comes from the collision of shells with different Lorentz factors in the coasting phase, in principle one can estimate the gamma-ray radiative efficiency according to energy and momentum conservations. So far different results have been presented. In general, too high radiative efficiency would bring doubt.

As a note here, actually there are a number of observations and/or theoretical considerations that pose difficulties for the internal shock model. Internal shocks have only a modest efficiency $1 - 10\%$ for converting jet energy to the radiation observed in the 20 keV - 1 MeV band (Kumar, 1999; Panaitescu, Spada, & & Mészáros 1999; Lazzati, Ghisellini, & Celotti 1999). Even a $\sim 10\%$ radiative efficiency is low compared to the burst efficiency implied by measurements of the jet kinetic energy through modeling GRB afterglow lightcurves. Another difficulty with the internal shock model is the large distance from the central explosion that one estimates ($R > 10^{16}$cm) for the γ-ray-producing region in a number of GRBs (Kumar 2007). This distance is significantly larger than what one expects in the internal shock model. Moreover, the estimated distance is within a factor of a few of the deceleration radius where the jet begins to interact with the external medium. This coincidence between two unrelated radii is unexpected. These difficulties, along with the problem of avoiding excessive baryon loading, motivate some people to consider an alternative to the internal shock model. Naturally, a model invoking magnetic dissipation as
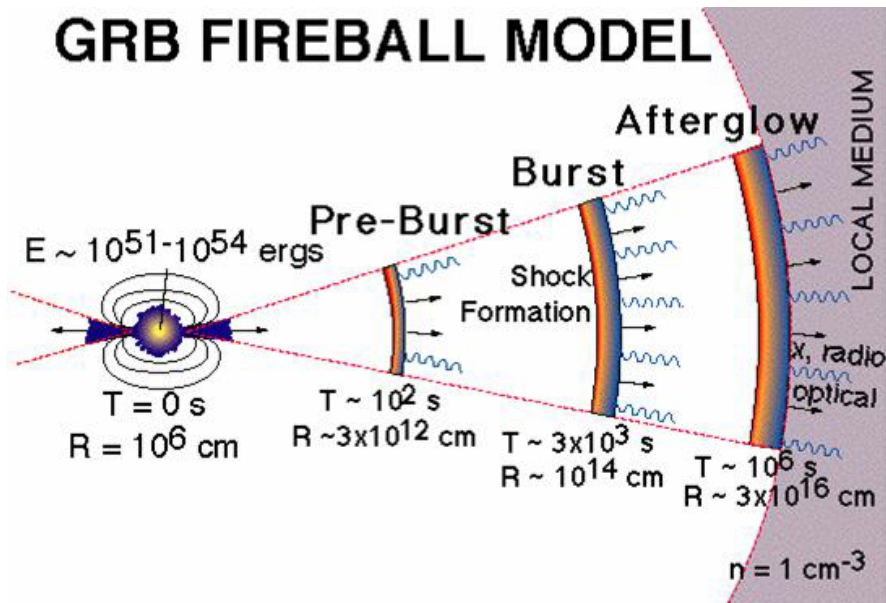
Figure 1.15: Schematic illustration of the fireball model (from Ghisellini 2001). This picture shows the various steps of the basic standard model with the internal and external shock and the various radiations they emit.
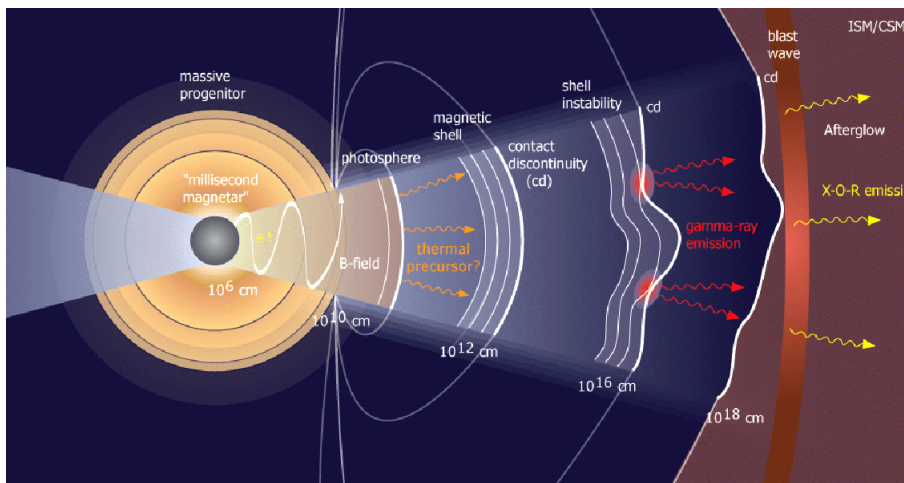
Figure 1.16: Schematic illustration of the electromagnetic model (from Lyutikov & Blandford 2003).

the energy extract mechanism seems quite attractive. This model may differentiate itself from the fireball model via a much higher polarization in radiation since it contains large scale regular magnetic field. Fig. 1.16 is a schematic illustration of this model.

Chapter 2
GRB afterglow temporal and spectral evolution

2.1 Introduction

After the GRB fireball undergoes the acceleration phase, the coasting phase, and the prompt phase of γ-ray emission, the min-shells in the fireball have merged into a big shell. This big shell would still move outwards and interact with the surrounding medium, giving rise the GRB afterglow emission.

Then a question naturally arises: where or under what conditions do we think the afterglow emerges? The answer is: at the so-called *deceleration radius*. This radius is defined as a certain radius where the internal energy of the shock swept-up medium is comparable to the internal energy of the initial fireball. At this point, the fireball shell has swept up so much medium that its dynamical evolution has been significantly changed and after this point the afterglow emission cannot be neglected. Before this point, actually there would be little afterglow emission which can be reasonably neglected.

This principle for determining the deceleration radius also applies to the SN remnant case. For the SN case, because the shock is non-relativistic, then the condition naturally changes to: when the mass of the shock swept-up medium is comparable to the mass of the SN ejecta.

Since the afterglow evolution invokes the relativistic shock and non-thermal radiation mechanisms, from now on we discuss them one by one to get a whole evolution picture.

2.2 Two inertial reference frames

Two reference frames are invoked in GRB study which is essential for the transformation between different observational or physical quantities. Let's imagine the emitting material has been accelerated and it moves relativistically relative to central engine with a bulk Lorentz factor Γ. Therefore there are two inertial frames: the rest frame of the emitting region (the comoving frame), and the rest frame of the central engine. The observer's rest frame is actually the same as the rest frame of the central engine aside from a cosmological redshift factor (see also Zhang & Mészáros 2004). We denote the parameters measured in the observer frame with the subscript "$\oplus$", the parameters

measured in the comoving frame with the superscript "′", and the parameters measured in the central engine frame with the hat script or simply without any superscript or subscript. The physical quantities (e.g. scale length and time) as viewed in the two inertial frames are related via the special-relativity transformation. Along the moving direction of the emitting region in the central engine's frame, the length scales Δ' and Δ, and the time intervals elapsed for the same pair of events dt' and $d\hat{t}$ are related by

$$\Delta' = \Gamma\Delta, \quad dt' = d\hat{t}/\Gamma.$$

The time in the observer frame is related to the time in the central engine frame by

$$t_{\oplus} = \int_0^R (1 - \beta\cos\theta)\frac{dr}{c} \approx \frac{R}{2\Gamma^2 c}, \tag{2.1}$$

where $\beta = (1 - 1/\Gamma^2)^{-1/2}$, and θ is the angle between the motion of the matter in the comoving frame and the line of sight, which would lead to $\cos\theta \approx 1$ if it is small enough. Of course a cosmological time-dilation factor $(1+z)$ should be added to the above relation for GRB study. In short, in the time domain for GRBs we have

$$t_{\oplus} = \hat{t}/2\Gamma^2 = t'/2\Gamma, \tag{2.2}$$

which is sometimes called the propagation effect. Should the relativistic motion of the GRB ejecta disappear, the above three times are the same because $\Gamma \sim 1$, which is the very Newtonian transformation.

2.3   Relativistic shocks

When it comes to relativistic shock for GRB afterglows, we refer it to relativistic collisionless shock. Note that magnetic energy dissipation, for example via magnetic reconnection, can also accelerate the particles and then give rise to prompt and afterglow emissions (e.g., Usov 1994; Thompson 1994; Lyutikov & Blandford 2003).

Shocks involve sharp jumps in the physical conditions. Conservations of mass, energy, and momentum determine the Rankine-Hugoniot shock jump conditions across the relativistic shocks. For the perpendicular shocks, if the upstream matter is cold and magnetized, the jump conditions read (Kennel & Coroniti 1984; see also Fan, Wei, & Zhang 2004)

$$\frac{n'_{\rm d}}{n'_{\rm u}} \approx \gamma_{\rm ud}\frac{7 + \chi + \sqrt{1 + 14\chi + \chi^2}}{1 + \chi + \sqrt{1 + 14\chi + \chi^2}}, \tag{2.3}$$

$$\frac{e'_{\mathrm{d}}}{n'_{\mathrm{d}} m_{\mathrm{p}} c^2} \approx \frac{\gamma_{\mathrm{ud}}(1+\sigma)}{8}(7 + \chi + \sqrt{1 + 14\chi + \chi^2})$$
$$[1 - \frac{6\chi}{1 + \chi + \sqrt{1 + 14\chi + \chi^2}}], \tag{2.4}$$

$$\frac{B'_{\mathrm{d}}}{B'_{\mathrm{u}}} = k\frac{n'_{\mathrm{d}}}{n'_{\mathrm{u}}}, \tag{2.5}$$

where n'_{u}, n'_{d}, e'_{u}, e'_{d}, B'_{u} and B'_{d} are the number density, the energy density and the magnetic field strength measured in the rest frames of the upstream region u and downstream region d respectively, and γ_{ud} is the Lorentz factor of upstream u relative to downstream d. Also $\chi \equiv \frac{k^2 \sigma}{1+\sigma}$ ($0 \leq k \leq 1$) is the parameter describing the magnetic energy dissipation at the shock front ($k = 1$ for the ideal MHD limit) and σ is the ratio of the magnetic energy density to the particle energy density measured in the rest frame of the region u.

For the un-magnetized upstream (i.e., $\sigma = 0$), we have (Blandford & McKee 1976)

$$\frac{n'_{\mathrm{d}}}{n'_{\mathrm{u}}} \approx 4\gamma_{\mathrm{ud}}, \quad \frac{e'_{\mathrm{d}}}{n'_{\mathrm{d}} m_{\mathrm{p}} c^2} \approx \gamma_{\mathrm{ud}} - 1. \tag{2.6}$$

Different fractions of the internal energy of the post-shock fluid are given to protons, electrons, and the magnetic field. These fraction parameters are determined by the microscopic physical processes and are difficult to estimate from first principles. A simple and phenomenological approach is to assume the former two parameters are ε_{e} and ε_{B} respectively, which are normally regarded as constant throughout the whole GRB afterglow phase. Therefore, the energy density of electrons and the energy density of the magnetic field for downstream are given by

$$U'_e \equiv \varepsilon_{\mathrm{e}} n'_{\mathrm{d}} = 4\varepsilon_{\mathrm{e}} \gamma_{\mathrm{ud}}(\gamma_{\mathrm{ud}} - 1)n'_{\mathrm{u}} m_{\mathrm{p}} c^2$$

and

$$U'_{\mathrm{B}} \equiv \varepsilon_{\mathrm{B}} n'_{\mathrm{d}} = 4\varepsilon_{\mathrm{B}} \gamma_{\mathrm{ud}}(\gamma_{\mathrm{ud}} - 1)n'_{\mathrm{u}} m_{\mathrm{p}} c^2$$

respectively.

2.4 Particle acceleration

Particle acceleration can occur in GRBs through the first-order Fermi mechanism involving internal or external shocks, and through the second-order Fermi acceleration involving gyroresonant scattering of particles by magnetic turbulence in the magnetic field of the blast wave. In the first-order Fermi acceleration, the particles are accelerated when they repeatedly cross the shock's contact-discontinuity (CD) surface. It is the magnetic-field irregularities that keep scattering the particles back so that they keep crossing the CD surface. Repeated crossings would lead to a

power-law energy spectrum for the electrons with $p \sim 2.3$ if $\gamma_{\rm ud} \gg 1$ is satisfied (Gallant 2002). The second-order Fermi acceleration can work efficiently if magnetic turbulence in the magnetic field of the blast wave has been well developed (Dermer & Humi 2001). Again, the accelerated spectrum could be a power-law with an index $p \sim 2.2$ (Virtanen & Vainio 2005).

As mentioned above, in the shock front a fraction, $\varepsilon_{\rm e}$, of shock energy is given to the fresh electrons which were swept up by the shock. If the accelerated electrons have a power-law energy distribution $dn'/d\gamma'_e \propto (\gamma'_e - 1)^{-p}$ for $\gamma'_m \leq \gamma'_e \leq \gamma'_{\rm M}$, with the shock jump conditions of

$$\int_{\gamma'_m}^{\gamma'_{\rm M}} (dn'/d\gamma'_e)d\gamma'_e = n'_{\rm d} \tag{2.7}$$

and

$$\int_{\gamma'_m}^{\gamma'_{\rm M}} (\gamma'_e - 1)m_{\rm e}c^2(dn'/d\gamma'_e)d\gamma'_e = U'_{\rm e}, \tag{2.8}$$

then from these conditions we have

$$\gamma'_m \approx \varepsilon_{\rm e}(\gamma_{\rm ud} - 1)\frac{p - 2}{p - 1}\frac{m_{\rm p}}{m_e} + 1, \tag{2.9}$$

where the maximal Lorentz factor is given when the lifetime of the accelerated electron due to its non-thermal radiation loss is comparable to the timescale for it being accelerated since it was swept up. The from of the maximal Lorentz factor will be given below.

The magnetic field strength is given by

$$\begin{aligned}
B' &= \sqrt{8\pi U'_{\rm B}} = \sqrt{32\pi\varepsilon_{\rm B}\gamma_{\rm ud}(\gamma_{\rm ud} - 1)n'_{\rm u}m_{\rm p}c^2} \\
&\approx 0.04(\frac{\varepsilon_{\rm B}}{0.01})^{1/2}n'^{1/2}_{\rm u}\gamma_{\rm ud}\beta_{\rm ud} \text{ Gauss}, \tag{2.10}
\end{aligned}$$

where $\beta_{\rm ud} = \sqrt{1 - 1/\gamma^2_{\rm ud}}$. This form indicates that in the internal shocks or the early forward shock, B' could be (significantly) larger than 1 Gauss as $n'_{\rm u} \gg 1$ in internal shocks and $\gamma_{\rm ud} \sim \Gamma \gg 1$ in the early forward shock.

2.5 Synchrotron radiation

The typical energy of synchrotron photons as well as the synchrotron cooling time depends on the Lorentz factor of the relativistic electron and on the strength of the magnetic field. If the emitting region moves with a Lorentz factor Γ, the photons are blue-shifted[1]. The typical photon energy

---

[1]Note that the Lorentz factor, γ'_e, of the relativistic electrons in the comoving frame is different from the Lorentz factor, Γ, of the whole relativistic-electrons-contained shell relative to the observer.

in the observer frame is given by (Rybicki & Lightman 1979)

$$\nu_{\mathrm{syn},\oplus} = \frac{\mathcal{D}\nu'_{\mathrm{syn}}}{1+z} \approx \frac{q_e B'}{2\pi(1+z)m_e c}\gamma_e'^2\Gamma, \tag{2.11}$$

where $\mathcal{D} \equiv [\Gamma(1 - \beta\cos\theta)]^{-1} \approx 2\Gamma$ for a small θ.

The power emitted, in the comoving frame, by a single electron due to synchrotron radiation is given by

$$P'_{\mathrm{syn}} = \frac{4}{3}\sigma_{\mathrm{T}}cU'_{\mathrm{B}}(\gamma_e'^2 - 1). \tag{2.12}$$

where q_e and σ_{T} are the charge and the Thompson cross section of an electron, respectively. The synchrotron cooling time of an electron with a Lorentz factor γ_e' is $t'_c \approx \gamma_e' m_e c^2/P'_{\mathrm{syn}}$.

So now we can estimate the maximal Lorentz factor mentioned above. The electron acceleration timescale is approximately expressed as $t'_{acc} \approx 2\pi R_L/c = 2\pi(\gamma_e' m_e c^2/q_e B')/c$. With $t'_c \approx t'_{acc}$, we have

$$\gamma_{\mathrm{M}}' \approx \left(\frac{3q_e}{B'\sigma_{\mathrm{T}}}\right)^{1/2} \approx 4\times 10^7 B'^{-1/2}. \tag{2.13}$$

A third timescale involved here is the dynamical time for an electron in the comoving frame, which roughly measures the timescale for an electron to travel from its initial position at the very beginning of the fireball to the position where is accelerated by the shock in the comoving frame. It reads as $t'_d \approx R/\Gamma c$, where R is the radius of the shock front to the central engine. If $t'_c < t'_d$ holds, then the electron cools rapidly (i.e., *fast cooling*). We thus define the cooling Lorentz factor of the shocked electrons as γ_c', which satisfies $t'_c = t'_d$ and is given by

$$\gamma_c' \approx \frac{6\pi\Gamma m_e c^2}{\sigma_{\mathrm{T}} R B'^2}. \tag{2.14}$$

On the other hand, if $t'_c < t'_d$ holds, then the electron cools slowly, we call this case as *slow cooling*.

As can bee seen, the synchrotron radiation of shock-accelerated electrons with slow cooling (i.e., $\gamma_e' < \gamma_c'$) doesn't change their initial spectral energy distribution. But for shock-accelerated electrons with fast cooling (i.e., $\gamma_e' > \gamma_c'$ and $\gamma_e' > \gamma_m'$), the initial spectral energy distribution would be changed due to rapid synchrotron loss. The continuity equation of electrons in the energy phase (i.e., $E = \gamma_e' m_e c^2$) reads

$$\frac{\partial N(\gamma_e', t')}{\partial t'} + \frac{\partial}{\partial \gamma_e'}\left(N(\gamma_e', t')\frac{d\gamma_e'}{dt'}\right) = \dot{Q}(\gamma_e', t'), \tag{2.15}$$

where

$$\frac{d\gamma_e'}{dt'} = -\frac{P'_{\mathrm{syn}}}{m_e c^2} = \frac{-\sigma_{\mathrm{T}} B'^2}{6\pi m_e c}(\gamma_e'^2 - 1) \approx \frac{-\sigma_{\mathrm{T}} B'^2}{6\pi m_e c}\gamma_e'^2$$

and $\dot{Q}(\gamma_e', t')$ is the injection rate at γ_e' of the accelerated electrons. Let's take the injection energy

distribution as $Q(\gamma'_e, t') \propto \gamma'^{-p}_e$ for $\gamma'_m \leq \gamma'_e \leq \gamma'_M$ according to particle acceleration theory.

For the fast-cooling injection electrons, i.e., $\gamma'_m < \gamma'_c < \gamma'_e$, to maintain a quasi-steady distribution, there should be $\frac{\partial N_{\gamma'_e}}{\partial t'} = 0$; thus we have $\frac{\partial}{\partial \gamma'_e}(N_{\gamma'_e} \frac{d\gamma'_e}{dt'}) = \dot{Q}_{\gamma'_e}$. As a further step, we have

$$N_{\gamma'_e} \propto (d\gamma'_e/dt')^{-1} \int \dot{Q}_{\gamma'_e} d\gamma'_e \propto \gamma'^{-(p+1)}_e. \tag{2.16}$$

For $\gamma'_c < \gamma'_e < \gamma'_m$, we have $N_{\gamma'_e} \frac{d\gamma'_e}{dt'} \sim const$ and then $N_{\gamma'_e} \propto \gamma'^{-2}_e$. And naturally for $\gamma'_m < \gamma'_e < \gamma'_c$, the distribution is still $N_{\gamma'_e} \propto \gamma'^{-p}_e$. In summary, we have the following distributions:

$$N_{\gamma'_e} \propto \begin{cases} \gamma'^{-(p+1)}_e, & \text{for } \gamma'_e > \max\{\gamma'_c,\, \gamma'_m\}, \\ \gamma'^{-p}_e, & \text{for } \gamma'_c > \gamma'_e > \gamma'_m, \\ \gamma'^{-2}_e, & \text{for } \gamma'_m > \gamma'_e > \gamma'_c. \end{cases} \tag{2.17}$$

The synchrotron radiation spectrum can be easily estimated. The spectrum of one electron moving in a magnetic field B' can be approximated by

$$F'(x) \approx 2.149 \frac{\sqrt{3}e^3 B'}{m_e c^2} x^{1/3} e^{-x}, \tag{2.18}$$

where $x \equiv \nu'/\nu'_{\text{syn}}$ and $\nu' = (1+z)\mathcal{D}^{-1}\nu_\oplus$ ($\nu_\oplus$ is the observer's frequency). We see that $F'(x)$ peaks at $x = 1/3$. If the synchrotron self-absorption is unimportant (this case works for almost all GRB afterglows unless the surrounding medium is unexpectedly high), for $\nu_\oplus < \min\{\nu_{c,\oplus},\, \nu_{m,\oplus}\}$, the emission is the sum of the contributions of the tails of all the electrons' emissions $F_{\nu,\oplus} \propto \nu_\oplus^{1/3}$, where $\nu_{c,\oplus} \equiv \nu_{\text{syn}}(\gamma'_c)$ and $\nu_{m,\oplus} \equiv \nu_{\text{syn}}(\gamma'_m)$. In higher energy range, using $F_{\nu,\oplus}d\nu_\oplus \propto N_{\gamma'_e}P'_{\text{syn}}d\gamma'_e$ and $\nu_\oplus \propto \gamma'^2_e$, we have $F_{\nu,\oplus} \propto \nu_\oplus^{-1/2}$ for $\nu_{c,\oplus} < \nu_\oplus < \nu_{m,\oplus}$, $F_{\nu,\oplus} \propto \nu_\oplus^{-(p-1)/2}$ for $\nu_{m,\oplus} < \nu_\oplus < \nu_{c,\oplus}$ and $F_{\nu,\oplus} \propto \nu_\oplus^{-p/2}$ for $\max\{\nu_{m,\oplus},\, \nu_{c,\oplus}\} < \nu_\oplus$. In addition, because in GRBs $\nu_{a,\oplus} < \min\{\nu_{m,\oplus},\, \nu_{c,\oplus}\}$ holds, we then have $F_{\nu,\oplus} \propto \nu_\oplus^2$ in this case. In summary, the synchrotron radiation spectra can be approximated as (see also Sari, Piran, & Narayan 1998)

$$F_{\nu,\text{syn},\oplus} \propto \begin{cases} \nu_\oplus^{-p/2}, & \text{for } \nu_{M,\oplus} > \nu_\oplus > \max\{\nu_{c,\oplus},\, \nu_{m,\oplus}\}, \\ \nu_\oplus^{-(p-1)/2}, & \text{for } \nu_{c,\oplus} > \nu_\oplus > \nu_{m,\oplus}, \\ \nu_\oplus^{-1/2}, & \text{for } \nu_{m,\oplus} > \nu_\oplus > \nu_{c,\oplus}, \\ \nu_\oplus^{1/3}, & \text{for } \min\{\nu_{c,\oplus},\, \nu_{m,\oplus}\} > \nu_\oplus. \end{cases} \tag{2.19}$$

This above scaling relations are a summary for both fast cooling and slow cooling. They are separately shown in Fig. 2.1.

The maximal specific flux to the observer is estimated as

$$F_{\nu,\text{syn}-\max} \approx \frac{(1+z)q_e^3 N_{e,\text{tot}}\Gamma B'}{4\pi m_e c^2 D_L^2},$$
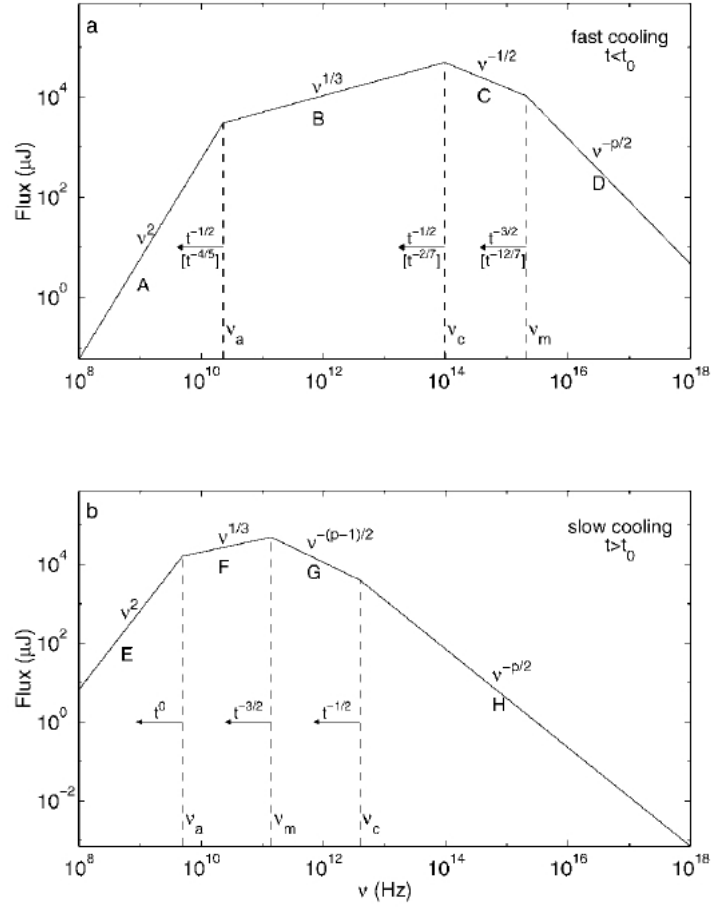
Figure 2.1: The synchrotron spectra in the fast cooling and slow cooling phases (from Sari, Piran, & Narayan 1998).

where $N_{e,\text{tot}}$ is the total number of swept-up electrons and D_L is the luminosity distance of the emitting source. We see the maximal specific flux is independent of the Lorentz factor γ'_e of electrons in the comoving frame because the maximal specific synchrotron radiation power for a single relativistic electron in the comoving frame is largely independent of its Lorentz factor γ'_e.

2.6 Inverse Compton scattering

An electron moving relative to a dense soft photon background will lose some of its energy via inverse Compton scattering (Rybicki & Lightman 1979) and produce an inverse Compton component at higher energies

$$\nu_{\text{ic},\oplus} = \frac{\mathcal{D}\nu'_{\text{ic}}}{1+z} \approx \frac{2\Gamma}{1+z}\frac{\gamma'^2_e \nu'_{\text{se}}}{1+g}, \tag{2.20}$$

where ν'_{se} is the frequency of the seed photon and $g \equiv \gamma'_e h\nu'_{\text{se}}/m_e c^2$.

In the Thompson regime, $g \ll 1$, so

$$\nu'_{\text{ic}} \approx {\gamma'_e}^2 \nu'_{\text{se}}. \tag{2.21}$$

In the Klein-Nishina regime, $g \geq 1$, we have

$$\nu'_{\text{ic}} \approx \gamma'_e m_e c^2 / h. \tag{2.22}$$

In this case, apart from the reduction in energy boost, the cross-section for scattering is also reduced to (Rybicki & Lightman 1979)

$$\sigma(\nu'_{\text{se}}, \gamma'_e) = \frac{3}{4} \sigma_T \{ \frac{(1+g)}{g^3} \left[\frac{2g(1+g)}{(1+2g)} - \ln(1+2g) \right] + \frac{1}{2g} \ln(1+2g) - \frac{(1+3g)}{(1+2g)^2} \}. \tag{2.23}$$

For convince, we define $A(g) \equiv \sigma(\nu'_{\text{se}}, \gamma'_e) / \sigma_{\text{T}}$.

The effect of inverse Compton scattering depends on the parameter

$$Y_{\text{ic}} \equiv P'_{\text{ic}} / P'_{\text{syn}}, \tag{2.24}$$

where P'_{ic} is the power of the inverse Compton radiation, which can be estimated as $P'_{\text{ic}} \approx A(g) \sigma_{\text{T}} c ({\gamma'_e}^2 - 1) U'_\gamma / (1+g)$, where U'_γ is the energy density of the seed photons. We then have

$$Y_{\text{ic}} \approx \frac{A(g)}{1+g} \frac{U'_\gamma}{U'_{\text{B}}} \approx \frac{U'_\gamma}{U'_{\text{B}}} \begin{cases} 1, & \text{for } g \ll 1, \\ \frac{1}{g^2}, & \text{for } g \gg 1. \end{cases} \tag{2.25}$$

If $Y_{\text{ic}} < 1$, the inverse Compton effect is unimportant and can be ignored. On the other hand if $Y_{\text{ic}} > 1$ IC is important. Note that second order IC could be even more important and so for even higher orders. This divergence will be stopped by the Klien-Nishina cutoff.

In general, the IC power in the comoving frame is give by

$$P'_{\text{ic}}(\gamma'_e) = \int_0^\infty h\nu'_{\text{ic}} \frac{dN'_\gamma}{dt' d\nu'_{\text{ic}}} d\nu'_{\text{ic}}. \tag{2.26}$$

The quantity $dN'_\gamma / dt' d\nu'_{\text{ic}}$ is the scattered photon spectrum per electron (Blumenthal & Gould 1970). Supposing the seed photons are isotropic in the rest frame of the IC scattering region, we can express $dN'_\gamma / dt' d\nu'_{\text{ic}}$ as

$$\frac{dN'_\gamma}{dt' d\nu'_{\text{ic}}} = \frac{3\sigma_T c}{4{\gamma'_e}^2} \frac{n'_{\nu'_{\text{se}}} d\nu'_{\text{se}}}{\nu'_{\text{se}}} [2q \ln q + (1+2q)(1-q) + \frac{1}{2} \frac{(4gq)^2}{1+4gq}(1-q)], \tag{2.27}$$

where $f \equiv h\nu'_{\text{ic}} / (\gamma'_e m_e c^2)$ satisfying $h\nu'_{\text{se}} / (\gamma'_e m_e c^2) \leq f \leq 4g/(1+4g)$, $q \equiv f/[4g(1-f)]$, and $n'_{\nu'_{\text{se}}}$

is the frequency distribution of the seed photons in unit volume (Blumenthal & Gould 1970).

The cooling of electrons caused by synchrotron and IC radiation and adiabatic cooling is described by

$$\frac{d\gamma'_e}{dR} = -\frac{4\sigma_{\rm T}}{3m_{\rm e}c^2}\frac{U'_B}{\beta_\Gamma\Gamma}[1 + Y_{\rm ic}]\gamma'^2_e - \frac{\gamma'_e}{R}, \tag{2.28}$$

where $dR \approx \Gamma\beta cdt'$. Thus the corresponding cooling Lorentz factor is given by

$$\gamma'_c = \frac{6\pi\Gamma m_{\rm e}c^2}{(1 + Y_{\rm ic})\sigma_{\rm T} RB'^2}. \tag{2.29}$$

Considering the spherical curvature of the emitting region, the observed IC emission flux is

$$F_{\nu_{\rm ic,\oplus}} = \frac{(1 + z)}{16\pi^2 D_L^2} \int \mathcal{D}^3 h\nu'_{\rm ic}\frac{dN'_\gamma}{dt'd\nu'_{\rm ic}}N_{\gamma'_e}d\gamma'_e d\Omega \tag{2.30}$$

where Ω is the solid angle of the emitting region.

For electrons having a power-law energy distribution $N_{\gamma'_e} \propto \gamma'^{-p}_e$, the IC spectrum is only weakly dependent on $n'_{\nu'_{\rm se}}$ and can be approximated as

$$F_{\nu_{\rm ic}} \propto \begin{cases} \nu_{\rm ic}^{-(p-1)/2}, & \text{for } g \ll 1, \\ \nu_{\rm ic}^{-p}, & \text{for } g \gg 1. \end{cases} \tag{2.31}$$

See Blumenthal & Gould (1970) for more details on the IC spectra.

2.7 GRB afterglow dynamics

The durations of GRB prompt emission are usually a few to tens seconds while the timescale of their observable afterglows is as long as a few months or even a few years, therefore the relativistic shock leading to the afterglow can be regarded as an instantaneous injection from the central engine. The blast wave undergoes short-duration interaction of the forward and revers shocks, and then the forward shock enters its self-similar phase. This self-similar phase means two aspects: firstly, the shock front moves outwards in a power-law with respect to its radius and time; secondly, the distribution of the post-shock fluid remains unchanged with respect to the shock front.

Suppose the radial particle density profile of the circumburst medium takes the form $n(R) \propto R^{-k}$, then $k = 0$ if the medium is interstellar medium-like (ISM-like) while $k = 2$ if the medium stellar wind-like (WIND-like). As pointed in Blandford & McKee (1976) (BM hereafter if needed), the shock's total energy is given by

$$E = \frac{8\pi}{17 - 4k}n(R)R^3\Gamma^2 m_p c^2. \tag{2.32}$$

Normally, the post-shock fluid is assumed to be a uniform and thin shell.

Again due to the propagation effect mentioned at the beginning of this chapter, we have

$$R = \frac{\beta_{sh}}{1 - \beta_{sh}} \frac{ct_\oplus}{1 + z} \approx 2\Gamma_{sh}^2 \frac{ct_\oplus}{1 + z} = 4\Gamma^2 \frac{ct_\oplus}{1 + z} \qquad (2.33)$$

where Γ_{sh} and Γ are Lorentz factors for the shock front and the post-shock fluid, relative to the observer respectively, $1 + z$ is due to the cosmological time dilation.

Normally, the shock can be regarded as expanding adiabatically. The full radiative scenario is not realistic because it requires $\varepsilon_e \approx 1$ and all the electrons are in the fast cooling phase.

2.7.1   The ISM Case

In this case, $k = 0$ is applied to equation 2.32. Then combing equation 2.32 and equation 2.33, we have

$$R = \left[\frac{17Et_\oplus}{4\pi n m_p c(1 + z)} \right]^{1/4} = 5.8 \times 10^{17} \left(\frac{1 + z}{2} \right)^{-1/4} E_{53}^{1/4} n_0^{-1/4} t_{day,\oplus}^{1/4} \text{ cm}$$

and

$$\Gamma = \left[\frac{17E(1 + z)^3}{1024\pi n m_p c^5 t_\oplus^3} \right]^{1/8} = 10.6 \left(\frac{1 + z}{2} \right)^{3/8} E_{53}^{1/8} n_0^{-1/8} t_{day,\oplus}^{-3/8}.$$

Now we combine the above two dynamical equations with the spectral equations in the Section of Synchrotron radiation, then the characteristic frequencies in the synchrotron radiation and the maximal specific flux will be written as

$$\nu_{c,\oplus} = 8.6 \times 10^{12} \left(\frac{1 + z}{2} \right)^{-1/2} \varepsilon_{B,-1}^{-3/2} E_{53}^{-1/2} n_0^{-1} t_{day,\oplus}^{-1/2} \text{ Hz},$$

$$\nu_{m,\oplus} = 1.1 \times 10^{14} x_p \left(\frac{1 + z}{2} \right)^{1/2} \varepsilon_{B,-1}^{1/2} \bar{\varepsilon}_{e,-1}^2 E_{53}^{1/2} t_{day,\oplus}^{-3/2} \text{ Hz},$$

and

$$F_{\nu,\max,\oplus} = 4.3 \times 10^5 \varphi_p \left(\frac{1 + z}{2} \right) \varepsilon_{B,-1}^{1/2} E_{53} n_0^{1/2} D_{L,28}^{-2} \text{ } \mu\text{Jy}$$

where $\bar{\varepsilon} = \varepsilon_e(p - 2)/(p - 1)$, $x_p \approx 0.3$, and φ_p is a coefficient related to the energy index p of electrons (Wijers & Galama 1999).

As can be seen, in this case $\nu_{m,\oplus} \propto t_\oplus^{-3/2}$, $\nu_{c,\oplus} \propto t_\oplus^{-1/2}$, and $F_{\nu,\max,\oplus} \propto t_\oplus^0$. The electrons will change from fast cooling into slow cooling at

$$t_{cm,\oplus} = 12.8 x_p \left(\frac{1 + z}{2} \right) \varepsilon_{B,-1}^2 \bar{\varepsilon}_{e,-1}^2 E_{53} n_0 \text{ day}$$
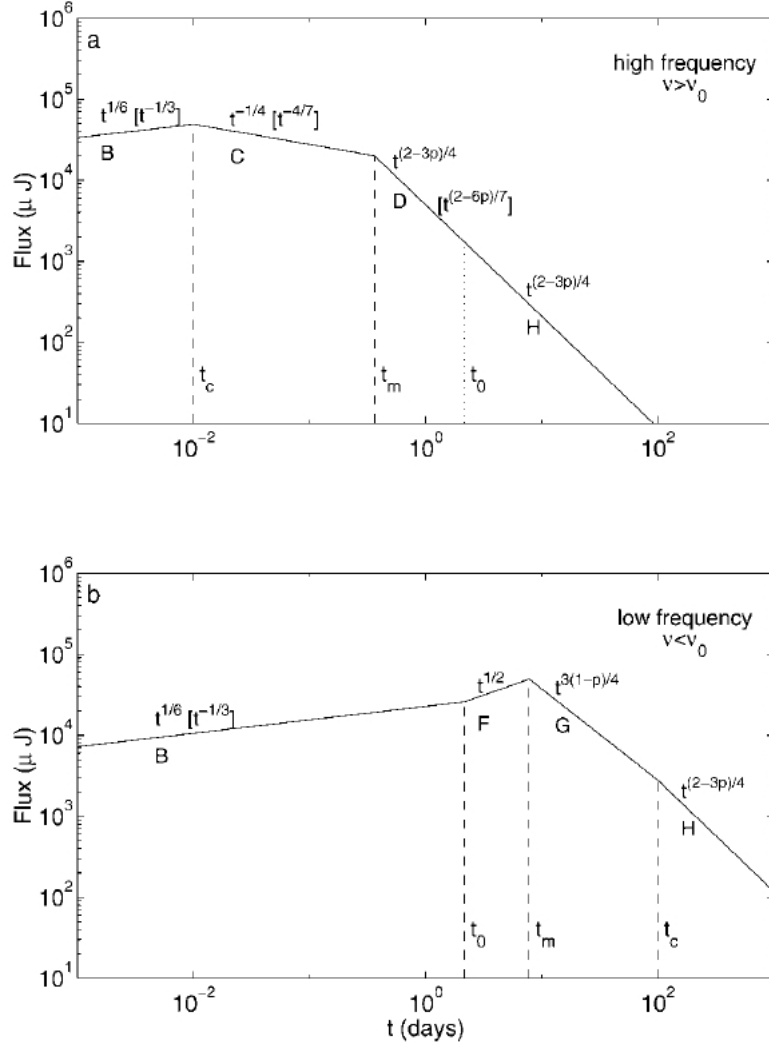
Figure 2.2: Synchrotron light curve (ignoring self-absorption). (a) High-frequency case ($\nu_\oplus > \nu_{cm,\oplus}$). The four segments that are separated by the critical times, t_c , t_m , and t_0 , correspond to the spectral segments in Fig. 2.1 with the same labels (B, C, D, and H). The observed flux varies with time as indicated; the scalings without square brackets are for adiabatic evolution discussed in this chapter. (b) Low-frequency case ($\nu_\oplus < \nu_{cm,\oplus}$). From Sari, Piran, & Narayan (1998).

with

$$\nu_{cm,\oplus} = 2.4 \times 10^{12} x_p^{-1/2} \left(\frac{1+z}{2}\right)^{-1} \varepsilon_{B,-1}^{-5/2} \bar{\varepsilon}_{e,-1}^{-1} E_{53}^{-1} n_0^{-3/2} \text{ Hz.}$$

Depending on whether the observational frequency is higher or lower than $\nu_{cm,\oplus}$, the afterglow lightcurves in the higher frequency phase and in the lower frequency phase are shown in the top and bottom panels of Fig. 2.2, respectively.

2.7.2　The WIND Case

In this case, $k = 2$ is applied to equation 2.32. Then combing equation 2.32 and equation 2.33, we have

$$R = 3.5 \times 10^{17} \left(\frac{1+z}{2} \right)^{-1/2} E_{53}^{1/2} A_*^{-1/2} t_{day,\oplus}^{1/2} \text{ cm}$$

and

$$\Gamma = 10.5 \left(\frac{1+z}{2} \right)^{1/4} E_{53}^{1/4} A_*^{-1/4} t_{day,\oplus}^{1/4}.$$

As in the ISM case, combining the above two dynamical equations with the spectral equations in the Section of Synchrotron radiation would give rise to the temporal evolutions for the characteristic frequencies in the synchrotron radiation and the maximal specific flux as

$$\nu_{c,\oplus} = 2.8 \times 10^{12} \left(\frac{1+z}{2} \right)^{-2/3} \varepsilon_{B,-1}^{-3/2} E_{53}^{1/2} A_*^{-2} t_{day,\oplus}^{1/2} \text{ Hz},$$

$$\nu_{m,\oplus} = 2.1 \times 10^{14} x_p \left(\frac{1+z}{2} \right)^{1/2} \varepsilon_{B,-1}^{1/2} \bar{\varepsilon}_{e,-1}^2 E_{53}^{1/2} t_{day,\oplus}^{-3/2} \text{ Hz},$$

and

$$F_{\nu,\max,\oplus} = 1.2 \times 10^5 \varphi_p \left(\frac{1+z}{2} \right)^{3/2} \varepsilon_{B,-1}^{1/2} E_{53}^{1/2} A_* D_{L,28}^{-2} t_{day,\oplus}^{-1/2} \mu \text{ Jy}.$$

As can be seen, in this case $\nu_{m,\oplus} \propto t_\oplus^{-3/2}$, $\nu_{c,\oplus} \propto t_\oplus^{1/2}$, and $F_{\nu,\max,\oplus} \propto t_\oplus^{-1/2}$. The electrons will change from fast cooling into slow cooling at

$$t_{cm,\oplus} = 7.8 x_p^{1/2} \left(\frac{1+z}{2} \right) \varepsilon_{B,-1} \bar{\varepsilon}_{e,-1} A_* \text{ day}$$

with

$$\nu_{cm,\oplus} = 8.2 \times 10^{12} x_p^{1/4} \left(\frac{1+z}{2} \right)^{-1} \varepsilon_{B,-1}^{-1} \bar{\varepsilon}_{e,-1}^{1/2} E_{53}^{1/2} A_*^{-3/2} \text{ Hz}.$$

Because the density of the circumburst medium corresponding to the very early afterglow is very high in the WIND case, the synchrotron-self absorption (SSA) becomes significant, especially for the low frequency. In the fast cooling phase, the SSA frequency is given by

$$\nu_{a,\oplus} \approx \begin{cases} 1.3 \times 10^{10} \left(\frac{1+z}{2} \right)^{3/5} \varepsilon_{B,-1}^{6/5} E_{53}^{2/5} A_*^{11/5} t_{day,\oplus}^{-8/5} \text{ Hz} & \nu_{a,\oplus} < \nu_{c,\oplus} \\ 2.1 \times 10^{11} \left(\frac{1+z}{2} \right)^{-1/3} A_*^{1/3} t_{day,\oplus}^{-2/3} \text{ Hz} & \nu_{c,\oplus} < \nu_{a,\oplus} < \nu_{m,\oplus} \end{cases}$$

In the slow cooling phase, the SSA frequency is written as

$$\nu_{a,\oplus} \approx 2.2 \times 10^{10} \left(\frac{1+z}{2} \right)^{-2/5} \varepsilon_{B,-1}^{1/5} \bar{\varepsilon}_{e,-1}^{-1} E_{53}^{2/5} A_*^{6/5} t_{day,\oplus}^{-3/5} \text{ Hz}$$

where $\nu_{a,\oplus} < \nu_{m,\oplus} < \nu_{c,\oplus}$ holds (Chevalier & Li 2000).
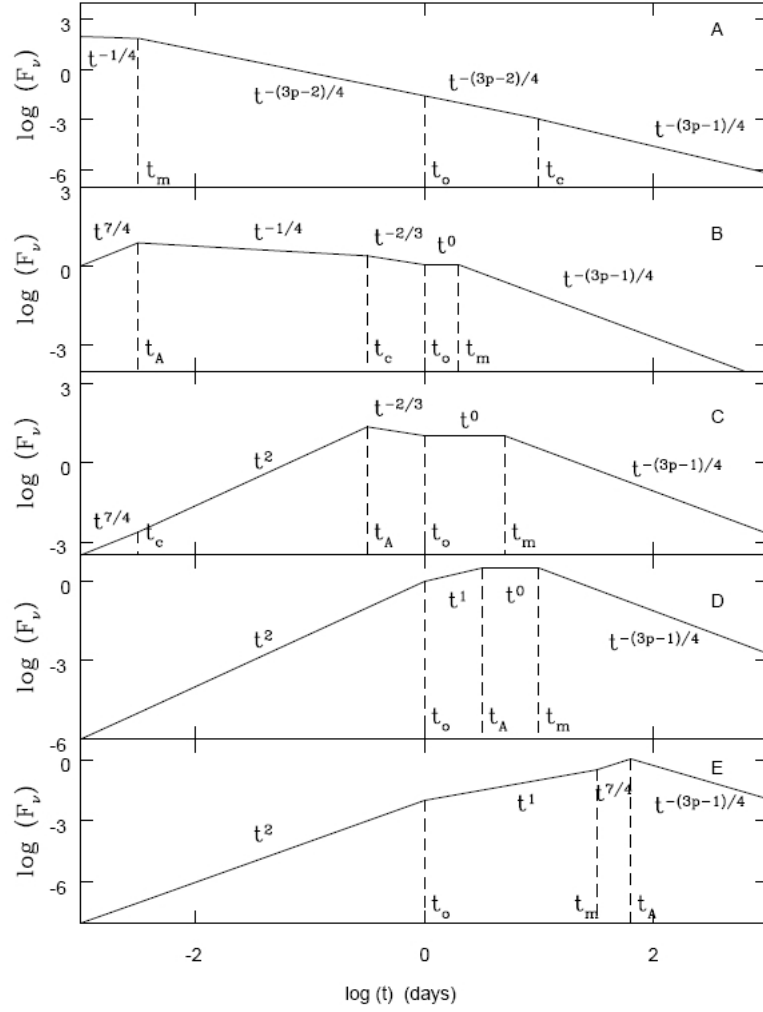
Figure 2.3: Characteristic light curves for wind interaction models in various frequency ranges. The light curves are sorted from (a) high frequency (type A) to (e) low frequency (type E). X-ray and optical light curves are typically of type A and radio of type D. From Chevalier & Li (2000).

Comparing the values between $\nu_{a,\oplus}$, $\nu_{m,\oplus}$, and $\nu_{c,\oplus}$, the afterglow lightcurves are shown in the four panels of Fig. 2.3, respectively.

2.8 Closure relations for GRB afterglows

According to the derivations in the ISM and WIND cases, we now can clearly see that for any specific flux $F(\nu_\oplus, t_\oplus)$ at the frequency $\nu_\oplus$ at the time $t_\oplus$, it always can written as

$$F(\nu_\oplus, t_\oplus) = K(E, \epsilon_e, \epsilon_B, p, n, A_*)\, t_\oplus^\alpha\, \nu_\oplus^\beta \tag{2.34}$$

where E, ϵ_e, ϵ_B, p, n, and A_* are six constant input parameters for a given GRB afterglow. Therefore, the specific flux form can be simplified as

$$F(\nu_\oplus, t_\oplus) \propto t_\oplus^\alpha \, \nu_\oplus^\beta \qquad\qquad (2.35)$$

where α and β are connected by the parameter p. This is the so-called *closure relation* for GRB afterglows.

Table 2.1 lists the detailed relation in various of cases. From this table, it's easy to get some direct information. For instance, the afterglow optical decay ($\alpha_O \sim -1.5$ for $p \sim 2.3$) would be faster than the X-ray decay ($\alpha_X \sim -1.2$ for the same $p \sim 2.3$) in the slow cooling phase of the WIND case. This is just our argument in chapter 5 to infer the origin of SN-less nearby long GRBs.

Table 2.1. Temporal index α and spectral index β in various afterglow models, the convention $F(\nu, t) \propto t^\alpha \nu^\beta$ is adopted. The assumption $\nu_a < \min(\nu_m, \nu_c)$ is made. (Under certain conditions, e.g. for the WIND fast cooling case in some limited regime, the higher ν_a case is relevant, so that the values collected here are no longer valid). The jet model applies for the sideways expanding phase, which is valid for both ISM and wind cases and is usually in the slow cooling regime. From Zhang & Mészáros (2004).

	β	α ($p > 2$, $p \sim 2.3$)	$\alpha(\beta)$
ISM, slow cooling			
$\nu < \nu_a$	2	$\frac{1}{2}$	
$\nu_a < \nu < \nu_m$	$\frac{1}{3}$	$\frac{1}{2}$	$\alpha = \frac{3\beta}{2}$
$\nu_m < \nu < \nu_c$	$-\frac{p-1}{2}$	$\frac{3(1-p)}{4} \sim -1.0$	$\alpha = \frac{3\beta}{2}$
$\nu > \nu_c$	$-\frac{p}{2}$	$\frac{2-3p}{4} \sim -1.2$	$\alpha = \frac{3\beta+1}{2}$
ISM, fast cooling			
$\nu < \nu_a$	2	1	
$\nu_a < \nu < \nu_c$	$\frac{1}{3}$	$\frac{1}{6}$	$\alpha = \frac{\beta}{2}$
$\nu_c < \nu < \nu_m$	$-\frac{1}{2}$	$-\frac{1}{4}$	$\alpha = \frac{\beta}{2}$
$\nu > \nu_m$	$-\frac{p}{2}$	$\frac{2-3p}{4} \sim -1.2$	$\alpha = \frac{3\beta+1}{2}$
Wind, slow cooling			
$\nu < \nu_a$	2	1	
$\nu_a < \nu < \nu_m$	$\frac{1}{3}$	0	$\alpha = \frac{3\beta-1}{2}$
$\nu_m < \nu < \nu_c$	$-\frac{p-1}{2}$	$\frac{1-3p}{4} \sim -1.5$	$\alpha = \frac{3\beta-1}{2}$
$\nu > \nu_c$	$-\frac{p}{2}$	$\frac{2-3p}{4} \sim -1.2$	$\alpha = \frac{3\beta+1}{2}$
Wind, fast cooling			
$\nu < \nu_a$	2	2	
$\nu_a < \nu < \nu_c$	$\frac{1}{3}$	$-\frac{2}{3}$	$\alpha = -\frac{\beta+1}{2}$
$\nu_c < \nu < \nu_m$	$-\frac{1}{2}$	$-\frac{1}{4}$	$\alpha = -\frac{\beta+1}{2}$
$\nu > \nu_m$	$-\frac{p}{2}$	$\frac{2-3p}{4} \sim -1.2$	$\alpha = \frac{3\beta+1}{2}$
Jet, slow cooling			
$\nu < \nu_a$	2	0	
$\nu_a < \nu < \nu_m$	$\frac{1}{3}$	$-\frac{1}{3}$	$\alpha = 2\beta - 1$
$\nu_m < \nu < \nu_c$	$-\frac{p-1}{2}$	$-p \sim -2.3$	$\alpha = 2\beta - 1$
$\nu > \nu_c$	$-\frac{p}{2}$	$-p \sim -2.3$	$\alpha = 2\beta$

Table 2.1 (cont'd)

β	α ($p > 2$, $p \sim 2.3$)	$\alpha(\beta)$

2.9   The forward-reverse shocks in early the afterglow

As stated in Section 1.7, the afterglow's BM self-similar evolution starts after the reverse shock crosses the GRB ejecta to its termination, because before the reverse terminates both the forward and the reverse shocks are not adiabatic whereas BM requires an adiabatic blast shock. So we now turn to the forward-reverse shocks in the very early GRB afterglow.

Because the forward-reverse shocks invokes four regions, for convenience we may not strictly follow the previous superscript and subscript rules upon quantities in different frames. But we shall clearly explain in which frame the quantity of interest is measured, in case of confusion.

2.9.1   Hydrodynamics

Let's consider a uniform and cold relativistic coasting shell with isotropic kinetic energy E_0, Lorentz factor $\gamma_4 = \eta + 1 \gg 1$, and width in observer's frame Δ_0, ejected from the progenitor of the GRB. This shell sweeps up a free wind environment with number density $n_1 = Ar^{-2}$, where η is the initial ratio of E_0 to the rest mass of the ejecta (Piran, Shemi & Narayan 1993). The interaction between the shell and the wind develops a forward shock propagating into the wind and a reverse shock propagating into the shell. As shown in Fig. 2.4, the two shocks separate the system into four regions: (1) the unshocked approximately stationary wind (called region 1 hereafter), (2) the shocked wind (region 2), (3) the shocked shell material (region 3), and (4) the unshocked shell material (region 4). By using the shock jump conditions and assuming the equality of pressures and velocities beside the surface of the contact discontinuity, the values of the Lorentz factor γ, the pressure p, and the number density n in the shocked regions can be estimated as functions of n_1, n_4, and η, where $n_4 = E_0/(\eta 4\pi r^2 \gamma_4 \Delta_0 m_p c^2)$ is the comoving number density of region 4.

Analytical results can be obtained in both relativistic and Newtonian reverse shock limit. These two cases are divided by comparison between f and γ_4^2, where $f \equiv n_4/n_1$ is the ratio of the number densities between the unshocked shell and the unshocked wind (Sari & Piran 1995). As shown by Wu et al. (2003) for the wind environment case, $f = l/(\eta^2 \Delta_0)$, where $l = E_0/(4\pi A m_p c^2)$ is the Sedov length. If $f \gg \gamma_4^2$, the reverse shock is Newtonian (NRS), and if $f \ll \gamma_4^2$, the reverse shock is relativistic (RRS).

As discussed by Kobayashi & Sari (2000), even for NRS, the adiabatic index of the post-shocked
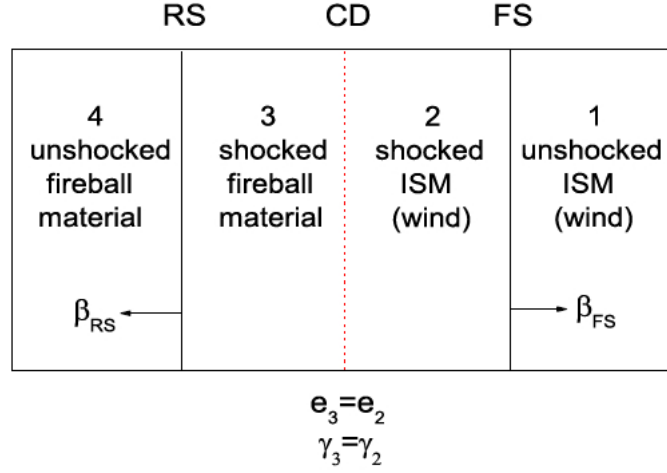
Figure 2.4: The forward and reverse shocks are generated due to the interaction of the fireball with the circum-burst surrounding medium. The forward shock sweeps up the outer medium while the reverse shock crosses the GRB ejecta. They are divided by the contact discontinuity surface.

fluid can be taken as a constant $\hat{\gamma} = 4/3$, because the electrons are still relativistic. Then the shock jump conditions can read

$$e_2/n_2 m_p c^2 = \gamma_2 - 1, n_2/n_1 = 4\gamma_2 + 3, \tag{2.36}$$

$$e_3/n_3 m_p c^2 = \bar{\gamma}_3 - 1, n_3/n_4 = 4\bar{\gamma}_3 + 3, \tag{2.37}$$

where m_p is the proton mass, e_2 and e_3 are the comoving energy densities of region 2 and region 3 respectively, and n_2 and n_3 are the corresponding comoving number densities of particles, which are assumed to consist of protons and electrons. The relative Lorentz factor between region 3 and region 4 is

$$\bar{\gamma}_3 = \gamma_3 \gamma_4 (1 - \sqrt{1 - 1/\gamma_3^2}\sqrt{1 - 1/\gamma_4^2}). \tag{2.38}$$

Assuming $\gamma_2 = \gamma_3$, and $\gamma_2, \gamma_4 \gg 1$, $\bar{\gamma}_3$ can be expressed as $\bar{\gamma}_3 \simeq (\gamma_4/\gamma_2 + \gamma_2/\gamma_4)/2$. The asymptotic solution is $\gamma_3 \simeq \frac{1}{\sqrt{2}}\gamma_4^{1/2} f^{1/4}$, $\bar{\gamma}_3 \simeq \frac{1}{\sqrt{2}}\gamma_4^{1/2} f^{-1/4}$ for RRS, while $\gamma_3 \simeq \gamma_4$ and $\bar{\gamma}_3 - 1 \simeq \frac{4}{7}\gamma_4^2 f^{-1}$ for NRS.

The time it takes the reverse shock to cross the shell in the burster's frame is given by (Sari & Piran 1995)

$$t_\Delta = \frac{\Delta_0}{c(\beta_4 - \beta_3)}\left(1 - \frac{\gamma_4 n_4}{\gamma_3 n_3}\right). \tag{2.39}$$

There are two simple limits involved in the problem: NRS and RRS, in which we can get analytical results. The relative Lorentz factor $\bar{\gamma}_3$ is constant in the whole reverse-shock period for RRS. t_Δ can be derived as $t_\Delta = \alpha\Delta_0\gamma_4 f^{1/2}/c$, and the corresponding radius of the shell at time t_Δ is $r_\Delta \simeq ct_\Delta = \alpha\Delta_0\gamma_4 f^{1/2} \simeq \alpha\sqrt{l\Delta_0}$, where the coefficient $\alpha = 1/2$ for RRS and $\alpha = 3/\sqrt{14}$ for

NRS. We will discuss both cases separately in the following.

2.9.2 Relativistic reverse shock case

In the RRS case, $f \ll \gamma_4^2$ (i.e., $\eta \gg 114 E_{53}^{1/4} \Delta_{0,12}^{-1/4} A_{*,-1}^{-1/4}$), using the relation between the observer's time and the radius $t_\oplus \simeq (1+z)r/2\gamma_3^2 c$, where z is the redshift of the GRB, we obtain $T \simeq (1+z)\Delta_0/2c \simeq 16.7(1+z)\Delta_{0,12}$s as the RRS-crossing time in the observer's frame. Using $e_2 = e_3$, $\gamma_2 = \gamma_3$, together with the above equations, we get the scaling-laws of the hydrodynamic variables for time $t_\oplus < T$,

$$\bar{\gamma}_3 \simeq 1.9\eta_{2.5} E_{53}^{-1/4} \Delta_{0,12}^{1/4} A_{*,-1}^{1/4} \tag{2.40}$$

$$\gamma_3 = \gamma_2 \simeq 81.5 E_{53}^{1/4} \Delta_{0,12}^{-1/4} A_{*,-1}^{-1/4} \tag{2.41}$$

$$e_3 = e_2 \simeq 1.4 \times 10^4 E_{53}^{-1/2} \Delta_{0,12}^{-3/2} A_{*,-1}^{3/2} \left(\frac{t_\oplus}{T}\right)^{-2} \text{ erg cm}^{-3} \tag{2.42}$$

$$N_{e,3} \simeq 2.1 \times 10^{53} E_{53} \eta_{2.5}^{-1} \frac{t_\oplus}{T} \tag{2.43}$$

$$N_{e,2} \simeq 3.5 \times 10^{51} E_{53}^{1/2} \Delta_{0,12}^{1/2} A_{*,-1}^{1/2} \frac{t_\oplus}{T} \tag{2.44}$$

where $A_* = 3 \times 10^{35}$ cm^{-1}, and $N_{e,i}$ is the number of electrons in the shocked region i. Note that γ_3 and $\bar{\gamma}_3$ do not depend on time. This is the property of wind environments, since the densities of the shell and the ambient environment have the same power-law relation with radius, i.e., $n(R) \propto R^{-2}$.

After the reverse shock crosses the shell ($t_\oplus > T$), the shocked shell can be roughly described by the BM solution (Wu et al. 2003; Kobayashi & Zhang 2003; Kobayashi et al. 2004),

$$\gamma_3 \propto t_\oplus^{-3/8}, n_3 \propto t_\oplus^{-9/8}, e_3 \propto t_\oplus^{-3/2}, R \propto t_\oplus^{1/4}, N_{e,3} \propto t_\oplus^0, \tag{2.45}$$

$$\gamma_2 \propto t_\oplus^{-1/4}, n_2 \propto t_\oplus^{-5/4}, e_2 \propto t_\oplus^{-3/2}, R \propto t_\oplus^{1/2}, N_{e,2} \propto t_\oplus^{1/2}. \tag{2.46}$$

These variables can be scaled to the initial values ($t_\oplus = T$), which are given by the expressions for the time $t_\oplus < T$.

2.9.3 Newtonian reverse shock case

In the NRS case, $f \gg \gamma_4^2$, the time for the reverse shock crossing the shell is $T' \simeq t_\eta \simeq 2.9 \times 10^3(1+z)E_{53}\eta_{1.5}^{-4}A_{*,-1}^{-1}$s in the observer's frame, if we consider the spreading of the cold shell

(Piran et al. 1993). The evolution of the hydrodynamic variables before the time T' are

$$\bar{\gamma}_3 - 1 \simeq 0.57\frac{t_\oplus}{T'} \tag{2.47}$$

$$\gamma_3 = \gamma_2 \simeq \gamma_4 \tag{2.48}$$

$$e_3 = e_2 \simeq 5.8E_{53}^{-2}\eta_{1.5}^6 A_{*,-1}^3 \left(\frac{t_\oplus}{T'}\right)^{-2} \text{ erg cm}^{-3} \tag{2.49}$$

$$N_{e,3} = 2.1 \times 10^{54} E_{53}\eta_{1.5}^{-1} \left(\frac{t_\oplus}{T'}\right)^{1/2} \tag{2.50}$$

$$N_{e,2} \simeq 6.6 \times 10^{52} E_{53}\eta_{1.5}^{-2}\frac{t_\oplus}{T'} \tag{2.51}$$

What should be noted is that the values for NRS are not suitable for mildly relativistic reverse shock case. Nakar & Piran (2004) showed the difference between the approximated analytical solution and the numerical results in the case of uniform environments. And for the spreading of the shell, f decreases with radius. At the crossing time, $\bar{\gamma}_3 \simeq 1.57$ (see equation (2.47)), which deviates from the Newtonian reverse shock approximation. More accurate values should be calculated numerically.

After the NRS crosses the shell, the Lorentz factor of the shocked shell can be assumed to be a general power-law relation $\gamma_3 \propto r^{-g}$ (Mészarós & Rees 1999; Kabayashi & Sari 2000). However, the forward shock is still relativistic, and can be described by the BM solution. The dynamic behavior is the same as the one in the RRS case. The scaling-law of the two regions are

$$\gamma_3 \propto t_\oplus^{-g/(1+2g)}, n_3 \propto t_\oplus^{-6(3+g)/7(1+2g)},$$
$$e_3 \propto t_\oplus^{-8(3+g)/7(1+2g)}, R \propto t_\oplus^{1/(1+2g)}, N_{e,3} \propto t_\oplus^0, \tag{2.52}$$
$$\gamma_2 \propto t_\oplus^{-1/4}, n_2 \propto t_\oplus^{-5/4},$$
$$e_2 \propto t_\oplus^{-3/2}, R \propto t_\oplus^{1/2}, N_{e,2} \propto t_\oplus^{1/2}. \tag{2.53}$$

2.9.4 Emission in the two cases

The above two subsections have given the dynamical evolution laws for both RRS and BRS. The emission mechanisms for electrons in the two cases are still synchrotron radiation, which has been explained in the first five sections of this chapter. Therefore we don't repeat it here.

Combining the hydrodynamical equations and the synchrotron radiation equations, we obtain the typical frequencies and the peak flux density in the shocked shell and the shocked wind for

the RRS case,

$$\nu_{m,3} \simeq 5.9 \times 10^{15}(1+z)^{-1}\bar{\epsilon}_e^2 \epsilon_{B,-1}^{1/2} E_{53}^{-1/2} \eta_{2.5}^2 A_{*,-1} \Delta_{0,12}^{-1/2} \left(\frac{t_\oplus}{T}\right)^{-1} \text{ Hz}, \qquad (2.54)$$

$$\nu_{m,2} \simeq 1.0 \times 10^{19}(1+z)^{-1}\bar{\epsilon}_e^2 \epsilon_{B,-1}^{1/2} E_{53}^{1/2} \Delta_{0,12}^{-3/2} \left(\frac{t_\oplus}{T}\right)^{-1} \text{ Hz} \qquad (2.55)$$

$$\nu_{c,2} = \nu_{c,3} \simeq 1.5 \times 10^{12}(1+z)^{-1}\epsilon_{B,-1}^{-3/2} E_{53}^{1/2} \Delta_{0,12}^{1/2} A_{*,-1}^{-2} \frac{t_\oplus}{T} \text{ Hz}, \qquad (2.56)$$

$$F_{\nu,\max,3} \simeq 95.3(1+z)\epsilon_{B,-1}^{1/2} E_{53} \eta_{2.5}^{-1} A_{*,-1}^{1/2} \Delta_{0,12}^{-1} D_{28}^{-2} \text{ Jy}, \qquad (2.57)$$

$$F_{\nu,\max,2} \simeq 1.6(1+z)\epsilon_{B,-1}^{1/2} E_{53}^{1/2} A_{*,-1} \Delta_{0,12}^{-1/2} D_{28}^{-2} \text{ Jy} \qquad (2.58)$$

where $\bar{\epsilon}_e \equiv \epsilon_{e,-0.5} \cdot 3(p-2)/(p-1)$. Note that $F_{\nu,\max,3} > F_{\nu,\max,2}$, i.e. region 3 dominates the emission for the early afterglow, mainly because the number of electrons in region 3 is much larger than that in region2.

For the NRS case, before the reverse shock crosses the shell ($t_\oplus < T'$), we have

$$\nu_{m,3} \simeq 4.1 \times 10^{12}(1+z)^{-1}\bar{\epsilon}_e^2 \epsilon_{B,-1}^{1/2} E_{53}^{-1} \eta_{1.5}^4 A_{*,-1}^{3/2} \frac{t_\oplus}{T'} \text{ Hz} \qquad (2.59)$$

$$\nu_{m,2} \simeq 1.3 \times 10^{16}(1+z)^{-1}\bar{\epsilon}_e^2 \epsilon_{B,-1}^{1/2} E_{53}^{-1} \eta_{1.5}^6 A_{*,-1}^{3/2} \left(\frac{t_\oplus}{T'}\right)^{-1} \text{ Hz} \qquad (2.60)$$

$$\nu_{c,3} = \nu_{c,2} \simeq 2.7 \times 10^{13}(1+z)^{-1}\epsilon_{B,-1}^{-3/2} E_{53} \eta_{1.5}^{-2} A_{*,-1}^{-5/2} \frac{t_\oplus}{T'} \text{ Hz} \qquad (2.61)$$

$$F_{\nu,\max,3} \simeq 7.6(1+z)\epsilon_{B,-1}^{1/2} \eta_{1.5}^3 A_{*,-1}^{3/2} D_{28}^{-2} \left(\frac{t_\oplus}{T'}\right)^{-1/2} \text{ Jy} \qquad (2.62)$$

$$F_{\nu,\max,2} \simeq 0.2(1+z)\epsilon_{B,-1}^{1/2} \eta_{1.5}^2 A_{*,-1}^{3/2} D_{28}^{-2} \text{ Jy} \qquad (2.63)$$

After the reverse shock crosses the shell ($t_\oplus > T'$), the temporal indices of the typical frequencies and the observed flux density can be inferred in a way similar to that for the afterglow BM self-similar evolution. But ν_a in the reverse shock could be very high (Wu et al. 2003) so it would bring more possible behaviors of the lightcurve evolution in the reverse shock case than the forward shock case.

Chapter 3

The central-engine driven X-ray afterglow of GRB 060218

3.1 Abstract

The nearby GRB 060218/SN 2006aj was an extremely long, weak and very soft GRB. It was peculiar in many aspects. We show here that the X-ray, ultraviolet/optical and radio afterglow of GRB 060218 have to be attributed to different physical processes arising from different emission regions. From the several components in this burst's afterglow only the radio afterglow can be interpreted in terms of the common external shock model. We infer from the radio that the blast wave's kinetic energy was $\sim 10^{50}$ erg and the circumburst matter had a constant rather than a wind profile. The lack of a "jet break" up to 22 days implies that the outflow was wide $\theta_j > 1$ rad. Even though the late X-ray afterglow decays normally it cannot result from an external shock because of its very steep spectrum. Furthermore, the implied kinetic energy would have produced far too much radio. We suggest that this X-ray afterglow could be attributed to a continued activity of the central engine that within the collapsar scenario could arise from fall-back accretion. "Central engine afterglow" may be common in under-luminous GRBs where the kinetic energy of the blast wave is small and the external shock does not dominate over this component. Such under-luminous GRBs might be very common but they are rarely recorded because they can be detected only from short distances.

3.2 Introduction

GRB 060218 (Cusumano et al. 2006a) was a nearby (z=0.033) burst (Mirabal & Halpern 2006; Cusumano et al. 2006b) associated with a bright type Ic broad-lines SN (Modjaz et al. 2006; Sollerman et al. 2006; Pian et al. 2006; Mirabal et al. 2006; Mazzali et al. 2006). It is distinguished in several aspects from other bursts: (i) It is very long ($T_{90} \sim 2000$ sec). (ii) The prompt $\gamma-$ray and X$-$ray luminosity is extremely low $\sim 10^{47}$ erg s^{-1} (Sakamoto et al. 2006) and the overall isotropic equivalent γ-ray energy, a few $\times 10^{49}$ erg, is small compared to typical bursts. (iii) The prompt emission is very soft and it contains a soft thermal component in the X-ray

band. The thermal emission begins at ~ 152 sec and continues up to ~ 0.1 day. (iv) A second thermal component in the UV/optical band peaks at $t \sim 1$ day after the GRB trigger (Campana et al. 2006). (v) For $t > 0.1$ day, the XRT lightcurve is simple and is well described a single power-law decay $t^{-1.15}$ with no break (Campana et al. 2006). (vi) For $t > 1.8$ day, the "8.46 GHz" radio afterglow lightcurve decays as $t^{-0.85}$ without break (Soderberg et al. 2006a). While the prompt emission is very different from a typical GRB and the optical emission is complicated by the appearance of the thermal bump and the supernova signal this last component, the X-ray and the radio afterglow, seem to be rather typical.

We focus here on the X-ray and the radio afterglow, and use them as keys to understand what has happened in this burst. The X-ray afterglow decays normally and at first[1] one could have interpreted it as arising from a standard external shock. However, the X-ray spectrum is too steep (De Luca 2006; Cusumano et al. 2006b) to be consistent with this interpretation. Furthermore, the radio observations (Soderberg et al. 2006a) are not compatible with the kinetic energy required to produce the X-ray emission by an external shock. We suggest that the X-ray afterglow should be attributed to a "central engine afterglow" resulting from a continued activity of the central engine, as suggested already in 1997 by Katz & Piran (1997). We argue that such afterglow could be common in the under-luminous nearby GRBs (see section 2 for details).

The radio afterglow, on the other hand, can be interpreted in terms of the standard afterglow model. One can infer from it the kinetic energy, $E_k \sim 10^{50}$ erg, as well as the wide opening angle, $\theta_j > 1$ rad, of the relativistic component of the ejecta. The association with a type Ic SN suggests that the progenitor was a WR-star (Campana et al. 2006). One expects, therefore, that the central engine is surrounded by a dense stellar wind, like the one seen in GRB 980425 that was associated with SN 1998bw (Li & Chevalier 1999; Waxman 2004). However, the density nearest to the progenitor depends on the mass loss rate during the latest phases of the WR-star, which is unknown at present (Woosley, Zhang, & Heger 2003). With the radio data, we show that a dense wind profile is not favored (see section 3 for details).

We examine possible sources for the thermal emission in section 4. Our conclusions and the implications for the GRB/SN connection are discussed in section 5.

In this work/chapter we use the notation $F(\nu, t) \propto t^\alpha \nu^\beta$ for the afterglow monochromatic flux as a function of time, where ν represents the observed frequency, α is the temporal index, and β is the energy spectrum index.

---

[1]The first XRT spectral index β_X was quite uncertain. For example, (De Luca 2006) suggested that $\beta_X \sim -2.3 \pm 0.6$, whereas (Cusumano et al. 2006b) give later $\beta_X \sim -2.3 \pm 0.2$ and the radio observations (Soderberg et al. 2006a) were not available for a while.

3.3 The long term X-ray emission from the central engine

The late (> 0.1 day) X-ray afterglow is similar to the one seen in typical GRBs in its overall intensity as well as in the almost standard power law decay index $\alpha_X \sim -1.1$. However, the time averaged XRT spectral index $\beta_X = -2.2 \pm 0.2$ is too steep to be reproduced in an external shock. For $\beta_X = -2.2 \pm 0.2$, the power-law distribution index of the shocked electrons $p = 5.4$ or 4.4, depending on the X-ray band being below or above the cooling frequency ν_c. In the constant density circumburst medium case, the expected temporal index $\alpha = (2-3p)/4 < -2.8$ for $\nu_X > \nu_c$ otherwise $\alpha = 3(1-p)/4 < -2.6$ (Sari, Piran, & Narayan 1998; Piran 1999). In the wind case, the expected temporal index $\alpha = (2-3p)/4 < -2.8$ for $\nu_X > \nu_c$ otherwise $\alpha = (1-3p)/4 < -3$ (Chevalier & Li 2000). All are far from consistent with the observation ~ -1.1.

The steep X-ray spectrum enables us to rule out the possibility that the X-ray emission arises due to inverse Compton. (Sari & Esin 2001) have shown that the inverse Compton spectra is much shallower than -2.2 unless it is in the Klein-Nishina regime. Clearly the observed X-ray cannot be in the Klein-Nishina regime. Therefore we can rule out the possibility that the X-ray afterglow arises due to either synchrotron-self inverse Compton (SSC) or the inverse Compton scattering of the SN optical photons with the external forward shock electrons.

Even if we ignore the very steep spectrum, the external shock model is still inconsistent because the X-ray emission is strong but the radio emission is very weak. Parameters $E_k \sim 10^{51}$erg, $\epsilon_e \sim 0.1$, $\epsilon_B \sim 0.01$ and $n \sim 1$ cm^{-3} are needed to reproduce the late X-ray emission ($t > 0.1$ day). With these parameters the resulting radio emission would have been about 1-2 orders brighter than the observation (Soderberg et al. 2006a).

An attractive alternative possibility for the production of the X-ray afterglow is the a continued activity of the central engine. This idea was first proposed by Katz & Piran (1997) and had been discussed in the context of GRB 970228 by Katz, Piran & Sari (1998). However, the agreement of the predictions of the external shock afterglow model with most subsequent multi-wavelength afterglows observation and in particular the smooth light curves seen in most afterglow lead to the understanding that afterglows are produced by external shocks. The energetic soft X-ray flares observe recently in many afterglows of *Swift* GRBs (O'Brien et al. 2006) lead Fan & Wei (2005) and Zhang et al. (2006) to re-introduce this model and to interpret these flares as arising from a continued activity of the central engine. When proposing the so-called "late internal shock" model, Fan & Wei (2005) speculated that in some GRBs, the X-ray and IR/optical afterglow might be attributed to different physical processes and thus from different regions. However, these X-ray flaring afterglows are quite different from the current long term power-law decaying lightcurve. This X-ray afterglow of GRB 060218 provides us an indication for a power-law decaying afterglow arising from the activity of the central engine. Such indications were also seen earlier in some

pre-Swift GRBs (Björnsson et al. 2002; Björnsson, Gudmundsson, & Johannesson 2004). If the corresponding outflow is from the central engine and there is a significant energy dissipation converting the kinetic energy into the X-ray emission, a power-law decaying X-ray central engine afterglow should be detected.

In the following we call the usual afterglow from external shocks a "fireball afterglow" or "afterglow" and the afterglow attributed to the long lived activity of the GRB central engine a "central engine afterglow". The central engine afterglow, besides those flares detected in *Swift* GRB X-ray afterglows, are expected to be detected in sub-luminous GRBs whose regular afterglows is weak and hence they do not over shine this activity. As such sub-luminous GRBs can be detected only from relatively short distances we will detect only few such bursts even if the total number of such under-luminous bursts is larger than the total number of regular GRBs. Alternatively, the "central engine afterglow" component may emerge if (i) The forward shock parameters ϵ_e and/or ϵ_B taken in eq. (3.4) are much smaller than the value normally used there; (ii) Some or all the free parameters ϵ, f_x and f_b^{-1} taken in eqs. (3.1-3.3) have been underestimated significantly. In this case, a burst with a "central engine afterglow" component may be detectable at high redshift[2].

To estimate the possible flux from a "central engine afterglow" we consider, as an example, the "Type II collapsar" model of (MacFadyen, Woosley, & Heger 2001). Clearly if dM/dt that follows an under-luminous $\gamma-$ray burst is significantly lower than the value taken in Eq.(3.1), the "central engine afterglow" emission should be dimmer or even undetectable (unless other free parameters ϵ, f_X, and/or f_b^{-1} taken below are much larger). As the difference between the progenitors of bright and dim bursts is not clear we assume that this accretion rate, which was originally suggested for bright bursts, is applicable also for sub-luminous ones. Here we take the lowest accretion rate dM/dt presented in Fig. 5 of MacFadyen, Woosley, & Heger (2001):

$$dM/dt \sim 10^{-6} t_{d,-1}^{-5/3} M_\odot \ \mathrm{s}^{-1}, \tag{3.1}$$

where t_d is the observer's time measured in days. Following MacFadyen, Woosley, & Heger (2001), we take an energy conversion coefficient $\epsilon \sim 0.001 - 0.01$ and the beam correction factor $f_b \sim 0.01 - 1$, (note that for this particular burst $f_b \sim 1$) thus the outflow luminosity can be estimated by

$$L \sim \epsilon(dM/dt)c^2/f_b \sim 2 \times 10^{46} \ \mathrm{erg} \ \mathrm{s}^{-1} \epsilon_{-3} f_{b,-1}^{-1} t_{d,-1}^{-5/3}. \tag{3.2}$$

Assuming that the fraction of the outflow converted into soft X-ray emission is $f_x \sim 0.01 - 0.1$

---

[2]A possible candidate is GRB 060210, a burst at $z \sim 4$ (Stanek et al. 2006b). For this burst, the R-band flux is just about 10 times that of the X-ray (at 3.5 keV) and is decaying with time as $t^{-1.3}$ for $t > 500$ s. On the other hand, the XRT spectral index is -1.17 ± 0.04 (X. Y. Dai, 2006, private communication). It is thus quite difficult to interpret these data self-consistently within the standard external shock model. This inconsistency could be resolved if the X-ray emission is a "central engine afterglow" while the optical emission is the normal external shock afterglow.

and for a luminosity distance $D_L \sim 10^{27}$ cm, the XRT flux

$$
\begin{aligned}
F_{\rm x} &\sim f_{\rm x} L/(4\pi D_L^2) \\
&\sim 2 \times 10^{-10} \epsilon_{-3} f_{\rm x,-1} f_{b,-1}^{-1} t_{d,-1}^{-5/3} \\
&\quad D_{L,27}^{-2} \ {\rm erg \ s}^{-1} \ {\rm cm}^{-2}.
\end{aligned}
\tag{3.3}
$$

On the other hand, the forward shock X-ray emission is expected to be (Fan & Piran 2006):

$$
\begin{aligned}
F_{\rm x} &\sim 3 \times 10^{-12} \ {\rm ergs \ s}^{-1} \ {\rm cm}^{-2} \ (1+z)^{(p+2)/4} D_{L,27}^{-2} \\
&\quad \epsilon_{B,-2}^{(p-2)/4} \epsilon_{e,-1}^{p-1} \bar{E}_{k,50}^{(p+2)/4} (1+Y)^{-1} t_{d,-1}^{(2-3p)/4},
\end{aligned}
\tag{3.4}
$$

where $\bar{E}_k$ is the total isotropic equivalent energy of the outflow, ϵ_e and ϵ_B are the fraction of shock energy given to the electrons and to the magnetic filed, respectively. The energy $\bar{E}_k$ must include both the energy of the initial GRB outflow and that of the "central engine afterglow" outflow $= \int (1 - f_{\rm x}) L dt$ that is added later. As we show later, for GRB 060218 this additional energy is a small fraction (less than 10%) of the total energy and its inclusion is insignificant. To get this and the following numerical coefficients, we take $p = 2.3$. $Y = (-1 + \sqrt{1 + 4\eta\eta_{KN}\epsilon_e/\epsilon_B})/2$ is the Compoton parameter, where $\eta = \min\{1, (\nu_m/\nu_c)^{(p-2)/2}\}$ (Sari, Narayan, & Piran 1996; Wei & Lu 1998, 2000), $0 \le \eta_{KN} \le 1$ is a coefficient accounting for the Klein-Nishina effect (Fan & Piran 2006).

Comparing eqs.(3.3) and (3.4) we see, as one could expect, that if the GRB outflow is significantly less energetic ($\bar{E}_k \sim E_k \sim 10^{50}$ erg) than typical GRB ($E_k \sim 10^{53}$ erg), the "central engine afterglow" component dominates. So the central engine afterglow may be common for the sub-luminous GRBs. This prediction could be tested in the coming months or years.

Note that in this particular model the temporal decay ($-5/3$) is too steep as compared with the observations of -1.1. However this temporal decay (Eq.(3.3)) is dictated simply by the accretion rate used in Eq.(3.1) and surely, there is enough freedom to allow for a different slope there.

3.4 The late radio afterglow: constraint on the density profile of the medium

Multi-wavelength radio data have been presented in (Soderberg et al. 2006a). There are 11 detections, 8 of which are at 8.46 GHz, ranging from $1.8 - 22$ days. The good quality 8.46 GHz lightcurve can be well fitted by a single power law $t^{-0.85}$. This decline slope (-0.85) is significantly different from that of GRB 980425 (~ -1.5). The radio emission is very weak and has already been discussed when ruling out the external shock origin for the X-ray afterglow. We examine it

now within the contexts of a constant density and a wind circumburst medium.

3.4.1　A constant density medium

For a constant density medium and for $\nu_m < \nu_a < \nu_{\rm obs} < \nu_c$, $F_{\nu_{\rm obs}} \propto t^{3(1-{\rm p})/4}$ (Sari, Piran, & Narayan 1998; Piran 1999). To reproduce the current 8.46 GHz lightcurve $t^{-0.85}$, we need $p \sim 2.1$. The bulk Lorentz factor of the outflow can be estimated by:

$$\Gamma \approx 3.4 E_{k,51}^{1/8} n_0^{-1/8} t_d^{-3/8} (1+z)^{3/8}. \tag{3.5}$$

The lack of a jet break in the radio afterglow up to 22 days after the burst suggests a very wide jet opening angle $\theta_j > 1$ rad (Rhoads 1999; Sari, Piran & Halpern 1999; Halpern et al. 1999).

In the radio band, the synchrotron self-absorption effect should be taken into account. Through the standard treatment (Rybicki & Lightman 1979), for $\nu_a < \nu_m < \nu_c$, we have

$$\nu_a \approx 1.3 \times 10^{10} \text{ Hz } \epsilon_{B,-2}^{1/5} E_{k,51}^{2/5} \epsilon_{e,-1}^{-1} C_p^{-1} (1+z)^{-1} n_0^{3/5}. \tag{3.6}$$

For $\nu_m < \nu_a < \nu_c$, we have

$$\begin{aligned}
\nu_a \approx\ & 2.6 \times 10^{10} \text{ Hz } \epsilon_{B,-2}^{(p+2)/[2(p+4)]} E_{k,51}^{(p+2)/[2(p+4)]} n_0^{2/(p+4)} \\
& \epsilon_{e,-1}^{2(p-1)/(p+4)} C_p^{2(p-1)/(p+4)} (1+z)^{(p-6)/[2(p+4)]} \\
& t_d^{-(2+3p)/[2(p+4)]}.
\end{aligned} \tag{3.7}$$

With the available radio data, we have three constraints on the physical parameters of the afterglows. One is the self-absorption frequency $\nu_a \sim 4 \times 10^9$ Hz $> \nu_m$ at $t_d \sim 5$. The other is the 22.5 GHz flux $F(22.5\text{GHz}) \sim 0.25$ mJy at $t_d \sim 3$. Another is the cooling frequency $\nu_c \leq 5 \times 10^{15}$ Hz, which has not been presented in Soderberg et al. (2006a) but one can deduce this from their Fig. 2, provided that the synchrotron spectrum of the external shock electrons is not dominated in the XRT band. We thus have the following relations:

$$\begin{aligned}
& \epsilon_{B,-2}^{(p+2)/[2(p+4)]} E_{k,51}^{(p+2)/[2(p+4)]} n_0^{2/(p+4)} \\
& \epsilon_{e,-1}^{2(p-1)/(p+4)} C_p^{2(p-1)/(p+4)} \sim 0.44,
\end{aligned} \tag{3.8}$$

$$\epsilon_{e,-1}^{{\rm p}-1} \epsilon_{B,-2}^{({\rm p}+1)/4} C_p^{{\rm p}-1} E_{k,51}^{({\rm p}+3)/4} n_0^{1/2} \sim 3.2 \times 10^{-3}, \tag{3.9}$$

$$E_{k,51}^{-1/2} \epsilon_{B,-2}^{-3/2} n_0^{-1} \leq 0.43. \tag{3.10}$$

These relations are satisfied with $(E_k,\ \epsilon_e,\ \epsilon_B,\ n) \sim (10^{50}$ erg, 0.01, 0.001, 100 cm$^{-3})$. A similar estimate of ϵ_e has also been suggested by (Dai, Zhang, & Liang 2006) and it is within the range
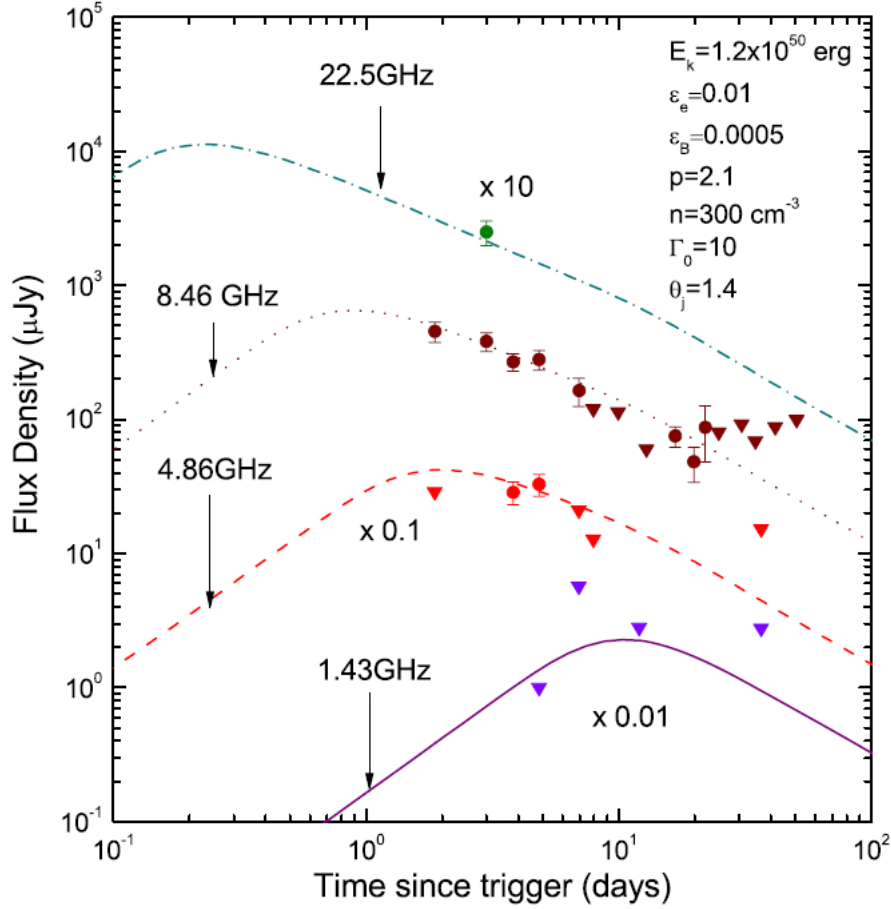
Figure 3.1: A fit to the observed radio afterglow lightcurves of GRB 060218 for a constant density circumburst medium. The inverted triangles are upper limits(3σ). Different colors are for different bands. From Fan, Piran & Xu (2006).

seen in detailed afterglow modelling of other bursts (Panaitescu 2005).

Fig. 3.1 depicts our numerical fit to the radio data. The code is the same as that used in Fan & Piran (2006b). One novel effect taken into account is the synchrotron self-absorption, following the standard treatment (Rybicki & Lightman 1979). The external inverse Compton cooling, caused by the long term X-ray emission from the central engine, has been calculated. However, this cooling effect changes the current radio emission only slightly because the inverse Compton parameter $Y_{\mathrm{EIC}} \sim 2L_{\mathrm{ph},41.5}\epsilon_{B,-3}^{-1}E_{k,50}^{-1}t_{d,1}$ (Fan & Piran 2006b) is too small to change the distribution of the shocked electrons significantly (The cooling Lorentz factor is $\sim 10^6$ and the random Lorentz factor electrons accounting for the radio afterglow emission is just $\sim$ a few hundreds). L_{ph} is the luminosity of the X-ray photons from the central source.

Since we are discussing a relatively late radio afterglow at $t_d > 1.8$, and since the kinetic energy is small the blast wave is in the sub-relativistic phase at this stage, the results do not depend on the initial shape of the ejecta and in particular the results are insensitive to whether it is thin or

thick (Sari & Piran 1995; Lazzati & Begelman 2006).

So far we have ignored the effects of the injection of additional energy into the initial GRB blast wave. This happens when the "central engine afterglow" outflow catches up with the decelerating initial GRB outflow. The energy injection rate is $dE_{inj}/dt_d = L(t_d) \sim (1 - f_{\rm x})L_X(t_d)/f_{\rm x}$ for $t > t_o$, where $L_X(t_d) \sim 6.9 \times 10^{43}$ erg s^{-1} cm^{-2} $t_{d,-1}^{-1.15}$ is the observed X-ray luminosity and $f_{\rm x}$ is conversion efficiency, t_o is the time at which the "central engine afterglow" begins. Here we take $t_o \sim 0.035$ day, i.e, slightly larger than T_{90}. For the prompt emission the conversion efficiency is $E_\gamma/(E_\gamma + E_k) \sim 0.3$, where $E_\gamma \sim 6 \times 10^{49}$ erg is the prompt $\gamma-$ray energy of GRB 060218. With this efficiency the total energy injected into the initial GRB ejecta is $E_{inj} \sim \int_{t_o}^{12} L(t_d) dt_d = 6.3 \times 10^{48}$erg. It is much smaller than the initial kinetic energy $E_k \sim 10^{50}$ erg. Such a weak energy injection cannot influence significantly the dynamics and emission of the forward shock emission. Indeed, detailed numerical calculation taking into account the energy injection show that the forward shock emission is nearly unchanged.

A more serious effect is the reverse shock emission that will arise from the interaction of the ejecta of the late continuous emission with the blast wave formed from the initial outflow. As an example we consider the reverse shock emission from a baryonic outflow with a bulk Lorentz factor $\sim \Gamma_o = 10$. At $t > 0.1$ day, the initial GRB ejecta have been decelerated so the reverse shock is relativistic. Since the weak energy injection does not accelerate the initial GRB ejecta significantly, we can approximate the Lorentz factor of the reverse shock as $\gamma_{\rm rs} \approx (1-\beta_o\beta)\Gamma_o\Gamma$, where $\beta_o = \sqrt{1 - 1/\Gamma_o^2}$, $\beta = \sqrt{1 - 1/\Gamma^2}$. The magnetic field generated in the reverse shock can be estimated by $B_{\rm rs} \sim [8\epsilon_B\gamma_{\rm rs}(\gamma_{\rm rs} - 1)L(t)/(\Gamma_0^2 R^2 c)]^{1/2} \approx 0.1$ Gauss $\epsilon_{B,-3.3}^{1/2}[\gamma_{\rm rs}(\gamma_{\rm rs} - 1)/12]^{1/2}t_{d,-1}^{-0.58}R_{16.3}^{-1}\Gamma_{o,1}^{-1}$. The number of electrons in the reverse shock region is $N_{\rm e,tot}(t) = E_{inj}(t)/(\Gamma_o m_p c^2) \approx 6.1 \times 10^{50}\Gamma_{o,1}^{-1}(1.17 - t_{d,-1}^{-0.15})$. The maximum spectral flux is thus $F_{\rm max,rs} \approx 1.1$ Jy $(1+z)N_{\rm e,tot}(t)\Gamma B_{rs}/D_L^2 = 46 \ \mu$Jy $\epsilon_{B,-3.3}^{1/2}[\gamma_{\rm rs}(\gamma_{\rm rs} - 1)/12]^{1/2}R_{16.3}^{-1}\Gamma_{o,1}^{-2}\Gamma t_{d,-1}^{-0.58}(1.17 - t_{d,-1}^{-0.15})$ Sari, Piran, & Narayan (1998); Fan & Wei (2005). For these parameters $F_{\rm max,rs} < 100 \ \mu$Jy at $t \sim 0.1$ day and decreases with time continually. This flux is much lower than the optical and radio observations (Note that the reverse shock emission flux in any bands is $\leq F_{\rm max,rs}$). The reverse shock X-ray flux is also far below the observations. We thus conclude that the radio afterglow is dominated by the forward shock and the model is self-consistent.

3.4.2 A circumburst wind

For a stellar wind (Dai & Lu 1998c; Mészáros, Rees, & Wijers 1998), $n = 3 \times 10^{35}A_*R^{-2}$ cm^{-3}, where $A_* = [\dot{M}/10^{-5}M_\odot \text{ yr}^{-1}][v_w/(10^8\text{cm s}^{-1})]$ (Chevalier & Li 2000), $\dot{M}$ is the mass loss rate of the progenitor, v_w is the velocity of the wind.

In the relativistic regime the bulk Lorentz factor of the ejecta $\Gamma^{\rm w} \propto t^{-1/4}$, where the superscript "w" represents the wind model. Following (Chevalier & Li 2000), we have the max-

imal spectrum flux $F_{\nu,\max}^{\mathrm{w}} \propto t^{-1/2}$, $\nu_m^{\mathrm{w}} \approx 1.3 \times 10^{10}$ Hz $\epsilon_{e,-1}^2 C_p^2 E_{k,50}^{\frac{1}{2}} \epsilon_{B,-2}^{\frac{1}{2}} (1+z)^{\frac{1}{2}} t_d^{-3/2}$ and $\nu_c^{\mathrm{w}} \approx 3.2 \times 10^{13}$ Hz $\epsilon_{B,-2}^{-3/2} E_{k,50}^{\frac{1}{2}} A_*^{-2} (1+z)^{-3/2} t_d^{\frac{1}{2}}$, where $C_p \equiv 13(p-2)/[3(p-1)]$. For $\nu_m^{\mathrm{w}} < \nu_a^{\mathrm{w}} < \nu_{\mathrm{obs}} < \nu_c^{\mathrm{w}}$ (where $\nu_{\mathrm{obs}} = 8.46$ GHz is the observer frequency), as suggested by the observation at $t_d > 1.8$, the observed lightcurve is

$$F_{\nu_{\mathrm{obs}}} = F_{\nu,\max}^{\mathrm{w}} (\nu_{\mathrm{obs}}/\nu_m^{\mathrm{w}})^{(p-1)/2} \propto t^{(1-3\mathrm{p})/4}. \tag{3.11}$$

In the Newtonian regime the velocity of the ejecta satisfies $\beta \propto t^{-1/3}$, the radius of the shock front $R \propto t^{2/3}$, the magnetic field strength $B \propto \beta R^{-1} \propto t^{-1}$. Furthermore, we have $F_{\nu,\max}^{\mathrm{w}} \propto RB \propto t^{-1/3}$, $\nu_m^{\mathrm{w}} \propto \beta^4 B \propto t^{-7/3}$, $\nu_c^{\mathrm{w}} \propto t$. Therefore, for $\nu_m^{\mathrm{w}} < \nu_a^{\mathrm{w}} < \nu_{\mathrm{obs}} < \nu_c^{\mathrm{w}}$, we have

$$F_{\nu_{\mathrm{obs}}} \propto t^{(5-7\mathrm{p})/6}. \tag{3.12}$$

For $p \geq 2$, the resulting temporal indexes are ≤ -1.25 and ≤ -1.5, (for Eqs. (3.11) and (3.12) respectively) are much steeper than the observed slope of -0.85.

While the $p < 2$ possibility cannot be ruled out it is less likely as particles accelerated at relativistic shocks usually have a power law distribution index $p \geq 2$ (Gallant 2002). On the other hand, as shown earlier, in a constant density medium a $p \sim 2.1$ can reproduce the data quite well. So we conclude that a dense wind model is less likely.

An important question is whether the energy injection caused by the late activity of the central engine can flatten the lightcurve significantly and thus render the wind profile likely. The answer is negative. Consider an energy injection with the form $dE_{inj}/dt \propto (t/t_o)^{-q}$, where q is a constant. In this case $q \sim 0.4$ is needed to flatten the afterglow lightcurve at $t \gg t_o$ significantly (see Table 2 of Zhang et al. 2006 and the references therein and the detailed numerical calculation of Fan & Piran 2006b). However, the X-ray light curve requires $q \sim 1.15$. For such a large q and as the total energy of this outflow is small compared to the initial energy, the energy injection cannot modify the temporal behavior of the forward shock emission in such an energy injection. Similar to the constant density medium case, it is straightforward to show that the corresponding reverse shock emission in the radio band is unable to account for the data. We thus are left with the conclusion that the wind profile is unlikely.

3.5 The thermal emission

A soft thermal component is seen (Campana et al. 2006) in the X-ray spectrum comprising $\sim 20\%$ of the 0.3-10 keV flux. It begins at ~ 152 sec and lasts up to $\sim 10^4$ sec. The fitted black body temperature shows a marginal decrease ($kT \simeq 0.16 - 0.17$ keV, where k is the Boltzmann constant) and a clear increase in luminosity, by a factor of 4 in the time range 300s-2600s, corresponding to

an increase in the apparent emission radius from $R_{\text{BB,XRT}} = (5.2 \pm 0.5) \times 10^{11}$ cm to $R_{\text{BB,XRT}} = (1.2 \pm 0.1) \times 10^{12}$ cm (Campana et al. 2006). In the sharp decline phase, the XRT emission is dominated by a thermal component ($kT = 0.10 \pm 0.05$ keV, the corresponding apparent emission radius is $R_{\text{BB,XRT}} = 6.6^{+14}_{-4.4} \times 10^{11}$ cm). This thermal component is undetectable in later XRT observation.

A second thermal component is detected by the UVOT. At 1.4 days (i.e., ~ 120 ksec) the black body peak is centered within the UVOT passband. The fitted values are $kT = 3.7^{+1.9}_{-0.9}$ eV and $R_{\text{BB,UVOT}} = 3.29^{+0.94}_{-0.93} \times 10^{14}$ cm, implying an expansion speed of $(2.7 \pm 0.8) \times 10^{9}$ cm s^{-1}. This speed is typical for a supernova and it is also comparable with the line broadening observed in the optical spectra (Pian et al. 2006). The UVOT thermal component is therefore very likely dominated by the expanded hot stellar envelope (see also Campana et al. 2006).

The nature of the X-ray thermal emission is less clear. Campana et al. (2006) suggest that it arises from a shock break out from a very dense wind ($A_* > 30$) surrounding the SN progenitor. As we have shown earlier the medium surrounding the progenitor is not likely to be a dense wind, as required in this model (Campana et al. 2006). We suggest, therefore, that the XRT thermal component arises from a shock heated stellar matter. As the size of the emitting black body region ($6 \times 10^{11} - 10^{12}$ cm) is larger than the size of a typical WR- star (10^{11} cm) there are two possibilities: The emission could be from a hot cocoon surrounding the GRB ejecta (Ramirez-Ruiz, Celotti, & Rees 2002; Zhang, Woosley, & Heger 2004) and expanding initially with $v \sim 0.1c$. An alternative possibility is that the X-ray thermal emission arises from the shock break out from the stellar envelope. This would require, however, a progenitor's size of $\sim 10^{12}$ cm (see also Li 2007). This is much larger than $\sim 10^{11}$ cm or less, that is expected from a star stripped from its H, He and probably O, as inferred from the spectroscopic analysis of the SNe (Pian et al. 2006). It is not clear if stellar evolution models can accommodate such a progenitor, but surprises of this nature have happened in the past. A relativistic radiation-hydrodynamics calculations are needed to test the viability of these two possibilities. This is beyond the scope of this work.

Here we just show that a hot and optical thick outflow could account for the temporal behavior of the XRT and UVOT thermal emission. After the central engines turns off (i.e., there is no fresh hot material injected), the hot outflow expands and cools adiabatically as $T \propto n_p^{1/3} \propto R^{-\alpha/3}$, where $\alpha = 3$ if the hot outflow is spreading and $\alpha = 2$ otherwise, n_p is the number density of the particle. Once the hot region cools adiabatically so that $kT \ll 0.2$ keV the thermal emission recorded by XRT in the range 0.2 to 10 keV decrease quickly with time as

$$L_{\text{th,XRT}} \propto R^2 e^{-0.2\text{keV}/kT} \propto R^2 e^{-\alpha R/3R_0}, \qquad (3.13)$$

where R_0 is the radius of the outflow at the turning off time of the central engine. The V-band flux

is $L_{\rm th,V} \approx 4\pi\sigma R^2 T^4 \frac{y^3 \Delta y}{e^y-1}$, where $y = 2.3{\rm eV}/kT$, $\Delta y \approx 0.13y$, accounting for the FWHM width of V-band. For $y \ll 1$,

$$L_{\rm th,V} \propto TR^2 \propto R^{2-\alpha/3} \propto t^{2-\alpha/3}, \tag{3.14}$$

increases with time until $y \sim 1$ and then it decreases rapidly. As noted by Campana et al. (2006), such a behavior is in agreement with the *Swift* observations.

3.6   Discussion and Summary

The recent nearby burst GRB 060218 had many peculiar features. There are several components of the observed afterglow, X-ray, optical and radio and there is no simple afterglow model that can fit two out of the three. From these components only the observed radio afterglow at $t \sim 10^5$ sec is rather usual and its lightcurve is compatible with a weak burst with a low kinetic energy. We summarize the situation below:

- The temporal decay of the bright (non-thermal) X-ray afterglow ($t > 10^4$ s) seems to be typical. However, the very steep spectrum and the very weak radio afterglow rule out an external shock origin (both form synchrotron radiation and from inverse Compton emission). We suggest following the earlier suggestion of (Katz & Piran 1997) and (Katz, Piran & Sari 1998) that this emission arises due to continued activity of the central engine. This is the first time that a power-law decaying X-ray afterglow is attributed to the activity of the central engine, though it has been suggested by Fan & Wei (2005) and Zhang et al. (2006) that the flare-rich X-ray afterglow that have been detected in a good fraction of *Swift* GRBs (O'Brien et al. 2006) also trace the long term activity of the central engine.

- The radio afterglow can be understood within the standard blast wave model, provided that the medium is ISM-like, the overall kinetic energy is 10^{50}erg, and the fraction of shock energy given to the electrons is ~ 0.01. A wind profile is disfavored as it requires $p \sim 1.5$ and even then it is not clear if one can reproduce the observations.

- The lack of a "jet break" of 8.46 GHz afterglow lightcurve up to 22 day indicates that the outflow is very wide ($\theta_j > 1$ rad). This is somewhat at odds with the standard Collapsar model that involves a narrow jet.

- The X-ray and optical/UV thermal emission cannot arise from the relativistic ejecta. A shock heated envelope of the progenitor is the most natural source. The question whether the envelope has expanded rapidly or was it initially large is open.

There are several implications to these conclusions. First we note that in the current event, the long term power-law decaying X-ray afterglow, the ultraviolet/optical afterglow and the radio

afterglow cannot be attributed to the same physical process and they arise from different regions. While this is sort of expected for the thermal optical and X-ray components it is somewhat puzzling and alarming that the two nonthermal X-ray and radio components do not seem to arise from the same source. While it may indicate a serious problem in the overall fireball model we suggest that this is a manifestation of the fact that GRBs are much more complex than anticipated earlier and that indeed different components such as external shocks as well as continued activity of the central engine might take place simultaneously. Of course GRB 060218 is not unique in this case and such a complexity might have been seen in other peculiar multi-wavelength afterglows which have been poorly interpreted within the standard external shock model (Fan & Piran 2006b).

We have argued that there is a clear indication that a power-law decaying, non-thermal X-ray afterglow that cannot be produced by an external shock and we have shown in §2 that fall-back accretion within a collapsar might be energetic enough to power a detectable "central engine afterglow". This component is in particular important for the sub-luminous GRBs, for which the ejecta is significantly less energetic than that of the typical GRBs and the late activity of the central engine is not hidden by the external shock afterglow. Such sub-luminous GRBs can be detected only from small distances. As it is possible and even likely (Nakar 2006, private communication) that the real rate of such GRBs is significantly higher than the rate of regular GRBs they should dominate the nearby bursts population. We thus predict that such central engine afterglow would be detected in a good fraction of nearby GRBs. In fact with a slight change of the paraments it is possible that the central engine afterglow might dominate over the external shock afterglow even for brighter GRBs. This, for example, could arise in GRB 060210.

The power-law decaying "central engine afterglow" of GRB 060218 was identified by its very steep X-ray spectrum. However, the inconsistency of the strong X-ray afterglow with the weak radio signal was essential to verify this idea. In general the X-ray spectrum of the central engine afterglow is not necessarily so steep. For example, within the well detected X-ray flares, that have been attributed to continues activity of the central engine, just a few have a very steep spectrum (see Table 8 of Butler 2007). Therefore, a multi-wavelength afterglow analysis is essential to identify the "central engine afterglow" component.

Finally we mention two observed features that seem to be inconsistent with the canonical Collapsar model. The first among the two is the lack of a clear wind profile. The afterglows arises at a distance of $R \sim 10^{17}$ cm from the central engine. It could be that the observed profile arose from the interaction of the wind with the surrounding matter or it may reflect a low mass-loss rate of the progenitor star during the post-helium burning phases. A similar feature was seen also in many GRBs but here we have information on regions that are nearer to the central engine. The wide angle of the relativistic ejecta is also incompatible with the usual Collapsar model, in which a narrow jet punches a narrow hole in the envelope of a WR star (Zhang, Woosley, & Heger 2004).

This may indicate that GRB 060218 was an almost "failed GRB". Due to some unique feature of the progenitor (a larger than usual size? or a smaller than typical mass?) the relativistic ejecta almost did not make it across the envelope. This has lead to a wide relativistic outflow with an unusually low initial Lorentz factor. This, in turn, lead to the softer spectrum (possibly due to internal shocks taking place in a region with optical depth of order unity). A significant fraction of the energy was given to a hot cocoon and was reprocessed as thermal emission - seen both in X-ray and later in the UV/optical. One can speculate that in many other cases the relativistic ejecta would have stopped completely and we would have a "failed GRB". It is possible that this is the reason why GRBs are not seen in most SNe Ibc (Berger et al. 2003b; Soderberg et al. 2006b).

3.7 Acknowledgements

Chapter 4

Magnetar as the central engine of short GRB 051221A

4.1 Abstract

The flat segment lasting $\sim 10^4$ seconds in the X-ray afterglow of GRB 051221A represents the first clear case of strong energy injection in the external shock of a short GRB afterglow. In this work, we show that a millisecond pulsar with dipole magnetic field $\sim 10^{14}$ Gauss could well account for that energy injection. The good quality X-ray flat segment thus suggests that the central engine of this short burst might be a millisecond magnetar.

4.2 Introduction

GRB 051221A was localized by the Burst Alert Telescope (BAT) onboard the *Swift* satellite (Parsons et al. 2005) and promptly observed by both *Swift*/BAT and the Konus-Wind instrument. The Swift observations reveal this is a short hard burst, with $T_{90} = 1.4\pm0.2$ s, a hard photon index $\alpha = -1.39 \pm 0.06$, and a fluence $1.16 \pm 0.04 \times 10^{-6}$ ergs cm^{-2} in the 15-150 keV band (Cummings et al. 2005). The Konus-Wind cutoff power-law spectral fitting, in the 20-2000 keV band, shows a fluence $3.2^{+0.1}_{-1.7} \times 10^{-6}$ erg cm^{-2}, a low-energy photon index $\alpha = -1.08 \pm 0.14$, and an observed peak energy $E_{\text{peak}} = 402^{+93}_{-72}$ keV (Golenetskii et al. 2005). With a redshift $z = 0.5459$ (Soderberg et al. 2006a), this burst's isotropic prompt emission energy is $E_\gamma \sim 2.4 \times 10^{51}$ erg, using the ΛCDM concordance model of $\Omega_M = 0.27$, $\Omega_\Lambda = 0.73$, and $h = 0.71$.

Both the X-ray ($\sim 10^2 - 2 \times 10^6$ s) and the optical ($\sim 10^4 - 4 \times 10^5$ s) afterglow light curves of GRB051221A have been well detected, while in the radio band only one data point followed by several upper limits is available. This burst is distinguished by an X-ray flattening at $t \sim 0.03 - 0.2$ day, which strongly suggests a significant energy injection (Soderberg et al. 2006a; Burrows et al. 2006). However, the nature of that energy injection is not clear. In the widely accepted double neutron star merger model for the short/hard bursts, supported by the lack of detection of the bright supernova component in the current event (Soderberg et al. 2006a), the material ejected in the merger is $\sim (10^{-4} - 10^{-2})M_\odot$ (Rosswog et al. 1999; Ruffert & Janka 2001). Given an energy

conversion efficiency ~ 0.001, the fall-back accretion of part of that material onto the central post-merger object is not likely to be able to pump energy up to $\sim 10^{52}$ erg, even with moderate beaming correction. So the fall-back accretion model, which may give rise to significant energy injection in the collapsar scenario of long/soft GRBs (MacFadyen, Woosley, & Heger 2001), does not work in the current case.

In this Letter, we'll show that the afterglow undergoing an energy injection from a millisecond pulsar with a dipole magnetic field $\sim 10^{14}$ Gauss (i.e., a magnetar) well accounts for the multi-wavelength data. The good quality X-ray flat segment thus suggests that the central engine of this short burst may be a millisecond magnetar.

4.3   Analytical investigation

In the long/soft GRB scenario, the energy injection caused by a millisecond pulsar has been discussed in some detail (Dai & Lu 1998b; Wang & Dai 2001; Zhang & Mészáros 2001; Dai 2004; Ramirez-Ruiz 2004; Zhang et al. 2006. Similarly, provided that the gravitational wave radiation is not important, the dipole radiation luminosity of a magnetar can be estimated by

$$L_{\mathrm{dip}}(t_b) \simeq 2.6 \times 10^{48} \text{ erg s}^{-1} \ B_{\perp,14}^2 R_{s,6}^6 \Omega_4^4 (1 + t_b/T_o)^{-2}, \tag{4.1}$$

where $B_\perp$ is the dipole magnetic field strength of the magnetar, R_s is the radius of the magnetar, Ω is the initial angular frequency of radiation, the subscript "b" represents the time measured in the burst frame, $T_o = 1.6 \times 10^4 B_{\perp,14}^{-2} \Omega_4^{-2} I_{45} R_{s,6}^{-6}$ s is the initial spin-down timescale of the magnetar, $I \sim 10^{45}$ g cm^2 is the typical moment of inertia of the magnetar (Pacini 1967; Gunn & Ostriker 1969).

The energy emitted at t_b will be injected into the previous GRB ejecta at time T_b satisfying

$$\int_{t_b}^{T_b} [1 - \beta(\tau_b)] c d\tau_b = c \int_0^{t_b} \beta(\tau_b) d\tau_b \approx c t_b, \tag{4.2}$$

where β, in units of the speed of light c, is the velocity of the ejecta moving toward us. The corresponding observer time is

$$t \approx (1 + z) \int_0^{T_b} [1 - \beta(\tau_b)] d\tau_b. \tag{4.3}$$

Equations (4.2) and (4.3) yield $t \approx (1 + z)t_b + (1 + z) \int_0^{t_b} [1 - \beta(\tau_b)] d\tau_b \approx (1 + z)t_b$.

At time T_b, the energy injected into the ejecta satisfies $dE/dT_b = [1 - \beta(T_b)]L_{\mathrm{dip}}(t_b)$. With

the relation $dt = (1 + z)[1 - \beta(T_b)]dT_b$, we have

$$\frac{dE}{dt} \approx \frac{1}{1+z} L_{\text{dip}}(\frac{t}{1+z})$$
$$= \frac{2.6 \times 10^{48}}{(1+z)} \text{ erg s}^{-1} B_{\perp,14}^2 R_{s,6}^6 \Omega_4^4 [1 + \frac{t}{(1+z)T_o}]^{-2}. \tag{4.4}$$

So the energy injection rate $dE/dt \sim$ const for $t \ll (1+z)T_o$ and $dE/dt \propto t^{-2}$ for $t \gg (1+z)T_o$.

A general energy injection form can be written as $dE/dt = A(1+z)^{-1}(t/t_o)^{-q}$ for $t_i < t < t_f$, where t_i and t_f are the times when the energy injection takes place and turns off, respectively (Zhang & Mészáros 2001; Zhang et al. 2006). GRB ejecta's dynamical evolution, at a time t_c, is significantly changed when the injected energy roughly equals to its initial kinetic energy, i.e., $\int_{t_i}^{t_c} (dE/dt)dt \sim E_k$. We thus derive $At_o^q(t_c^{1-q} - t_i^{1-q}) \sim (1+z)(1-q)E_k$. Accordingly, our magnetar model requires $t_o = 1$, $t_i \sim 0$ and $q \sim 0$ for $t_c < (1+z)T_o$, which leads to $A \sim (1+z)E_\gamma/t_c$, and so

$$2.6 \times 10^{48} \text{ erg s}^{-1} B_{\perp,14}^2 R_{s,6}^6 \Omega_4^4 \sim (1+z)E_k/t_c. \tag{4.5}$$

For $t > (1+z)T_o$, the rate of the energy injection drops sharply or even the central supermassive magnetar has collapsed when it has lost significant part of the angular momentum, which indicates that the afterglow lightcurve flattening weakens at the time $t_f \geq (1+z)T_o$. So we have

$$1.6 \times 10^4 (1+z) B_{\perp,14}^{-2} \Omega_4^{-2} I_{45} R_{s,6}^{-6} \sim t_f. \tag{4.6}$$

From eqs. (4.5) and (4.6), the total injected energy could be estimated as $E_{\text{inj}} = t_f E_k/t_c \sim 5 \times 10^{52}$ erg $I_{45}\Omega_4^2$. On the other hand, with and without energy injection, the contrast of forward shock X-ray emission flux can be estimated by (Kumar & Piran 2000)

$$f \sim (E_{\text{inj}}/E_k)^{(\text{p}+2)/4} \sim [5 \times 10^{52} \text{ erg } I_{45}\Omega_4^2/E_k]^{(\text{p}+2)/4}, \tag{4.7}$$

where $p \sim 2.4$ is the power-law index of the shocked electrons. Equations (4.5)−(4.7) are our main relations to constrain the physical parameters of the underlying magnetar.

From the X-ray observations of GRB051221A, we measure $t_c \sim 3000\,$s, $t_f \sim 1.5 \times 10^4\,$s, and $f \sim 6$. Substitute p and f into equation (4.7), we find $E_k \sim 7.6 \times 10^{51} I_{45}\Omega_4^2$ erg is well consistent with the observational result $E_k \sim 2E_\gamma \sim 4.8 \times 10^{51}$ erg when taking typical $I_{45} \sim 1.5$, $\Omega_4 \sim 0.65$ (i.e., 1 millisecond period), and the GRB efficiency $\eta = E_k/(E_k + E_\gamma) \sim 30\%$. Furthermore, the measurements of t_c, t_f, f, and p are well consistent with the constraint relation $f \simeq (t_f/t_c)^{(\text{p}+2)/4}$. *So we conclude that the central engine may be a magnetar.* Its physical parameters are $(\Omega, R_s, B_\perp, I) \sim (6500\,\text{s}^{-1}, 13\,\text{km}, 10^{14}\,\text{Gauss}, 1.5 \times 10^{45}\,\text{g cm}^2)$ according to the above constraint relations.

An additional constraint is on the ellipticity ϵ of the magnetar. As shown in Shapiro & Teukolsky (1983), the spin-down timescale due to the gravitational wave radiation is $\tau_{\mathrm{gw}} \sim 3 \times 10^{-3} \epsilon^{-2} I_{45}^{-1} \Omega_4^{-4}$ s. Now $\tau_{\mathrm{gw}} > t_f \sim 1.5 \times 10^4$ s, we have $\epsilon < 5 \times 10^{-4} I_{45}^{-1/2} \Omega_4^{-2}$.

4.4   Numerical fit to the afterglows of GRB 051221A

We interpret the apparent flattening in the X-ray light curve being caused by an energy injection from the central magnetar. Yet the flattening episode is unapparent in the optical and radio bands because of limited observations. The code here to fit the multi-band lightcurves has been used in Fan & Piran (2006). The dynamical evolution of the outflow is calculated using the formulae in Huang, Dai, & Lu (2000), which are able to describe the dynamical evolution of the outflow for both the relativistic and the non-relativistic phases. One modification is that now we have taken into account the energy injection (for instance see equation (12) of Fan & Piran (2006)). The electron energy distribution is calculated by solving the continuity equation with the power-law source function $Q = K\gamma_e^{-p}$, normalized by a local injection rate (Moderski, Sikora, & Bulik 2000). The cooling of the electrons due to both synchrotron and inverse Compton has been considered. The synchrotron radiation of the forward shock electrons on the "equal arriving surface" (on which the emission reaches us at the same time) has been calculated strictly. The synchrotron self-absorption has also been taken into account strictly.

We consider a uniform relativistic jet undergoing the energy injection from the central source and sweeping up its surrounding uniform medium. The energy injection has been taken as $dE/dt = 2 \times 10^{48}$ erg s$^{-1}(1+t/1.5 \times 10^4)^{-2}$ for $t < 1.5 \times 10^4$ s otherwise $dE/dt = 0$ (i.e., we assume that the supermassive magnetar collapses when it has lost significant part of its angular momentum). As usual, the fractions of shock energy given to the electrons and the magnetic field (i.e., ϵ_e and ϵ_B) are assumed to be constant. Shown in Figure 4.1 is our numerical fit in the X-ray and optical bands with the following jet parameters: $E_k = 10^{52}$ erg, $\epsilon_e = 0.3$, $\epsilon_B = 0.0002$, the circumburst density $n = 0.01$ cm^{-3}, the half-opening angle $\theta_j = 0.1$, and the viewing angle $\theta_{\mathrm{obs}}{=}0$ (i.e. on-beam viewing).

In addition, we find that a reverse shock emission component, besides the forward shock emission, should be evoked to account for the radio data, which is consistent with the finding in Soderberg et al. (2006a). In the pulsar/magnetar energy injection scenario, the reverse shock emission has been calculated in Dai (2004), assuming that the outflow is electron/positron pairs dominated and the reverse shock parameters are similar to, or even larger than that of the forward shock. The resulting reverse shock emission is so bright that a long-duration flat bump should be evident in the multi-band afterglow lightcurves. This prediction is not confirmed by current observations. This puzzle, however, could be resolved if the fraction of the reverse shock energy
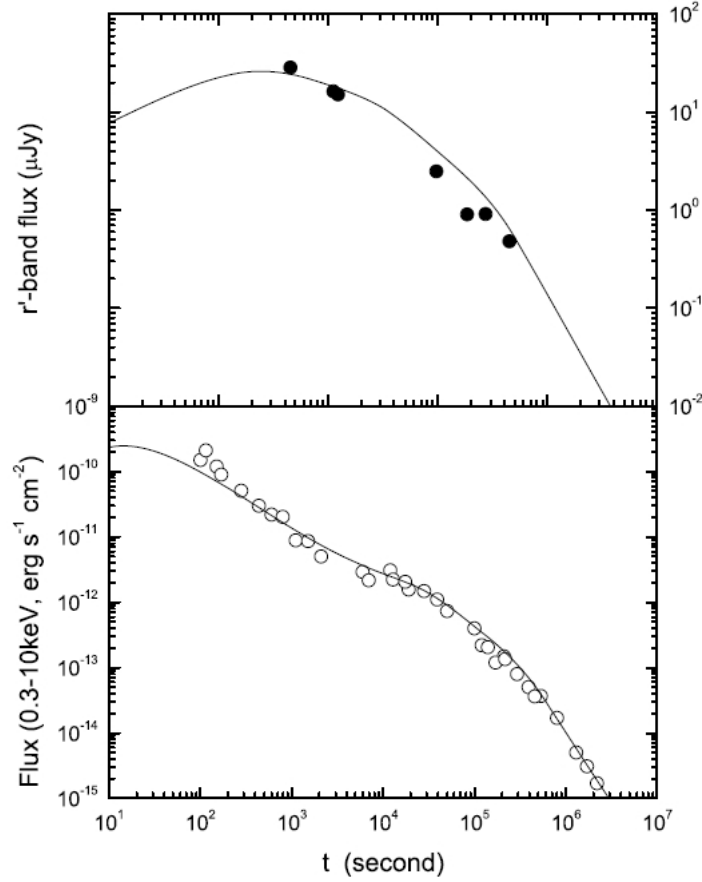
Figure 4.1: Modelling the XRT and R-band afterglow light curves of GRB 051221A with energy injection from an underlying millisecond magnetar. The optical and X-ray data are taken from Soderberg et al. (2006a) and Burrows et al. (2006), respectively. The r'-band extinction of our Galaxy ~ 0.19 mag and that of the host galaxy ~ 0.2 mag (Verkhodanov et al. 2000) have been taken into account. The solid lines are our numerical results. Fitted parameters of the GRB jet undergoing energy injection are presented in Section 4 of this Chapter. From Fan & Xu (2006).

given to the electrons is very small, as shown below.

In our numerical code, the reverse shock dynamics/emission has not been taken into account. It is investigated analytically instead. We assume that the reverse shock emission accounting for the radio data is powered by the energy injection. Following Sari & Piran (1999), after the reverse shock crosses the ejecta at $t_\times$ (note that at $t \sim t_\times \sim 0.2$ day the central magnetar collapses), the observed reverse shock emission flux $F_{\nu_\oplus} \propto (t/t_\times)^{-2}$ for $\nu_m < \nu_\oplus < \nu_c$, where ν_m is the typical synchrotron emission frequency of the shocked electrons and ν_c is the cooling frequency. On the other hand, $F_{\nu_\oplus} \propto (t/t_\times)^{-1/2}$ for $\nu_\oplus < \nu_m < \nu_c$. The current radio observation thus requires a $\nu_m(t_\times) \leq 8.46$ GHz. At $t_\times \sim 0.2$ day, the ejecta is at a radius $R \sim 7 \times 10^{17}$ cm and moves with a bulk Lorentz factor $\Gamma(t_\times) \sim 20$ (obtained in our numerical calculation), thus the comoving toroidal magnetic field of the magnetar wind is $B_w \sim [2L_{\rm dip}/(R^2\Gamma_w^2 c)]^{1/2} \sim 20/\Gamma_w$ Gauss, where Γ_w is the

bulk Lorentz factor of the magnetar wind. In the reverse shock phase, the toroidal magnetic field will be amplified by a factor $\sim \Gamma_{\rm rsh} \approx \Gamma_w/2\Gamma(t_\times)$ for $\Gamma_w \gg \Gamma(t_\times)$ (Kennel & Coronitti 1984). On the other hand, the constraint $\nu_m(t_\times) \approx 2.8 \times 10^6 {\rm Hz}\, \gamma_{m(t_\times)}^2 \Gamma(t_\times)\Gamma_{\rm rsh}B_w/(1+z) \leq 8.46\,{\rm GHz}$ yields $\gamma_{m(t_\times)} \leq 20$, where $\gamma_{m(t_\times)}$ is the minim random Lorentz factor of the electrons accelerated in the reverse shock front. Such a small $\gamma_{m(t_\times)} \equiv 3\epsilon_e(p-2)(\Gamma_{\rm rsh}-1)m_p/[4(p-1)m_e]$ requires that the fraction of shock energy given to the electrons ϵ_e is in order of m_e/m_p because it is very likely that now $\Gamma_w \gg \Gamma(t_\times)$, where m_e and m_p are the rest mass of the electron and the proton, respectively. Taking $\epsilon_e \sim m_e/m_p$ and $p \sim 2.3$, we thus have $\Gamma_{\rm rsh} \leq 115$ and $\Gamma_w \simeq 2\Gamma_{\rm rsh}\Gamma(t_\times) \leq 4600$. After the reverse shock phase, the magnetic energy may be translated to the forward shock mainly by the magnetic pressure working on the initial GRB ejecta and the shocked medium. However, the details are far from clear.

At $t \sim 0.91$ day, the 8.46 GHz emission flux is 0.155 mJy. Therefore the optical (4.6×10^{14} Hz) flux at $t_\times \sim 0.2$ day is $\leq 0.155{\rm mJy}(0.91/0.2)^2(4.6 \times 10^{14}{\rm Hz}/8.46{\rm GHz})^{-0.65} = 2.7\ \mu{\rm Jy}$. It is about one order lower than the forward shock optical emission. As for the X-ray, now $\nu_c(t_\times) \approx 2 \times 10^{15}$ Hz, the X-ray (at 2 keV) flux at $t_\times \sim 0.2$ day is $\leq 0.155{\rm mJy}(0.91/0.2)^2(2 \times 10^{15}{\rm Hz}/8.46{\rm GHz})^{-0.65}(4.84 \times 10^{17}/2 \times 10^{15})^{-1.15} \sim 10^{-6}$ mJy, is also significantly lower than the forward shock X-ray emission. Our estimates made here are independent of the poorly known magnetized reverse shock dynamics. We thus conclude that the reverse shock X-ray/optical emission is unimportant and can be ignored.

One caveat is that the dipole radiation of the magnetar is almost isotropic. The medium surrounding the magnetar but out of the GRB ejecta cone would be accelerated by the energetic wind. Because the energy injected into the GRB ejecta is larger than that contained in the initial ejecta, the outflow contributing to the afterglow emission would be close to be an isotropic fireball rather than a highly jetted ejecta. So the magnetar energy injection model is somewhat challenged by the late jet break detected in GRB 051221A. However, this puzzle could be resolved if in other directions a large amount of baryons ($\sim 0.01\ M_\odot$) ejected in the double neutron star merger have existed there, as found in the previous numerical simulations (Rosswog et al. 1999; Ruffert & Janka 2001). The ejected material would be accelerated by the magnetar wind to a bulk Lorentz factor $\sim$ a few, provided that $E_{\rm inj} \sim 10^{52}$ erg. This wide but only mild-relativistic outflow will give rise to a very late ($\sim 10^6 - 10^7$ s after the burst) multi-wavelength re-brightening. However, for typical parameters taken in this Letter (the isotropic energy is 1.5×10^{52} erg and the initial Lorentz factor is 5.0, i.e., assuming the material ejected from the merger is about $1.5 \times 10^{-3}\ M_\odot$), the flux is not bright enough to be detectable. The emission peaks at $t \sim 3 \times 10^6$ s. The 0.3-10 keV flux is $\sim 1 \times 10^{-15}$ erg s^{-1} cm^{-2} which is marginal for the detection of *Chandra*, and the 8.46 GHz flux is ~ 0.01 mJy. Both are consistent with the extrapolation of current observations (Soderberg et al. 2006a; Burrows et al. 2006). If an event like GRB 051221A takes place much

closer, for example, at $z \sim 0.1$, such very late multi-wavelength re-brightening may be detectable for *Swift* XRT or *Chandra* and other radio telescopes. This predication could be tested in the coming months or years.

4.5 Discussion and Summary

Short hard GRBs may be powered by the merger of double neutron stars (e.g. Eichler et al. 1989). For GRB 051221A, ruling out of bright supernova component in the late optical afterglow lightcurve suggests that the progenitor probably is not a massive star and instead is consistent with the double neutron star merger model. After the energetic merger, a black hole (Eichler et al. 1989), or a differentially rotating neutron star (Kluźniak & Ruderman 1998; Dai et al. 2006), or a magnetar may be formed. Among the above cases the last one is based on various dynamo mechanisms (Rosswog, Ramirez-Ruiz, & Davis 2003) and in particular the MHD simulation of the two neutron star coalescence (Price & Rosswog 2006). How long can the supermassive magnetar survive? In the general-relativistic numerical simulation, the resulting hypermassive magnetar collapses in a very short time ~ 100 ms (Shibata et al. 2006). The hypermassive magnetar has a mass exceeding the mass limit for uniform rotating but the supermassive magnetar does not. Therefore a supermassive magnetar may be able to survive in a long time as shown in Duez et al. (2006). In view of the uncertainties involved in the numerical simulation, some constraints from the observation rather than just from the theoretical calculation are needed.

Thanks to the successful running of *Swift* and *Chandra*, now short GRBs could be localized rapidly and their X-ray afterglows could be monitored continuously. The X-ray flat segment in GRB 051221A strongly suggests a significant energy injection. Such an energy injection could be well accounted for if the central engine is a millisecond pulsar with a dipole magnetic field $\sim 10^{14}$ Gauss. The X-ray flat segment in GRB 051221A thus provides us a possible evidence for a long time living magnetar formed in the double neutron star merger. In this scenario, the material ejected from the merger would be swept and accelerated by the strong magnetar wind. This wide but mild-relativistic component would give rise to a very late multi-wavelength re-brightening and might be detectable for an event like GRB 051221A but much closer.

We would like to point out that the magnetar energy injection model is not unique to account for the data. For example, assuming the energy carried by the material of the initial GRB ejecta satisfies the relation $E(> \Gamma) \propto \Gamma^{-4.5}$ (Rees & Mészáros 1998), the X-ray afterglow lightcurve of GRB 051221A could also be well reproduced. However, the physical process pumping such kind of energy injection, in particular in the short GRB scenario, is not clear yet.

4.6 Acknowledgments

Chapter 5

The core-collapse origin for SN-less nearby long GRBs 060505 and 060614

5.1 Abstract

GRB 060505 and GRB 060614 are nearby long-duration gamma-ray bursts (LGRBs) without accompanying supernovae (SNe) down to very strict limits. They thereby challenge the conventional LGRB-SN connection and naturally give rise to the question: are there other peculiar features in their afterglows which would help shed light on their progenitors? To answer this question, we combine new observational data with published data and investigate the multi-band temporal and spectral properties of the two afterglows. We find that both afterglows can be well interpreted within the framework of the jetted standard external shock wave model, and that the afterglow parameters for both bursts fall well within the range observed for other LGRBs. Hence, from the properties of the afterglows there is nothing to suggest that these bursts should have another progenitor than other LGRBs. Recently, *Swift*-discovered GRB 080503 also has the spike + tail structure during its prompt γ-ray emission seemingly similar to GRB 060614. We analyse the prompt emission of this burst and find that this GRB is actually a hard-spike + hard-tail burst with a spectral lag of 0.8±0.4 s during its tail emission. Thus, the properties of the prompt emission of GRB 060614 and GRB 080503 are clearly different, motivating further thinking of the criteria for GRB classification. Finally we note that, whereas the progenitor of the two SN-less bursts remains uncertain, *the core-collapse origin for the SN-less bursts would be quite certain if a wind-like environment can be observationally established, e.g, from an optical decay faster than the X-ray decay in the afterglow's slow cooling phase.*

5.2 Introduction

Gamma-ray bursts (GRBs) are the most luminous explosions in the Universe since the Big Bang. They fall into two (partially overlapping) populations according to their observed duration: γ-ray durations (measured as the time in which 90% of the fluence is emitted) longer than 2 s are defined as long GRBs (LGRBs) while bursts with duration shorter than 2 s are defined as short GRBs

(SGRBs; Kouveliotou et al. 1993). It is widely accepted that at least the majority of LGRBs are driven by the collapse of massive stars (e.g., Woosley 1993), although some LGRBs may be generated by the merger of compact objects (e.g., Kluźniak & Ruderman 1998; Rosswog, Ramirez-Ruiz, & Davis 2003). The strongest evidence for the collapsar scenario is the detection of bright Type Ic supernova (SN) component photometrically and spectroscopically associated with nearby LGRBs such as GRB 980425, GRB 030329, GRB 031203, and XRF 060218 (Galama et al. 1998; Hjorth et al. 2003; Malesani et al. 2004; Sollerman et al. 2006; Pian et al. 2006; Campana et al. 2006). On the other hand, SGRBs may be powered by the merger of binary compact objects (e.g. Eichler et al. 1989; Narayan et al. 1992). This connection is observationally bolstered by the association of some SGRBs with old stellar populations and lack of accompanying bright SN components in cases such as GRB 050509B (Hjorth et al. 2005a), GRB 050709 (Fox et al. 2005; Hjorth et al. 2005b) and GRB 050724 (Berger et al. 2005; Malesani et al. 2007). However, challenging this simple picture some SGRBs displayed violent X-ray flares occurring at least ~ 100 s after the triggers, e.g., GRB 050709 (Fox et al. 2005) and GRB 050724 (Barthelmy et al. 2005b; Campana et al. 2006; Malesani et al. 2007). This suggests long-lasting activity of the central engine and hence the current understanding of the GRB progenitor mechanism may be too simple (e.g., Fan, Zhang, & Proga 2005; Dai et al. 2006; Rosswog 2007). There is also evidence for activity of the inner engine on much longer time-scales (several days) for GRB 050709 (Watson et al. 2006) and GRB 070707 (Piranomonte et al. 2008).

The whole picture became more complicated after the discovery of GRB 060505 and GRB 060614, because both bursts are nearby LGRBs according to the conventional taxonomy but they are observationally not associated with SNe down to very strict limits (Fynbo et al. 2006; Della Valle et al. 2006; Gal-Yam et al. 2006). In this sense, they share the expected observational properties of both conventional LGRBs and SGRBs.

GRB 060505 had a fluence of $(6.2 \pm 1.1) \times 10^{-7}$ erg cm^{-2} in the $15 - 150$ keV band, and a T_{90} duration of 4 ± 1 s (Hullinger et al. 2006; McBreen et al. 2008). It was found to be associated with a bright, star-forming H II region within its host galaxy at $z = 0.089$ (Ofek et al. 2007; Thöene et al. 2008a). In the compact-star merger scenario the diameter of the H II region and the location of the GRB within it suggest that the delay time from birth to explosion of GRB 060505 was $\lesssim 10$ Myr. This is marginally matching the lower limit of the delay-time region for SGRBs (Ofek et al. 2007). On the other hand, the age of the H II region of ~ 6 Myr (Thöene et al. 2008a) is consistent with the expectation for core-collapse in a massive star. The prompt emission of GRB 060614 consisted of a hard-spectrum component lasting ~ 5 s followed by a soft-spectrum component lasting ~ 100 s. Mangano et al. (2007) reported a photon index $\Gamma = 1.63 \pm 0.07$ for the time interval [-2.83,5.62] s since the BAT trigger ($\chi^2/\text{dof} = 48.2/56$) and $\Gamma = 2.21 \pm 0.04$ for 5.62-97.0 s since the BAT trigger ($\chi^2/\text{dof} = 40.9/56$). The fluences in the two components are

$(3.3\pm0.1)\times10^{-6}$ erg cm^{-2} and $(1.69\pm0.02)\times10^{-5}$ erg cm^{-2} in the 15-350 keV band, respectively (Gehrels et al. 2006). Its host galaxy has a redshift of $z = 0.125$ (Price, Berger, & Fox 2006). The host of GRB 060614 is very faint with an absolute magnitude of about $M_B = -15.3$ (Fynbo et al. 2006). Its specific star-formation rate is quite low, but within the range covered by LGRB hosts (similar, e.g., to that of the GRB 050824 host galaxy, Sollerman et al. 2007).

The spectral lag has been invoked as a quantity that can be used to classify bursts such that SGRBs have zero lag and LGRBs fall on a well defined lag-luminosity relation (Norris et al. 2000, 2006). For GRB 060614 Gehrels et al. (2006) found that the spectral lags for the hard and soft components in the prompt γ-ray emission are both consistent with zero lag, falling entirely within the range for SGRBs. For GRB 060505, on the other hand, McBreen et al. (2008) found using the *Suzaku*/WAM and *Swift*/BAT data that the spectral lag for the prompt γ-ray emission is 0.36 ± 0.05 s, consistent with a LGRB identity. Furthermore, lags of LGRBs and SGRBs, regardless of their physical origins, appear to overlap quite significantly according to statistics of 265 *Swift* bursts (see Fig. 1 in Bloom et al. 2008). Alternatively, the so-called Amati relation can be used to provide hints on which class GRB 060505 and GRB 060614 belong to. According to this relation derived from the observed GRBs with sufficient data, all SGRBs are outliers because of their relatively higher νF_ν peak energy, while all LGRBs, except the peculiar long GRB 980425, are consistent with this relation. Amati et al. (2007) find that GRB 060614 follows the relation whereas GRB 060505 does not. Hence, based on properties of the prompt emission other than the duration it seems impossible to establish clear evidence about which class of bursts GRB060505 and GRB060614 belong to.

To gain further insight on this topic, in this work we add our own observational data to already published data and study the afterglows of GRB 060505 and GRB 060614. We aim to determine from the afterglow properties whether these two bursts differ from other LGRBs, besides being SN-less, to provide further clues to the nature of their progenitors. The observations of the two afterglows and data reduction are presented in § 2.1 and § 2.2. At the beginning of § 3, we briefly introduce the leading external shock wave model employed to explain GRB afterglows, and apply it to GRB 060505 in § 3.1. GRB 060614 has been studied by Mangano et al. (2007); in § 3.2 and § 3.3 we re-analyze this burst and provide analytical and numerical constraints on the afterglow parameters, respectively. In § 4 we discuss possible progenitors of these two bursts in comparison with the recently discovered GRB 080503, which we define as the first hard-spike + hard-tail *Swift* GRB.

5.3   Observations and data reduction

5.3.1   GRB 060505

The field of GRB 060505 was observed with the European Southern Observatory (ESO) Very Large Telescope (VLT) and the FORS1 instrument on two epochs (see also Fynbo et al. 2006). On May 6.4, slightly more than one day after the burst, the field was observed in the B, V, R, I and z bands. In order to be able to subtract the underlying host galaxy, in particular the hosting star-forming region within the host galaxy (Thöene et al. 2008a), the field was observed again on September 14.2, again in the B, V, R, I and z bands. The journal of observations is given in Table 1. Due to strong fringing and lack of calibration data we decided not to include the z band data in the analysis.

The optical data were corrected for bias and flat-fielded using standard techniques. In order to subtract the underlying emission from the host galaxy we used the ISIS software (Alard & Lupton 1998). In Fig. 5.1 we show the result of the image subtraction. As can be seen, the afterglow is clearly detected in all four bands. We then performed photometry on the afterglow in the following way. We first duplicated an isolated, non-saturated star in each of the first epoch images to a new empty position such that it also appeared in the subtracted image. We then used Daophot (Stetson 1987) to perform relative photometry between the afterglow and the star. Finally, we obtained the photometry on the standard system by measuring the magnitude of the comparison star using aperture photometry and the photometric zeropoints obtained based on Landolt stars by the ESO observatory calibration plan on the same night.

The *Swift*/XRT data were processed in a standard way using the *Swift* software version 29 (released 2008 June 29 as part of HEAsoft 6.5.1). We also included in the analysis the *Swift*/UVOT data points/upper limits and the late X-ray data point using the ACIS-S detector on board the *Chandra* X-ray observatory in Ofek et al. (2007).

5.3.2   GRB 060614

Table 5.2 shows the comprehensive R-band data of the afterglow of GRB 060614 from the Watcher 0.4m telescope, DFOSC at the Danish 1.5m telescope (D1.5m), the 1m telescope at the Siding Spring Observatory (SSO), VLT/FORS1, and VLT/FORS2. The R-band data by the Watcher telescope were processed and made public for the first time, which not only are consistent with other R-band data but provide the accurate peak time, 0.3 days since the BAT trigger, of the R-band afterglow lightcurve. We have applied the correction for the Galactic extinction, $E(B - V) = 0.057$ mag (Schlegel et al. 1998), and subtracted the contribution of host galaxy, $R_{\mathrm{host}} = 22.46 \pm 0.04$ (Della Valle et al. 2006).

We collected *Swift*/UVOT data from Mangano et al. (2007). For the UVOT bands, we also

applied the correction for Galactic extinction and subtracted the contribution of host galaxy using the template in Mangano et al. (2007).

The *Swift*/XRT lightcurve and spectrum data were collected from the UK Swift Science Data Centre (Evans et al. 2007). The X-ray lightcurves at 0.3 keV and 1.5 keV are shown in Fig. 5.5 so that the spectral slope, $\beta_X \sim 0.89$, in the 0.3-10 keV band is taken into account when we performed the numerical fitting.

The *Swift*/BAT lightcurve in the 15-350 keV band was processed with the `batgrbproduct` task of the HEAsoft 6.5.1.

5.4 Interpretation of the two afterglows

Suppose the radial density profile of the circumburst medium takes the form $n(r) \propto r^{-k}$, then $k = 0$ if the medium is interstellar medium-like (ISM-like) while $k = 2$ if the medium stellar wind-like (WIND-like).

We use the standard fireball afterglow theory reviewed by, e.g., Piran (2005), with the simple microphysical assumptions of constant energy fractions imparted to the swept-up electrons, ϵ_e, and to the generated magnetic field, ϵ_B, respectively. For the evolution of the synchrotron spectrum, we adopt the prefactors of equation (1) in Yost et al. (2003) for the ISM scenario, and those of equations (11-14) in Chevalier & Li (2000) for the WIND scenario. We note that both cases lead to the afterglow closure relations made of the temporal decay index α and the spectral index β, depending upon the spectral segment and the electron energy distribution index, p (see Tables II and IV of Piran 2005).

For numerical calculation, we follow the general treatment of Huang, Dai, & Lu (2000), that is, one first calculates the overall dynamical evolution of the GRB outflow, and then calculates the synchrotron radiation at different times, including different corrections such as, e.g., the equal-arrival-time-surface effect and the synchrotron-self-absorption effect.

5.4.1 Constraints on GRB 060505

To establish a broadband spectral energy distribution (SED) we extrapolate the X-ray flux to the epoch of the optical data (i.e., 1.125 days after the burst). The optical data were corrected for foreground Galactic extinction of $A_B = 0.089$, $A_V = 0.068$, $A_R = 0.055$, $A_I = 0.040$ (Schlegel et al. 1998). We fit the SED in count space (see Starling et al. 2007) with an absorbed power law model, where Galactic absorption in the X-rays is fixed at $N_{\rm H} = 1.8 \times 10^{20}$ cm^{-2} (Kalberla et al. 2005) and intrinsic X-ray absorption and optical/UV extinction in the host galaxy are free parameters. Solar metallicity is assumed in the X-ray absorption model, and extinction in the host is assumed to be SMC-like (Pei 1992). The resulting SED is shown in Fig. 5.2. The derived

spectral slope is $\beta_{OX} = 0.97 \pm 0.03$. The host galaxy extinction is consistent with zero, but with a best fitting value of $E(B-V) = 0.015$ mag and a 90% upper limit of $E(B-V) = 0.05$ mag, while the X-ray absorption is found to be $N_{\rm H} = (0.2^{+0.2}_{-0.1}) \times 10^{22}$ cm^{-2} (where errors are quoted at the 90 % confidence level). The fit has a $\chi^2/$dof of 5.3/4.

The index $\beta_{OX} = 0.97 \pm 0.03$ indicates that the cooling frequency ν_c is already below the optical at this time and the energy spectral index p is slightly larger than 2. Indeed, the numerical fit, shown in Fig. 5.3, yields $p \sim 2.1$, and other afterglow parameters are $n \sim 1\,{\rm cm}^{-3}$, $\epsilon_e \sim 0.1$, $\epsilon_B \sim 0.006$, $E_k \sim 2.8 \times 10^{50}$ erg, and the half-opening jet angle $\theta_j \sim 0.4$ rad. These parameters are within the range of LGRB afterglows, but the limited data prevent us from getting more insight on the properties of this afterglow. Both the SED measurement and the numerical fit tend to render it unnecessary to employ *ad hoc* models (e.g., macronova in Ofek et al. 2007) to interpret this afterglow.

5.4.2   Preliminary constraints on GRB 060614

We constructed afterglow SEDs in GRB 060614 at three epochs, i.e., 0.187 days, 0.798 days, and 1.905 days. The results are listed in Table 5.3 and shown in Fig. 5.4. Our SEDs are fully consistent with those in Mangano et al. (2007) measured at 0.116, 0.347, 0.694, and 1.736 days. Both works show that there exists a spectral break between the optical and the X-ray before $\sim$0.26 days while afterwards both the optical and the X-ray are in the same spectral segment with the spectral index $\beta_{OX} \sim 0.8$.

The afterglow lightcurves show that energy injection exists between ~ 0.01 and ~ 0.26 days, which presumably would change the SED during this period. If the injection frequency is between the optical and the X-ray, then it may lead to that the lightcurves have a very shallow rising in the optical band and a very shallow decay in the X-ray band. Indeed, the observational data fit this interpretation very well (Mangano et al. 2007). We found that this optical-to-Xray lightcurve behavior still holds after performing different corrections. The result of our analysis shows that a flat or gradually increasing lightcurve is generally a description as good as a slow decaying except in the X-ray band. A temporal peak, clearly shown in optical bands, exists ~ 0.3 days after the burst. Afterwards the afterglow decays with $\alpha_1 \sim 1.1$ until $t_b \sim 1.4$ days when it steepens significantly to $\alpha_2 \sim 2.5$. There is only one V-band upper limit before ~ 0.01 days, the starting time of energy injection. Therefore, to constrain the afterglow properties we use data after ~ 0.26 days.

The index $\beta_{OX} \sim 0.8$ after ~ 0.26 days indicates that the afterglow is in the slow cooling case of

$$\nu_a < \nu_m < \nu_O < \nu_X < \nu_c$$

until at least a few days. Using the afterglow closure relations we find $\beta = (p-1)/2 \sim 0.8$, which gives the energy spectral index $p \sim 2.6$, which then gives the decay index $\alpha = 3(p-1)/4 \sim 1.2$, in good agreement with the observed decay law ($\alpha_1 \sim 1.1$). Furthermore, this p value of ~ 2.6 is very close to the observed decay index of 2.5 after $t_b \sim 1.4$ days, in good agreement with the theoretically predicted decay law after a jet break, i.e., $\alpha \sim p$ at any wavelength from X-ray to optical. Therefore, as discussed by Mangano et al. 2007, the break at $t \sim 1.4$ days is likely the so-called *jet break* (Rhoads 1999; Sari, Piran & Halpern 1999; Zhang et al. 2006; Nousek et al. 2006).

Since the optical decay is never faster than the X-ray decay, there is no indication of a WIND-like circumburst medium for this afterglow. Also since radio data are not available, analytical constraint on ν_a is impossible for this afterglow. Using the earliest useful data, we put a lower limit on F_ν^{max} and an upper limit on ν_m as

$$F_\nu^{max} = 1.6\,(z+1)\,D_{28}^{-2}\,\epsilon_{B,-2}^{0.5}\,E_{52}\,n^{0.5} > 105.5 \times 10^{-3} \;\; \text{mJy} \tag{5.1}$$

and

$$\nu_m = 3.3 \times 10^{14}\,(z+1)^{0.5}\,\epsilon_{B,-2}^{0.5}\,\bar{\epsilon}_e^2\,E_{52}^{0.5}\,t_d^{-1.5} < 4.69 \times 10^{14} \;\; \text{Hz} \tag{5.2}$$

where $t_d = 0.3$ and $z = 0.125$. Using the latest useful data, we put the lower limit on ν_c as

$$\nu_c = 6.3 \times 10^{15}\,(z+1)^{-0.5}\,\epsilon_{B,-2}^{-1.5}\,E_{52}^{-0.5}\,n^{-1}\,t_d^{-0.5} > 10^{18} \;\; \text{Hz} \tag{5.3}$$

where $t_d = 10$. In detail, the above three equations give rise to the constraints

$$
\begin{aligned}
&\epsilon_{B,-2}^{0.5}\,E_{52}\,n > 0.0019 \\
&\varepsilon_{B,-2}^{0.5}\,\varepsilon_e^2\,E_{52}^{0.5} < 1.564 \\
&\epsilon_{B,-2}^{-1.5}\,E_{52}^{-0.5}\,n^{-1} > 532.4.
\end{aligned}
\tag{5.4}
$$

5.4.3 Numerical constraints on GRB 060614

We find that the afterglow data can be reasonably reproduced by the following parameters (see Fig. 5.5 for a plot of our fit): $p \sim 2.5$, $\epsilon_e \sim 0.12$, $\epsilon_B \sim 0.0002$, $E_k \sim 6 \times 10^{50}$ erg, $n \sim 0.04$ cm^{-3}, and $\theta_j \sim 0.08$ rad. The energy injection takes place at $t_i \sim 8 \times 10^2$ s and ends at $t_e \sim 2 \times 10^4$ s after the burst, and the energy injection is nearly a constant with a rate $L_{\text{inj}} \sim 1.2 \times 10^{48}$ erg s^{-1}. Substituting these parameters into eq. (5.4), the numerical constraint is in agreement with the analytical constraint.

If the energy injection is from the wind of a millisecond magnetar, to fit the observational data at the late stage of the whole energy injection period, the magnetar is required to have dipole

radiation $L_{\mathrm{dip}}(t) \approx 2.6 \times 10^{48}/(1+z)$ erg s^{-1} $B_{\perp,14}^2 R_{s,6}^6 \Omega_4^4 [1 + t/((1+z)T_o)]^{-2}$, where $B_\perp$ is the dipole magnetic field strength of the magnetar, R_s is the radius of the magnetar, Ω is the initial angular frequency of radiation, $T_o = 1.6 \times 10^4 B_{\perp,14}^{-2} \Omega_4^{-2} I_{45} R_{s,6}^{-6}$ s is the initial spin-down timescale of the magnetar, and $I \sim 10^{45}$ g cm^2 is the typical moment of inertia of the magnetar (Pacini 1967). However, because the optical flux is roughly proportional to $\bar{E}_{\mathrm{k}}$, where $\bar{E}_{\mathrm{k}}$ is the sum of the isotropic-equivalent kinetic energy E_{k} and the injected energy, then the predicted optical flux at the early stage of the energy injection period (e.g., $t \sim 0.02$ days in Fig. 5) would be much higher than the observed flux. In detail, at $t \sim 0.02$ day, there would be $\bar{E}_{\mathrm{k}} \sim E_{\mathrm{k}} + L_{\mathrm{inj}} t \sim 3 E_{\mathrm{k}}$, indicating that the predicted optical flux should be ~ 3 times the observed flux. Therefore the magnetar model is not convincing.

Note that the prompt $\gamma-$ray lightcurve may have two components: the earlier hard spike with an isotropic energy $E_{\gamma,h} \sim 3.7 \times 10^{50}$ erg and the latter soft tail (sometimes called extended emission) with an isotropic energy $E_{\gamma,s} \sim 1.7 \times 10^{51}$ erg. The early part is spectrally hard thus the outflow might be ultra-relativistic, while the latter part is spectrally soft suggesting the bulk Lorentz factor of the outflow became lower. This is because the optically thin condition yields a lower limit on $\Gamma \geq 20(L_{\mathrm{outflow}}/10^{50}$ erg s$^{-1})^{1/5} \delta t^{-1/5}$, where L_{outflow} is the total luminosity of the outflow, and δt is the typical variability timescale of the late soft $\gamma-$ray emission (Rees & Mészáros 1994). In our numerical calculation, we find the bulk Lorentz factor of the forward shock $\Gamma \sim 26$ at $t \sim 10^3$ s while $\Gamma \sim 16$ at $t \sim 2 \times 10^4$ s. If the energy carried by the material of the late time GRB ejecta satisfies the relation $E(> \Gamma) \propto \Gamma^{-5}$ (Rees & Mészáros 1998) for $16 < \Gamma < 26$, the constant energy injection form taken in the afterglow modeling can be reproduced (Zhang et al. 2006). In this model, for the outflow accounting for the hard spike emission the energy efficiency is $\sim E_{\gamma,h}/(E_{\gamma,h} + E_{\mathrm{k}}) \sim 40\%$, while for the outflow accounting for the soft tail emission, the energy efficiency is $\sim E_{\gamma,s}/[L_{\mathrm{inj}}(t_e - t_i) + E_{\gamma,s}] \sim 8\%$. The decreasing efficiencies from early spike to late tail may be due to the smaller contrast between the Lorentz factors of the fast material and that of the slow material.

5.5　Discussion and Conclusion

As shown in several early papers, for GRB 060505 (Fynbo et al. 2006) and GRB 060614 (Fynbo et al. 2006; Della Valle et al. 2006; Gal-Yam et al. 2006) there is no accompanying SN emission, down to limits hundreds of times fainter than the archetypical SN 1998bw that accompanied GRB 980425, and fainter than any Type Ic SN ever observed. Multi-wavelength observations of the early afterglow exclude the possibility of significant dust obscuration. For GRB 060505 the properties of the host galaxy (Ofek et al. 2007; Thöene et al. 2008a) as well as the spectral lag of the prompt emission (McBreen et al. 2008) is most consistent with the properties expected for

the long-duration class of GRBs. For GRB 060614 the duration of the prompt emission places the burst firmly within the long-duration class of GRBs, but the negligible spectral lag (Gehrels et al. 2006) and the relatively modest star-formation activity of the host galaxy is more similar to the expected properties for the short-duration class of GRBs. In this paper we have investigated whether or not the properties of the two afterglows could provide some hints to the most likely progenitor types for these bursts.

For GRB 060505, the numerical fit of its afterglow shows that the standard jetted external shock wave model is consistent with the data, yielding a typical interstellar medium density of $n \sim 1\,\mathrm{cm}^{-3}$, a wide jet angle $\theta_j \sim 25°$, and a possible jet break at $t_b \sim 3$ days. For GRB 060614, the standard external shock wave model is again consistent with the data, but apparently needing to invoke energy injection. The afterglow shows the clearest achromatic jet break among all *swift* bursts studied so far, decaying in a broken power-law from $\alpha_1 \sim 1.1$ to $\alpha_2 \sim 2.5$ at $t_b \sim 1.4$ days. An achromatic peak, especially in the *UBVR* bands, occurs at ~ 0.3 days, which we interpret as resulting from an episode of strong energy injection as Mangano et al. (2007) suggested. Numerical fit yields a circumburst density of $n \sim 0.04\,\mathrm{cm}^{-3}$ and a jet angle of $\theta_j \sim 5°$. The inferred afterglow parameters for the two bursts fall within the range for other LGRBs. If it had not been for the observed absence of associated SNe we would have no reason, from the afterglow properties, to question their classification as LGRBs.

After discovery of these two GRBs, to reconcile all SN-observed and SN-less GRBs within the conventional framework of short ($\lesssim 2$ s) and long ($\gtrsim 2$ s) GRBs, a new classification was proposed, in which GRBs featuring a short-hard spike and a (possible) long-soft tail would be ascribed to the conventional short class, or Type I in the new taxonomy, while all other GRBs, or Type II, would comprise the conventional long class (Zhang et al. 2007, see also Kann et al. 2007). The new classification expands the range of the conventional short class, and is applicable to GRB 060505 and GRB 060614, which then would be SN-less due to a merger-related progenitor rather than SN-less massive stellar death.

However, a recent burst, GRB 080503, seems to challenge the new classification. This burst also has a temporal spike + tail structure in the prompt emission phase. The T_{90} values of the initial spike and the total emission in the 15-150 keV band are 0.32 ± 0.07 s and 232 s, respectively (Perley et al. 2008). The fluence of the non-spike emission measured from 5 s to 140 s after the BAT trigger in the 15-150 keV band is $(1.86 \pm 0.14) \times 10^{-6}\,\mathrm{erg\,cm}^{-2}$, being around 30 times that of the spike emission in the same band. This fluence ratio is much higher than the ratio of ~ 6 for GRB 060614, and higher than any previous similar *Swift* GRB. For GRB 060614 and GRB 080503 we extracted the BAT lightcurves in different energy bins, shown in Fig. 5.6, for comparison study. For GRB 080503 we have analysed the spectral evolution during the prompt emission period by BAT and XRT and list our analysis and that of other groups in Table 5.4. From

these we conclude that: (1) The results of different groups are fully consistent with each other. (2) The photon indices for the spike and non-spike emissions are consistent within their error regions (90% confidence level). A strong spectral softening from the spike phase to the non-spike phase can be excluded. A cutoff power-law fit does not improve the fitting, yielding the error of E_{peak} larger than 100%. (3) During the BAT-XRT overlap period, the XRT spectra are always harder than the BAT spectra, which implies that the BAT+XRT spectra (0.3-150 keV) would be harder than the BAT spectra (15-150 keV) alone. This adds more evidence that from spike to non-spike the spectra did not soften considerably. In addition, note that for all conventional LGRBs (e.g., from BATSE), there is a general trend that the spectra during the prompt emission would soften mildly from the beginning time to the ending time (Norris et al. 1986). Therefore, the prompt spectral evolution of GRB 080503 is different from that of GRB 060614.

In addition, we computed the spectral lags in different energy bands using the 64 ms binning lightcurves, following the method in Norris et al. (2000) and Chen et al. (2005). The lag during the initial spike phase is consistent with zero. From 5 to 50 s since BAT trigger, the lags are $0.8^{+0.3}_{-0.4}$ s for the 25-50 keV vs. 15-25 keV band and $0.8^{+0.4}_{-0.5}$ s for the 50-100 keV vs. 15-25 keV band respectively, both well above the lag range for SGRBs. Again the lag of GRB 080503 is in contrast with that of GRB 060614. The redshift of GRB 080503 was not measured mainly because its optical and X-ray afterglows became very faint shortly after the BAT trigger (never exceeding 25 mag in deep observations starting at ~ 1 hr since trigger), but the g-band photometric detection imposes a limit of approximately z<4 (Perley et al. 2008). In Fig. 5.7 we show the possible position of GRB 080503 in the spectral lag-peak luminosity plane relative to the positions of previous LGRBs and SGRBs. As can be seen, for the extended emission of GRB 080503, its position is outside the SGRB population at a very high confidence level regardless of its redshfit. For the spike emission of GRB 080503, its position is within the SGRB population because of a peak luminosity comparable to that of the extended emission, as well as a negligible spectral lag.

The very faint optical and X-ray afterglows of GRB 080503 may indicate the circumburst density is very low. This is consistent with the fact that the afterglow is located away from any host galaxy down to 28.5 mag in deep *Hubble Space Telescope* imaging (Perley et al. 2008). These observational signatures contribute to put GRB 080503 into the merger class. If we ignore the lag function in classifying GRBs and relax the restriction of "soft-tail" for a Type I GRB to "either soft- or hard- tail", then it would be (even more) ambiguous, also operationally difficult to define the type of spike+tail GRBs among all long GRBs, especially among those at $z \gtrsim 0.7$ for which a SN search in their afterglows is difficult or impossible. Bearing in mind that GRBs can be either luminous or under-luminous, and the redshift could be either high or low, then the problems would be: up to what duration should be classified as a spike, and how much should the flux ratio be for the spike component over the non-spike component? If GRB 080503 is interpreted as a merger

burst, then it enhances the possibility that a merger could produce a long GRB, at least in the prompt emission phase, mimicking the one produced by a collapsar. GRB 080503 is a dark burst with the optical-to-Xray spectral slope β_{OX} well below 0.5, the critical value for defining a dark burst (Jakobsson et al. 2004), at 0.05 days after the burst. We speculate that some other dark bursts may have similar progenitors GRB 080503.

The progenitors of GRB 060505 and GRB 060614 remain uncertain based on their observations and current GRB theory. Other than the lack of a SN component, their afterglows are actually not peculiar when compared with the afterglows of other LGRBs. According to the current theoretical study, in the core-collapse scenario the "fallback"-formed black holes or progenitors with relatively low angular momentum could produce such SN-less GRBs (e.g., Fryer et al. 2006; Sumiyoshi et al. 2006; Nakazato et al. 2008; Kochanek et al. 2008), or in the merger scenario the two compact objects also could produce such SN-less GRBs if the formed remnant, a differentially rotating neutron star or an uniformly rotating magnetar, has not collapsed into a black hole immediately (Kluźniak & Ruderman 1998; Rosswog, Ramirez-Ruiz, & Davis 2003). A difference existing in the afterglows between these two scenarios is that the collapsar model predicts a WIND-like circumburst medium created by the Wolf-Rayet progenitor star while the merger model does not. As a matter of fact the WIND signature is not clearly evident in most LGRBs, but this should not necessarily lead to the merger origin for these bursts because the definite WIND signature is an ideal case for a constant wind off a massive star. If lucky enough, the core-collapse origin for a SN-less GRB (no matter whether it has the hard-spike + soft-tail structure) will be quite certain if in the afterglow, either the X-ray flux $F_\nu(t)$ decays as $\propto t^{-\alpha}$ with its spectrum as $\propto \nu^{-(2\alpha-1)/3}$ for the $\nu_m < \nu_X < \nu_c$ stage (normally in early afterglow), or the optical decay index is larger than the X-ray decay index by a factor of $\sim 1/4$ for the slow cooling phase of the WIND scenario.

5.6 Acknowledgements

Figure 5.1: Multicolor imaging of the afterglow and host galaxy of GRB 060505. The top row shows the result of image subtraction, that is, imaging on May 6.4 minus imaging on September 14. The middle row shows the deeper, and better seeing imaging obtained on September 14, more than 4 months after the burst, while the bottom row shows the imaging of the field on May 6.4, ~ 1.125 days after the burst.
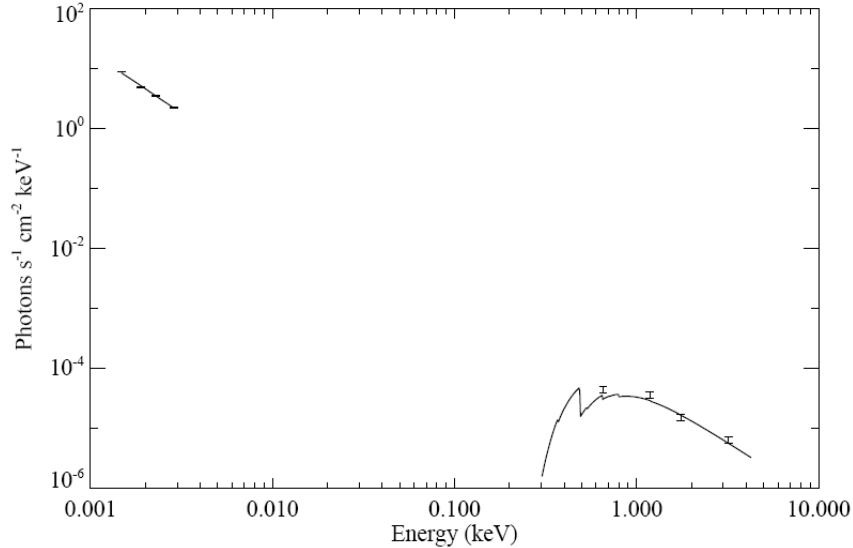
Figure 5.2: The broadband SED for GRB 060505 at the epoch of the multi-band optical observation (1.125 days after the burst). The SED can be fitted with a single absorbed power-law with slope $\beta = 0.97 \pm 0.03$.
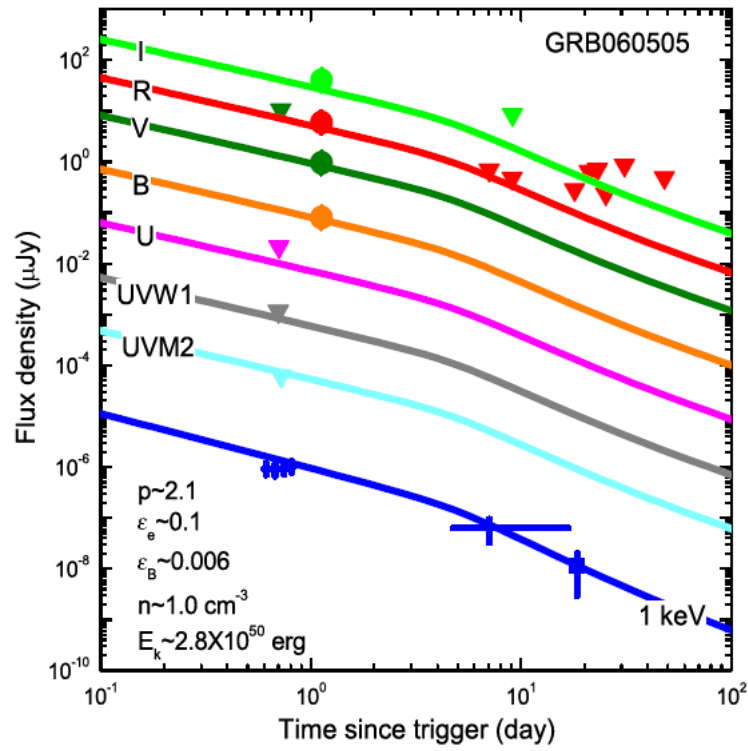
Figure 5.3: The multi-band lightcurves for the afterglow of GRB 060505. For clarity, the shown flux densities in the I, R, V, B, U, UVW1, UVM2, and 1 keV bandpass are 5, 1, 1/50, 1/500, 1/5000, 1/50000, 1/50000 times that of their real flux densities, respectively. Points and crosses represent the measurements with errorbars while triangles represent upper limits. Also marked are the parameters used for a good fit.
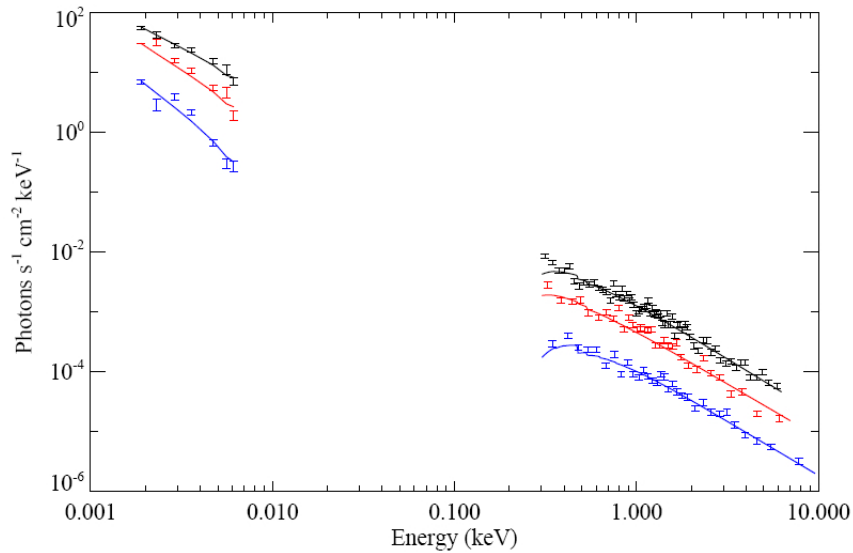
Figure 5.4: The broadband SEDs for GRB 060614 at the epochs of 0.187, 0.798, and 1.905 days from top to bottom. A broken power-law is only required during the first epoch. Refer to Table 5.3 for detailed measurements.
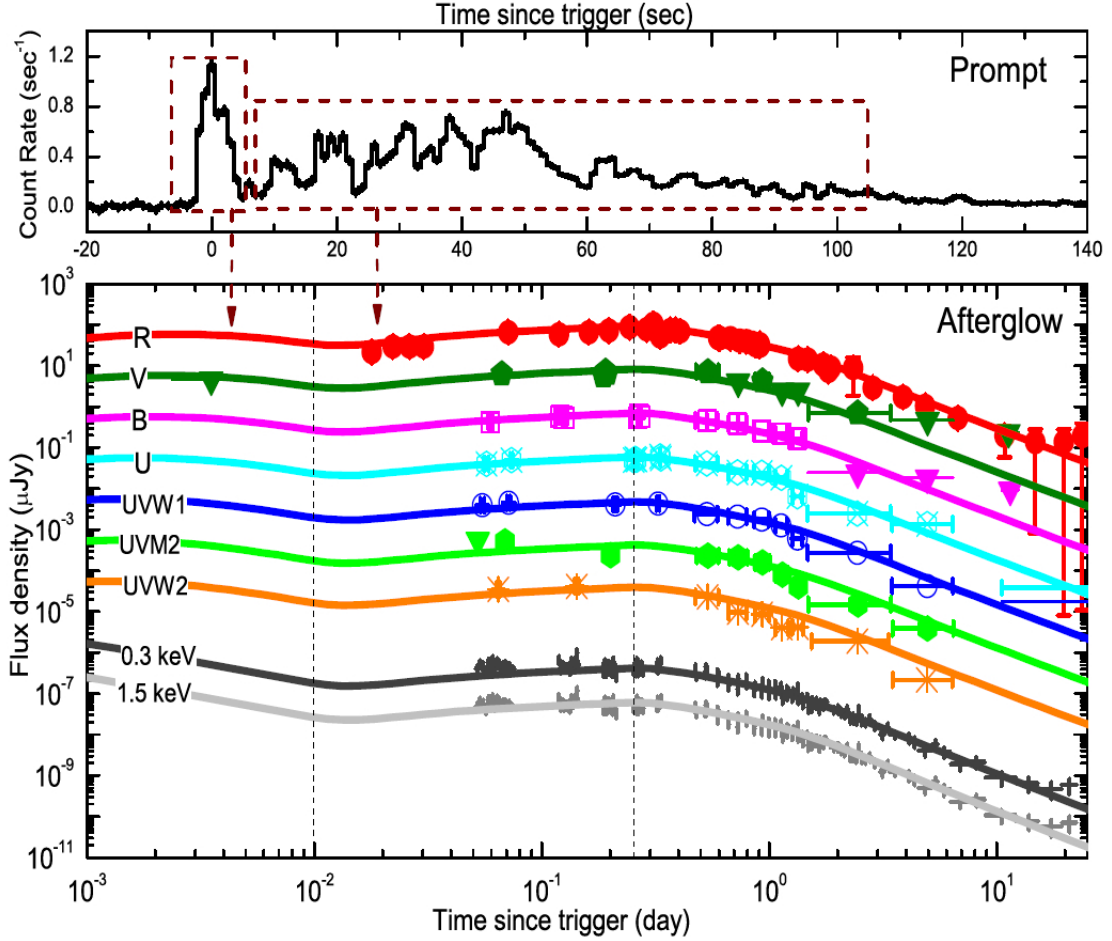
Figure 5.5: The temporal lightcurves for the prompt phase (upper panel) and for the afterglow (lower panel) of GRB 060614. *Upper:* the prompt lightcurve in the 15-350 keV band, consisting of a hard spike of duration ~ 5 s and a soft tail of ~ 100 s. *Lower:* numerical fit to the afterglow lightcurves which consists of an episode of energy injection enclosed by two vertical dashed lines. For clarity, the shown flux densities in the R, V, B, U, UVW1, UVM2, UVW2, 0.3 keV, and 1.5 keV bands are 10^0, 10^{-1}, 10^{-2}, 10^{-3}, 10^{-4}, 10^{-5}, 10^{-6}, 2×10^{-7}, 10^{-7} times that of their real flux densities, respectively. In our model, the energy injection corresponds to the soft tail in the prompt phase while the main afterglow corresponds to the hard spike−−this correlation is illustrated by two arrows from the upper prompt panel to the lower afterglow panel.
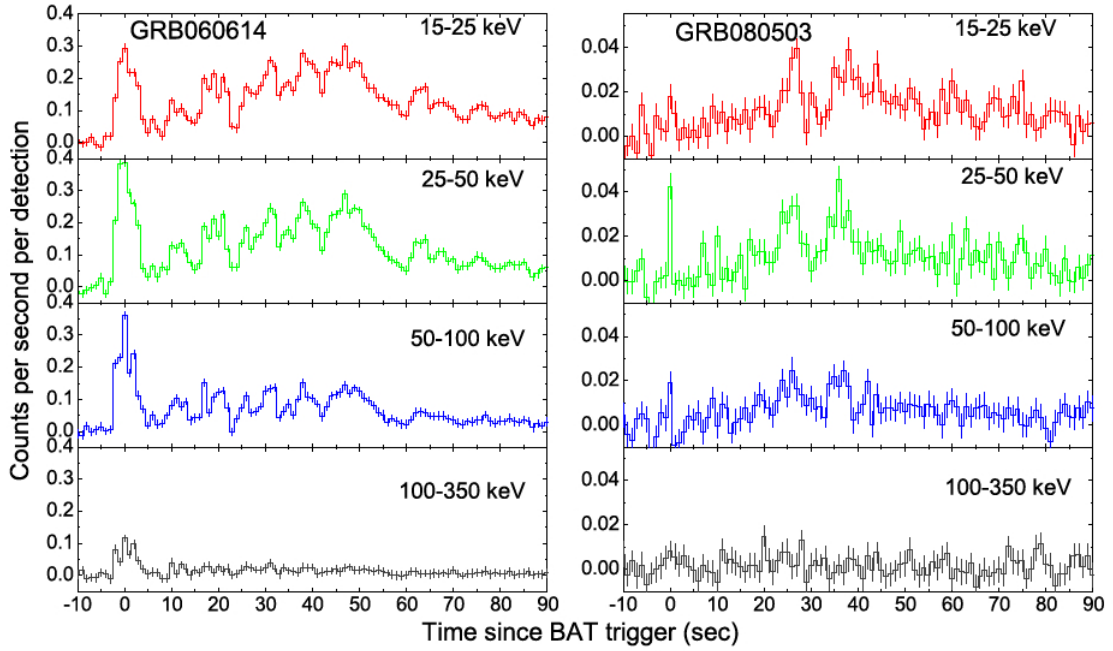
Figure 5.6: Comparison of the prompt lightcurves (1 s binning) of GRB 060614 (left column) and GRB 080503 (right column) detected by BAT in different energy bins. Morphologically both bursts consist of a spike emission followed by an extended emission, namely, a tail emission. For each energy bin of either burst, comparing the count rates in the spike phase and in the tail phase yields a rough estimate of the spectral hardness. In GRB 060614 the tail is considerably softer than the spike, while in GRB 080503 the tail is comparably as hard as the spike, being consistent with the comparison of spectral measurements in Table 5.4. The spectral lags for both spikes are consistent with zero; the lag for the tail of GRB 060614 is consistent with zero while the lags for the tail of GRB 080503 are $0.8^{+0.3}_{-0.4}$ s for the 25-50 keV vs. 15-25 keV band and $0.8^{+0.4}_{-0.5}$ s for the 50-100 keV vs. 15-25 keV band.
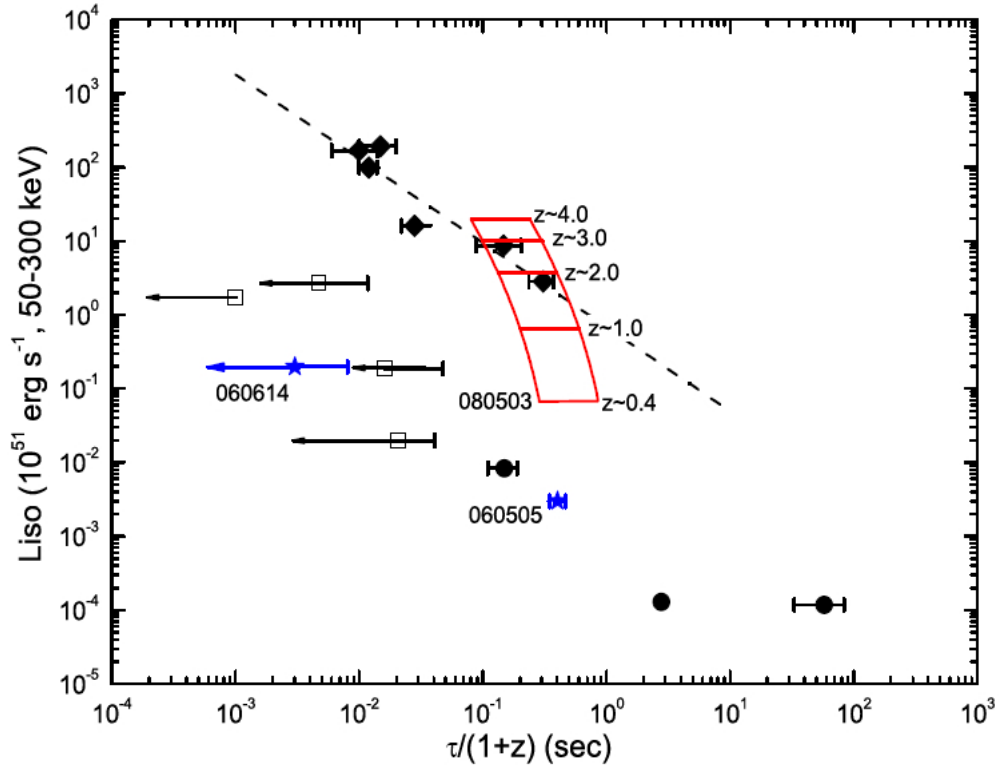
Figure 5.7: Spectral lag-peak luminosity relation for GRBs. The Norris LGRB data (diamonds) and the associated fit (dashed line) are from Norris et al. (2000). The data of SGRBs (open squares), the nearby SN-bright GRBs 980425, 031203, and 060218 (filled circles), the nearby SN-less GRBs 060505 and 060614 (stars) are from McBreen et al. (2008) and references therein. Also shown is the spectral lag-peak luminosity region for the extended emission of GRB 080503 (closed region) due to lacking the spectroscopic redshift of this burst. The position of this burst moves upward in the plane as its *assumed* redshift increases.

Table 5.1.   Log of optical observations of GRB 060505.

Time[a] [day]	Bandpass	Vega Mag[b]	σ(mag)	Instrument	Ref
0.702	UVW1	>20.71	–	UVOT	1
0.706	U	>20.31	–	UVOT	1
0.721	V	>20.34	–	UVOT	1
0.724	UVM2	>22.05	–	UVOT	1
1.102	r	21.65	0.16	GMOS	1
1.118	g	22.37	0.08	GMOS	1
1.125	I	21.21	0.04	VLT+FORS1	2
1.125	R	21.74	0.04	VLT+FORS1	2
1.125	V	22.14	0.04	VLT+FORS1	2
1.125	B	22.48	0.04	VLT+FORS1	2
7.041	g	>24.74	–	GMOS	1
7.055	r	>24.02	–	GMOS	1
9.078	g	>24.54	–	GMOS	1
9.092	r	>24.32	–	GMOS	1
9.105	i	>22.96	–	GMOS	1
18.0	R	>24.95	–	VLT+FORS2	3
21.1	R	>24.05	–	D1.5m+DFOSC	3
23.1	R	>23.95	–	D1.5m+DFOSC	3
25.3	R	>25.15	–	Keck+LRIS	3
31.1	R	>23.75	–	D1.5m+DFOSC	3
48.1	R	>24.35	–	D1.5m+DFOSC	3

[a]Time since BAT trigger.

[b]The Vega magnitude is after correction for the Galactic extinction of $E(B - V) = 0.02$ mag, and image subtraction to remove the host contribution.

References. — (1) Ofek et al. 2007; (2) This work; (3) Fynbo et al. 2006.

Table 5.2.   Log of R-band optical observations of GRB 060614

Date[a] [days]	Veg Mag[b]	σ(mag)	Instrument	Ref
0.67347	19.45	0.01	D1.5m+DFOSC	1
0.74059	19.60	0.01	D1.5m+DFOSC	1
0.79292	19.64	0.01	D1.5m+DFOSC	1
0.84034	19.73	0.01	D1.5m+DFOSC	1
0.89998	19.86	0.01	D1.5m+DFOSC	1
0.9037	19.88	0.01	D1.5m+DFOSC	1
0.90743	19.80	0.01	D1.5m+DFOSC	1
0.91146	19.92	0.01	D1.5m+DFOSC	1
1.82138	21.45	0.06	D1.5m+DFOSC	1
0.0179	20.29	0.34	SSO	2
0.0221	19.95	0.22	SSO	2
0.0262	19.95	0.22	SSO	2
0.0303	19.95	0.22	SSO	2
0.0713	19.10	0.10	SSO	2
0.1188	19.20	0.11	SSO	2
0.1608	19.10	0.10	SSO	2
0.1968	18.99	0.10	SSO	2
0.2427	18.79	0.10	SSO	2
0.28938	18.92	0.17	Watcher	3
0.30887	18.58	0.11	Watcher	3
0.36713	18.97	0.10	Watcher	3
0.38661	18.96	0.11	Watcher	3
0.40613	19.04	0.11	Watcher	3
0.33131	19.33	0.30	Watcher	3
1.33851	20.69	0.21	Watcher	3
1.47729	20.75	0.26	Watcher	3
2.33615	21.27	0.86	Watcher	3
0.59715	19.42	0.03	VLT+FORS2	4

Table 5.2 (cont'd)

Date[a] [days]	Veg Mag[b]	σ(mag)	Instrument	Ref
0.59885	19.43	0.02	VLT+FORS2	4
0.59989	19.42	0.02	VLT+FORS2	4
0.60094	19.45	0.02	VLT+FORS2	4
0.602	19.45	0.02	VLT+FORS2	4
0.60313	19.43	0.02	VLT+FORS2	4
0.60418	19.46	0.02	VLT+FORS2	4
0.60524	19.45	0.03	VLT+FORS2	4
0.6063	19.45	0.02	VLT+FORS2	4
0.8701	19.88	0.03	VLT+FORS2	4
0.89996	19.92	0.02	VLT+FORS2	4
1.72583	21.07	0.02	VLT+FORS1	4
1.86974	21.25	0.02	VLT+FORS1	4
2.84199	22.47	0.06	VLT+FORS1	4
3.86899	23.04	0.09	VLT+FORS1	4
4.84365	23.58	0.19	VLT+FORS1	4
6.74083	24.32	0.30	VLT+FORS1	4
10.81441	25.40	0.77	VLT+FORS1	4
14.77259	25.78	1.08	VLT+FORS1	4

[a]Time since BAT trigger.

[b]The Vega magnitude is after correction for the Galactic extinction of $E(B - V) = 0.057$ mag, and subtraction of the host contribution, $R_{\text{host}} = 22.46 \pm 0.04$.

References. — (1) Fynbo et al. 2006; (2) Schmidt et al. 2006; (3) This work; (4) Della Valle et al. 2006.

Table 5.3. Results (main parameters) of fits to the three spectral energy distributions of GRB 060614 at epochs 0.187, 0.798, and 1.905 days. For the broken power law models we fit both with the power law slopes free, and for the case of a cooling break where $\Gamma_1 = \Gamma_2 - 0.5$ (where $\Gamma = \beta + 1$). Galactic absorption, $N_{\mathrm{H,Gal}}$, is fixed at 1.87×10^{20} cm^{-2} (Kalberla et al. 2005) and Galactic extinction, $E(B-V)_{\mathrm{Gal}}$, is fixed at 0.057 mag (Schlegel et al. 1998). Solar metallicity is assumed in the X-ray absorption model and the extinction is modeled with an SMC extinction law (Pei 1992). All errors are quoted at the 90% confidence level.

Model	$E(B-V)$ (mag)	N_{H} (10^{22} cm^{-2})	Γ_1	E_{bk} (keV)	Γ_2	χ^2/dof
Epoch 1						
PL+SMC	<0.02	<0.02	1.75±0.02	-	-	60/68
BKNPL+SMC	<0.2	$0.03^{+0.03}_{-0.02}$	0.9±0.4	$0.005^{+0.010}_{-0.002}$	1.9±0.1	49/66
BKNPL+SMC	<0.04	$0.03^{+0.02}_{-0.01}$	Γ_2-0.5	$0.012^{+0.001}_{-0}$	$1.86^{+0}_{-0.02}$	50/67
Epoch 2						
PL+SMC	<0.04	<0.03	$1.78^{+0.02}_{-0.01}$	-	-	42/36
BKNPL+SMC	$0.3^{+0.1}_{-0.2}$	$0.10^{+0.04}_{-0.05}$	<1.3	$0.005^{+0.025}_{-0.001}$	2.2±0.2	27/34
BKNPL+SMC	<0.08	$0.09^{+0.03}_{-0.05}$	Γ_2-0.5	$0.2^{+0.7}_{-0.19}$	$2.1^{+0.2}_{-0.1}$	31/35
Epoch 3						
PL+SMC	$0.09^{+0.06}_{-0.05}$	$0.06^{+0.03}_{-0.02}$	1.81±0.04	-	-	26/35
BKNPL+SMC	0.2±0.1	$0.08^{+0.04}_{-0.03}$	>0.1	unbounded	1.9±0.1	24/33
BKNPL+SMC	$0.13^{+0.06}_{-0.07}$	0.07±0.03	Γ_2-0.5	<0.008	$1.86^{+0.07}_{-0.08}$	24/34

Table 5.4.   Comparison of power-law spectral evolution for GRB 060614 and GRB 080503.

GRB	Time Interval (s)	Photon Index	Index Error[a]	χ^2/dof	Bandpass (keV)	Ref
GRB 060614	-2.83-5.62	1.63	0.07	48.2/56	15-150	1
–	5.62-97.0	2.21	0.04	40.9/56	15-150	1
–	97.0-176.5	2.37	0.13	42.6/56	15-150	1
GRB 080503	0.2-0.6	1.74	0.28	78.1/58	15-150	2
–	10-200	1.93	0.14	38.3/58	15-150	2
–	0.0-0.7	1.59	0.28	69/59	15-150	3
–	10-170	1.91	0.12	52/59	15-150	3
–	81-282	1.27	0.03	–	0.3-10	3
–	81-280	1.33	0.05	696.3/714	0.3-10	4
–	83-107	1.00	0.13	–	0.3-10	5
–	107-128	1.11	0.13	–	0.3-10	5
–	128-150	1.42	0.14	–	0.3-10	5
–	150-185	1.66	0.16	–	0.3-10	5
–	185-256	1.77	0.16	–	0.3-10	5

[a]Errors are quoted at the 90% confidence level.

References. — (1) Mangano et al. 2007; (2) This work; (3) Mao et al. 2008; (4) The UK Swift Science Data Centre; (5) Perley et al. 2008.

Chapter 6

The mildly relativistic origin for the X-ray transient 080109 associated with SN 2008D

6.1 Abstract

We analyze the available X-ray, optical and radio data of the X-ray transient 080109/SN 2008D. From the data we suggest that (i) The initial transient ($\lesssim 800$ sec) is due to the reverse shock emission of a mildly relativistic ($\Gamma_i \sim$ a few) outflow stalled by the stellar wind with a wind parameter $A_* \sim 1$. The prompt UV/optical to X-ray spectrum is well consistent with the typical one for conventional GRBs/XRFs. (ii) The subsequent X-ray afterglow emission ($\lesssim 10^4$ sec) is from the blast wave of the transient remnant sweeping up the stellar wind medium, with a kinetic energy $\sim 10^{46}$ erg. (iii) The late X-ray and radio afterglow emissions ($\gtrsim 2 \times 10^4$ sec) are relevant to the shock driven by the ejecta of SN 2008D. (iv) The local event rate of X-ray transient may be of order $\sim 1 \times 10^4$ yr^{-1} Gpc^{-3}, comparable to that of the local Type Ibc SNe. (v) The X-ray transient 080109/SN 2008D indicates a continuum from GRB-SN to under-luminous GRB-/XRF-SN to X-ray transient-SN and to ordinary Type Ibc SN (unless every Type Ibc SN has a mildly relativistic jet), as shown in Fig. 6.3 of this work.

6.2 Introduction

During the past decade, long-duration ($\gtrsim 2$ sec) $\gamma-$ray bursts (GRBs), including the subclass of X-ray flashes (XRFs), have been found (1) to be driven by the core-collapse of massive stars (Woosley 1993); thus (2) to be associated with a rare variety ($\sim 1\%$) of Type Ibc supernovae (SNe), the so-called hypernovae (HN) (Galama et al. 1998; Hjorth et al. 2003; Stanek et al. 2003; Malesani et al. 2004; Pian et al. 2006) (see however Fynbo et al. 2006); and (3) in general to be hosted by star-forming dwarf galaxies with low metallicity (Fynbo et al. 2003; Fruchter et al. 2006; Stanek et al. 2006). Though the association of GRBs/XRFs and Type Ibc SNe has been pinned down, what channels make a dying star to produce a GRB or an XRF, and not just a Type Ibc SN, is still unclear. It is believed that the progenitor's mass, metallicity, angular momentum, and the configuration and strength of its internal magnetic field play important roles

for the generation of GRBs/XRFs and ordinary SNe Ibc.

The serendipitous discovery of the X-ray transient (XT) 080109/SN 2008D (Berger & Soderberg 2008a) may shed light on filling in this gap between energetic GRBs/XRFs and ordinary SNe Ibc. We will analyze space- and ground-based data of this transient and SN, focusing on X-ray/radio data because observationally they trace the fastest component of the transient/SN outflow while optical data trace the slower SN ejecta.

This work is structured as following. Section 3 presents the prompt and X-ray afterglow data of XT 080109 and the discussion of the shock breakout model. Section 4 gives the interpretations of X-ray and radio data. We attribute the prompt X-ray emission ($t < 800$ s) to the strong reverse shock radiation of a mildly relativistic outflow stalled by a normal wind medium. The XT outflow decelerated by the reverse shock, moves sub-relativistically and drives a blast wave. The early X-ray afterglow ($t < 10^4$ s) could be either the synchrotron radiation of the forward shock or the inverse Compton emission of the SN thermal photons upscattered by electrons in the blast wave. The late time radio afterglow is found to be fully consistent with the synchrotron self-absorbed radiation of the fastest ejecta of the main SN outflow. We summarize our results with some discussions in Section 5.

6.3 Swift Observations and Data Analysis

During *Swift*/XRT follow-up observations of the Type Ib SN 2007uy beginning at 13:32:49 UT on Jan 9, 2008, an X-ray transient (XT hereafter) was identified and reported on Jan 10.58 (Berger & Soderberg 2008a). X-ray emission was already underway at the time of the trigger. Both XT 080109 and SN 2007uy are in the same host galaxy, NGC 2770, at $z = 0.0065$. The galaxy was within the *Swift*/BAT field of view for approximately 30 minutes prior to the XRT observation but didn't trigger the BAT (Burrows et al. 2008).

From the beginning of the XRT observation, XT 080109 was observed to rise to a maximum flux in ~65 sec, and then decay until the end of the first orbit at ~800 sec. We reduced the XRT data in a standard way using the Swift analysis software (HEAsoft 6.4) and the latest calibration and exposure maps. The pile-up effect for early bright X-ray observation has been corrected. The contamination by nearby X-ray sources has been corrected too, making use of the *Chandra* data in Soderberg et al. (2008). As a whole, the first orbit data can be well fitted by an absorbed power-law $\Gamma = 2.3 \pm 0.2$ and a column density $N_H = 7.6^{+1.4}_{-1.2} \times 10^{21} \, \text{cm}^{-2}$ ($\chi^2_{dof} = 15.1/20$) with respect to the Galactic value of $1.7 \times 10^{20} \, \text{cm}^{-2}$. An absorbed blackbody spectrum with $kT = 0.73 \pm 0.05$ keV in the restframe gives a $\chi^2_{dof} = 24.2/20$. *Clearly the power-law fit is much better than the blackbody fit.* If the first orbit is divided into different periods, hard-to-soft spectral evolution is present. The spectrum of the X-ray data after the first orbit is found to be consistent

with the early value, indicating $\Gamma \sim 2.3$. The 0.3-10 keV unabsorbed light curve is presented in the upper panel of Fig. 6.1.

We also reduced the UVOT data in a standard way. The first 83.4 s UVOT/u exposure was taken starting from 13:35:49 UT on Jan 9, 2008; the first 83.5 s UVOT/b exposure starting from 13:37:18 UT on Jan 9, 2008; and the first 83.4 s UVOT/v exposure starting from 13:44:35 UT on Jan 9, 2008. These three exposures during the XT period reveal $u > 20.2$ mag, $b > 20.5$ mag, and $v > 19.9$ mag (all 3σ upper limits, see also Immler et al. 2008). The second u, b, v exposures were at $\sim 10^4$ sec since the XRT observation. Afterwards, UVOT observation confirms the presence of SN 2008D (Malesani et al. 2009). Our UVOT data reduction is fully consistent with the report in Immler et al. (2008) and Soderberg et al. (2008). Shown in the lower panel of Fig. 6.1 are the extinction-corrected early ubv light curves.

6.4 Interpretation of the follow-ups

6.4.1 Real onset time and spectra for XT 080109

As can be seen, it is almost impossible to know the exact onset time of XT 080109. However, firstly, *Swift*/BAT was not triggered for $\sim$30 mins prior to the XRT observation although XT 080109 was in BAT's field of view; Secondly, XT 080109 was associated with SN 2008D. These two factors give rise to the high possibility that XT 080109 is a low-luminosity outburst compared with previous bursts featuring low νF_ν peak energy such as XRF 060218. A generic Fast Rise Exponential Decay (FRED) profile fit of the X-ray light curve of XT 080109 gives constraint on the real onset time to be ~ 10 sec earlier (Soderberg et al. 2008). We don't adopt this small time shift in the following analysis because it doesn't affect the late afterglow power-law decay indices.

In the simplest shock breakout model, the shock wave forms a blackbody spectrum when it roughly breaks out of the surface of the progenitor star. Should this model work, according to the equation $L = \Omega R_e^2 \sigma T^4$, where $L \sim 10^{44} \mathrm{erg\,s^{-1}}$ is the isotropic luminosity, Ω is the solid angle of the outflow, R_e is the emission radius (not smaller than the radius of the progenitor $R_* \sim 10^{11}$ cm, as identified in Soderberg et al. (2008), σ is the Stefan-Boltzmann constant, and T is the temperature, we have $kT \sim 300\Omega^{-1/4}L_{44}^{1/4}R_{e,11}^{-1/2}\mathrm{eV}$. To match the measured $kT = 0.73$ keV, a jet-like outflow with extremely small $\Omega \sim 3 \times 10^{-2}L_{44}R_{e,11}^{-2}$ is needed, which suggests it is unlikely that the shock breakout contribution dominates the XT emission. In addition, the observed long X-ray duration of $\sim$800 sec would be contradictory with the short-duration prediction (i.e., a few seconds) in the simplified shock breakout model.

A realistic shock breakout is more complicated. Here we take the semi-analytical model constructed by Li (2007) to estimate whether the current data can be accommodated in the modified
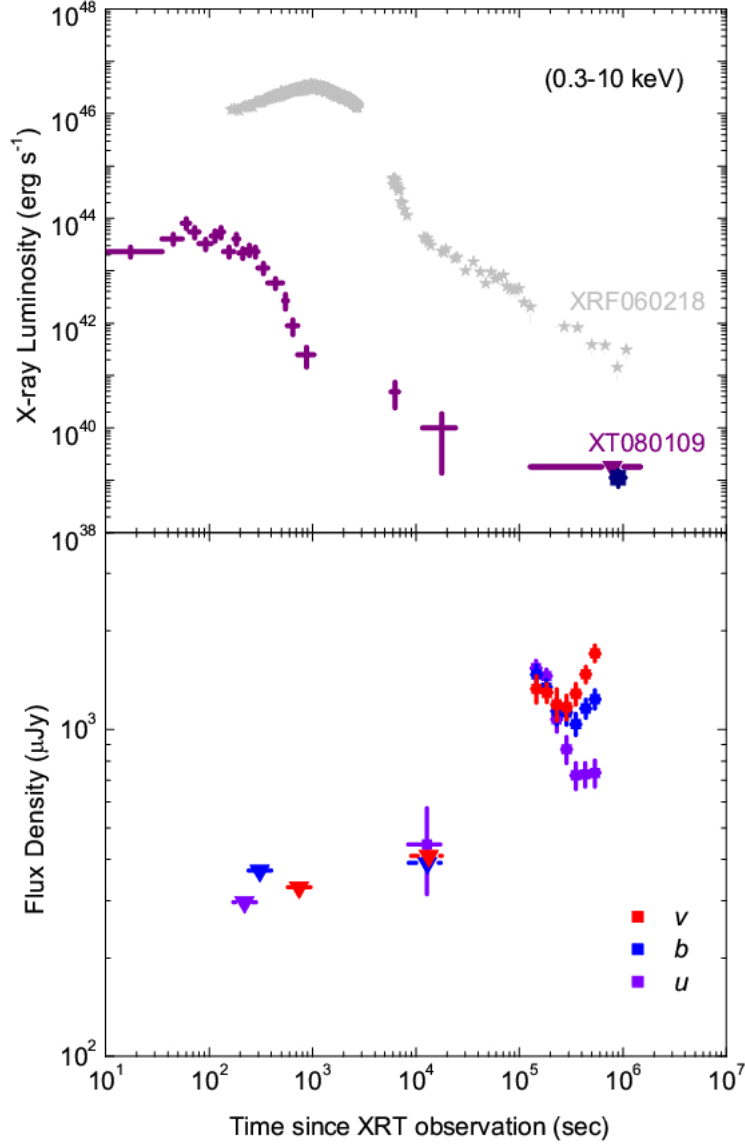
Figure 6.1: Multi-wavelength observation of XT 080109/SN 2008D. *Upper Panel*: The 0.3-10 keV unabsorbed light curves of XT 080109/SN 2008D (squares). The late upper limit from *Swift* measurement is nicely consistent with the *Chandra* measurement (navy square point). Note that the contamination from nearby X-ray sources has been corrected. Comparatively shown is the 0.3-10 keV unabsorbed light curves of XRF 060218/SN 2006aj (light grey) from Campana et al. (2006). *Lower Panel*: The *Swift*/UVOT's u (violet), b (blue), and v (red) light curves for XT 080109/SN 2008D. The Galactic extinction, $E(B-V)_{\mathrm{MW}} = 0.023$ (Schlegel et al. 1998), and the host extinction, $E(B-V)_{\mathrm{HOST}} = 0.7$ (Malesani et al. 2009), have been corrected.

model. The shock breakout emission is assumed to be in the wind and begin at a radius R_{br} where the optical depth of the stellar wind $\tau_{\mathrm{br}} \sim 1/\beta_{\mathrm{s}}$ (e.g., Matzner & McKee 1999), where β_{s} is the speed of the shock at the breakout point, in units of c. The duration of such a soft X$-$ray outburst lasts

$$T_{90} \sim (R_{\mathrm{ph}} - R_{\mathrm{br}})/(\beta_{\mathrm{s}}c), \tag{6.1}$$

where $R_{\rm ph}$ is the photospheric radius at which the optical depth of the wind $\tau_{\rm ph} \sim 2/3$.

The observed temperature ($T_{\rm br}$) and the luminosity ($L_{\rm obs}$) of the soft X-ray burst are thus related as

$$4\pi R_{\rm br}^2 \sigma T_{\rm br}^4 \sim \frac{R_{\rm ph}}{R_{\rm br}} L_{\rm obs}. \tag{6.2}$$

For simplicity, we assume that the number density of the wind can be estimated as $n = 3 \times 10^{35} \bar{A}_* R^{-2}$ cm^{-3}. This $\bar{A}_*$ can be much larger than the A_* identified in the late radio afterglow modeling because for $R < 100R_*$, the wind structure is very complicated and may be much denser than the simple extraction $n = 3 \times 10^{35} A_* R^{-2}$ cm^{-3} (e.g., Li 2007). So we have $\tau_{\rm br} \sim 2\bar{A}_* R_{\rm br,11}^{-1}$, $R_{\rm ph} \sim 1.5 \times 10^{11} \bar{A}_*$, and $R_{\rm ph}/R_{\rm br} \approx 1.5/\beta_{\rm s}$. Combing the last relation with eqs.(1) and (2), we have

$$\beta_{\rm s} \sim [\frac{27 L_{\rm obs}}{32\pi (cT_{90})^2 \sigma T_{\rm br}^4}]^{1/5} \sim 0.1\ L_{\rm obs,44}^{1/5} T_{90,2}^{-2/5} (\frac{kT_{\rm br}}{0.73\mathrm{keV}})^{-4/5}. \tag{6.3}$$

For a non-relativistic shock, $aT_{\rm br}^4/3 \approx n_{\rm br} m_{\rm p} (\beta_{\rm s} c)^2/2$ (e.g., Li 2007), where $n_{\rm br} = 3 \times 10^{35} \bar{A}_* R_{\rm br}^{-2}$ cm^{-3}. Combing with eq.(3), we have

$$\bar{A}_* \sim 10^4\ L_{\rm obs,44}^{2/5} T_{90,2}^{6/5} (\frac{kT_{\rm br}}{0.73\mathrm{keV}})^{12/5}. \tag{6.4}$$

With the observation data $L_{\rm obs,44} \sim 0.5$ and $T_{90,2} \geq 1$, for $kT_{\rm br} \sim (0.73,\ 0.36,\ 0.1)$ keV, we have $\beta_{\rm s} \leq (0.09,\ 0.15,\ 0.43)$ and $\bar{A}_* \geq (10^4,\ 1.7 \times 10^3,\ 77)$. The resulting $\bar{A}_*$ might be too large to be realistic even for $kT \sim 0.1$ keV and $T_{90} \sim 100$ sec. As can be seen, fine-tuning is needed for the shock breakout model to work in this particular event. Indeed, Chevalier & Fransson (2008) pointed out that if the observed emission is interpreted as blackbody emission, the temperature and radiated energy are close to expectations, considering that scattering dominates absorption processes so that spectrum formation occurs deep within the photosphere. Instead of going in this direction, we shall focus on another possible interpretation, i.e., the mildly relativistic outflow model for XT 080109.

In addition to the analysis of the X-ray spectrum itself, we also consider the simultaneous broadband UV/Optical-to-X-ray spectral energy distributions (SEDs). As shown in Fig. 6.1, there is no UVOT detection when the X-ray peaks at ~ 70 sec. Afterwards, during the first *ubv* exposures the X-ray light curve drops quite fast. To get reliable SED constraints, we integrate the X-ray flux over the *u*, *b*, *v* exposure times respectively (i.e., 180-263.4 s, 269-352.5 s, 706-789.4 s since the XRT observation) and then obtain the time-averaged flux in each filter. For each exposure period above, it is difficult to get meaningful X-ray spectral fitting. But if we combine the three periods into one, i.e., 180-789.4 sec, we find $\Gamma = 2.3 \pm 0.5$ ($\chi_{dof}^2 = 8.94/8$). Fig. 6.2 shows the time-averaged broadband SEDs, in which *u*, *b*, and *v* observations are combined and
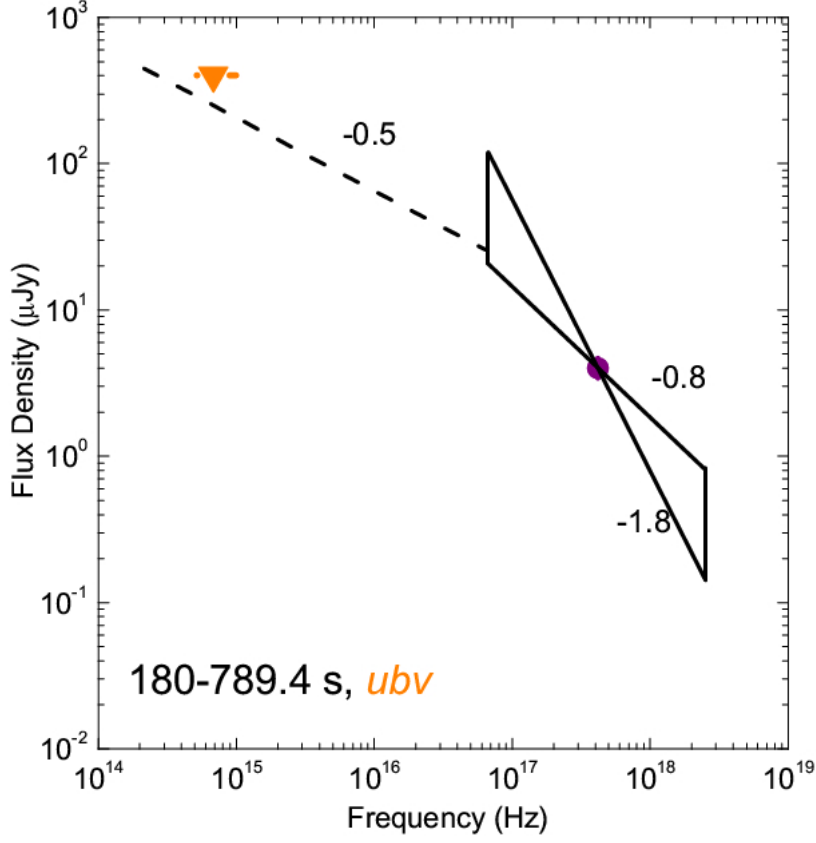
Figure 6.2: The time-averaged UV/Optical-to-X-ray SED during the prompt emission. The time considered covers the first *ubv* detections for XT 080109. A broken power-law from $F_\nu \propto \nu^{-0.5}$ in the UV/Optical to $\propto \nu^{-1.3}$ in the X-ray matches the 3σ *ubv* limit.

then averaged. As seen, a broken power-law from $F_\nu \propto \nu^{-0.5}$ in the UV/Optical to $\propto \nu^{-1.3}$ in the X-ray is consistent with the spectral observation. Even the real *ubv* flux is one order of magnitude lower than its upper limit, a Band function with the typical low-energy spectral index of ~ 0.0 and the typical high-energy spectral index of ~ 1.25 (see Figs. 7 and 9 in Preece et al. 2000) still matches the observation.

6.4.2   The XT powered by a mildly relativistic outflow

The XT's initial decline depends on its real onset time and should be steeper than $t^{-3.3}$ derived in the case of $\Delta t = t_{\mathrm{XT}} - t_{\mathrm{XRT}} \sim 0$ sec, where t_{XT} is the XT onset time and t_{XRT} the time for the XRT starting observation. If $\Delta t \sim -50$ sec, then the decline is as $\sim t^{-3.7}$. Such steep decays (i.e., decay index larger than $\sim$3) rules out that the XT is from the forward shock of an outflow. Therefore the overall smooth profile of this XT's light curve may favor the reverse shock model, in which the prompt X-rays are powered by the interaction of a relativistic outflow with its surrounding dense stellar wind. The number density of the stellar wind is $n = 3 \times 10^{35} A_* R^{-2}$ cm^{-3}, where

$A_* = [\dot{M}/10^{-5} M_\odot \text{ yr}^{-1}][v_w/(10^8 \text{ cm s}^{-1})] \sim 0.01 - 10$ is the wind parameter, $\dot{M}$ is the mass loss rate of the progenitor, and v_w is the velocity of the stellar wind (Chevalier 1998; Li & Chevalier 1999). Because of the low total luminosity of the XT outflow ($L_{\rm m} \sim 10^{44}$ erg s^{-1}) and the dense medium surrounding the progenitor, the XT outflow is almost stalled when the interaction takes places. So the reverse/forward shock regions move sub-relativistically

$$\Gamma_{\rm fr} \approx 1.1 L_{\rm m,44}^{1/4} A_{*,-1}^{-1/4}, \tag{6.5}$$

and the Lorentz factor of the shocked region with respect to the initial outflow is comparable to the initial Lorentz factor of the XT outflow ($\Gamma_{\rm i}$).

Eq. (6.5) suggests that a weak outflow with $L_{\rm m} \sim 10^{44}$ erg s^{-1} and $\Gamma_{\rm i} > \Gamma_{\rm fr}$ will be decelerated quickly. After the reverse shock crossed the outflow, essentially all the initial information of the outflow is lost. So our model ($\Gamma_{\rm i} \sim$ a few, see below) and Soderberg et al. (2008)'s ($\Gamma_{\rm i} \sim 1.5$) will give rise to almost the same late time afterglow emission and thus are undistinguishable. To reveal the nature of the XT outflow, the prompt Optical-to-Xray data, as plotted in Fig. 6.2, are crucially needed.

Now we estimate the synchrotron radiation of such a reverse shock at a distance $R_{\rm r} \sim 10^{13}$ cm. As usual we assume a fraction of $\epsilon_{\rm e}$ and $\epsilon_{\rm B}$ of the shock energy given to the electrons and magnetic field, respectively (Sari, Piran, & Narayan 1998). The minimum Lorentz factor of the reverse shock accelerated electrons is $\gamma_{\rm m,r} \sim (\Gamma_{\rm i} - 1)\epsilon_{\rm e}(p - 2)m_{\rm p}/[(p - 1)m_{\rm e}] \sim 1400$ for $\Gamma_{\rm i} \sim 3$, $p \sim 2.6$ and $\epsilon_{\rm e} \sim 0.5$, and the magnetic filed generated in the reverse shock region is $B_{\rm r} \sim 10^4$ Gauss $(\epsilon_{\rm B}/\epsilon_{\rm e})^{1/2} L_{44}^{1/2} R_{\rm r,13}^{-1}$. The typical synchrotron radiation frequency

$$\nu_{\rm m,r} \sim 2.8 \times 10^6 \text{ Hz } \gamma_{\rm m,r}^2 B_{\rm r} \sim 6 \times 10^{16} \text{ Hz},$$

which is in the soft X-ray band and matches the observations. The cooling Lorentz factor is $\gamma_{\rm c,r} \sim 7.7 \times 10^8/(B_{\rm r}^2 t) \ll \gamma_{\rm m,r}$, so the reverse shock is in the fast cooling phase and the UV/Optical to soft X-ray spectrum should be $F_\nu \propto \nu^{-0.5}$, which is consistent with the time-averaged prompt UVOT-XRT spectrum, as shown in Fig. 6.2. It is also possible that the prompt spectrum of XT 080109 may be harder than $\nu^{-0.5}$ and is inconsistent with a simple fast cooling synchrotron radiation spectrum. As shown in Fig. 7 of Preece et al. (2000), actually the low energy spectra of most GRBs are harder than $\nu^{-0.5}$ and the typical spectrum is $\propto \nu^{0.0}$ instead. So the possible hard low energy spectrum of XRT 080109 supports the idea that such an event is a low energy analogy of GRBs/XRFs.

Suppose the reverse shock ceases at a time $t_{\rm cea}$, the photons from higher latitude can extend the emission duration to $\sim 2t_{\rm cea}$ but not longer. After that the detectable X-ray emission would drop with time very sharply. As a result, with a reverse shock model we may be able to interpret

both the smoothness and the sharp decline of the XT light curve. The outflow is likely to be mildly relativistic, because for $\Gamma_i \sim$ tens$-$hundreds, $\gamma_{m,r} \sim 10^4 - 10^5$ and $\nu_{m,r} \sim 10 - 10^3$ keV, and as a result, the XRT spectrum should be $\propto \nu^{-0.5}$, which is inconsistent with the observed value. While at the other extreme, a marginally relativistic ($\Gamma_i \sim 1.2$) outflow model is also disfavored because the reverse shock would be very weak. With typical shock parameters, the emission of such a weak reverse shock could not peak in the soft X-ray band and would be likely to be outshone by the forward shock X-ray emission.

6.4.3 The early X-ray afterglow ($\lesssim 10^4$ sec) from the forward shock of XT remnant

As mentioned before, the mildly relativistic XT outflow has been decelerated in the reverse shock phase. We calculate the emission in the sub-relativistic blast wave when it sweeps up the surrounding stellar wind medium. Here two possibilities arise because we don't know when the thermal UV/optical emission emerged while observationally the earliest UV/optical component was at $t \sim 10^4$ sec. One possibility is that the thermal emission existed shortly after the XT. Therefore the X-ray afterglow is dominated by the inverse Compton scattering of the thermal photons by the forward shock electrons (i.e., the inverse Compton model). The other possibility is that for $t < 10^4$ sec the thermal emission can be ignored because the X-ray afterglow is dominated by the synchrotron radiation of the forward shock electrons (i.e., the synchrotron radiation model).

The inverse Compton model

At $t \sim 10^4$ sec, UVOT detected a thermal-like component. Very similar phenomena has been found in XRF 060218 and is likely contributed by the expanded hot stellar envelope with a velocity ~ 0.1 c (Campana et al. 2006). The thermal UV/optical photons with a luminosity $L_{\rm th} \sim 10^{42}$ erg s^{-1} will cool the forward shock electrons of the XT remnant. Now we assume such a component emerged shortly after the XT. In the blast wave, the generated magnetic field energy density can be estimated as $U_B \approx 430$ erg cm^{-3} $(\beta/0.23)^2 R_{14}^{-2} \epsilon_{B,-1} A_*$ while the thermal photon energy density is $U_{\rm th} \approx L_{\rm th}/(4\pi R^2 c) \approx 256$ erg cm^{-3} $L_{\rm th,42} R_{14}^{-2}$. For $t \lesssim 10^4$ sec and $\epsilon_B \ll 0.1$, we have $U_B < U_{\rm th}$. The cooling of the forward shock electrons is dominated by inverse Compton scattering thermal photons from the SN.

The electron with a random Lorentz factor $\gamma_e \sim 10$ will boost the thermal SN photons to keV energy range. To produce an X-ray spectrum $\propto \nu^{-1.1}$, usually we need $\max\{\gamma_m, \gamma_c\} < 10$ unless $p > 3$, where the typical Lorentz factor of the shock-accelerated electrons $\gamma_m \approx 8\, C_p (\beta/0.5)^2 \epsilon_{e,-1}$, and the cooling Lorentz factor of electrons $\gamma_c \approx 3 \times 10^7/(U_{\rm th} t) \sim 10 L_{\rm th,42}^{-1} R_{14}^2 t_4^{-1}$. So the requirement that $\max\{\gamma_m, \gamma_c\} < 10$ can be satisfied for $t < 10^4$ sec.

In this case, the X-ray luminosity is a fraction of the total radiation power of shocked electrons, i.e.,

$$
\begin{aligned}
L_{\rm rad} &\sim 2\pi\epsilon_e\beta^3 n m_p c^3 R^2 \min\{1, (\gamma_m/\gamma_c)^{p-2}\} \\
&\sim 6\times 10^{40}\ {\rm erg\ s^{-1}} \epsilon_{e,-1}(\beta/0.2)^3 A_* \min\{1, (\gamma_m/\gamma_c)^{p-2}\}.
\end{aligned}
\tag{6.6}
$$

For $\gamma_c > \gamma_m$, $\min\{1, (\gamma_m/\gamma_c)^{p-2}\} = (\gamma_m/\gamma_c)^{p-2} \propto t^{2-p}$. The early X-ray afterglow luminosity $L_{\rm X} \sim 10^{40} t_4^{-1.1}$ erg s^{-1} then suggests that $\beta \propto t^{-(p-3.1)/3}$ and $E_{\rm tran} \approx 4\pi\beta^2 R^3 n m_{\rm p} c^2 \approx 3 \times 10^{46}(\beta/0.2)^2 A_* R_{14}$ erg.

The synchrotron radiation model

We calculate the synchrotron radiation of the sub-relativistic forward shock when it sweeps up the surrounding stellar wind medium. The minimum Lorentz factor of the shocked electrons, the magnetic field and the cooling Lorentz factor are $\gamma_{\rm m} \approx 32\ C_{\rm p}\beta^2\epsilon_{e,-1}$, $B \approx 15$ Gauss $\beta R_{15}^{-1}\epsilon_{\rm B,-1}^{1/2}A_{*,-1}^{1/2}$, and $\gamma_{\rm c} \approx 34\ \beta^{-2}R_{15}^2\epsilon_{\rm B,-1}^{-1}A_{*,-1}^{-1}t_5^{-1}$, respectively, where $C_{\rm p} \equiv 3(p-2)/(p-1)$. The maximum specific flux, the typical synchrotron radiation frequency and the cooling frequency (Sari, Piran, & Narayan 1998) are respectively given by

$$
F_{\nu,{\rm max}} \approx 1\ {\rm Jy}\ \beta\epsilon_{\rm B,-1}^{1/2}A_{*,-1}^{3/2}D_{\rm L,25.9}^{-2},
\tag{6.7}
$$

$$
\nu_{\rm m} \approx 4.4 \times 10^{10}\ {\rm Hz}\ \beta^5 C_{\rm p}^2 R_{15}^{-1}\epsilon_{e,-1}^2\epsilon_{\rm B,-1}^{1/2}A_{*,-1}^{1/2},
\tag{6.8}
$$

$$
\nu_{\rm c} \approx 4.8 \times 10^{10}\ {\rm Hz}\ \beta^{-3} R_{15}^3\epsilon_{\rm B,-1}^{-3/2}A_{*,-1}^{-3/2}t_5^{-2},
\tag{6.9}
$$

where $D_{\rm L}$ is the luminosity distance of the source. So the X-ray flux can be estimated as

$$
\begin{aligned}
F_{\nu_{\rm X}} = 1.1 \times 10^{-2}\ \mu{\rm Jy}\ \nu_{\rm X,17}^{-p/2}\ &\beta^{(5p-6)/2}\epsilon_{e,-1}^{p-1}\epsilon_{\rm B,-1}^{(p-2)/4} \\
&A_{*,-1}^{(p+2)/4}D_{\rm L,25.9}^{-2}C_{\rm p}^{p-1}R_{15}^{(4-p)/2}t_5^{-1}.
\end{aligned}
\tag{6.10}
$$

If $\beta \sim$const., i.e., the outflow has not been decelerated significantly, we have $R \approx \beta c t$ and $F_{\nu_{\rm X}} \propto t^{(2-p)/2}$. The decline is thus too shallow to be consistent with the detected $\propto t^{-1.1}$ for the early X-ray afterglow. We then consider an alternative in which the outflow with an energy distribution $E(\geq \beta\Gamma) \propto (\beta\Gamma)^{-k}$ has entered the Sedov regime, thus we have $\beta \propto t^{-\frac{1}{3+k}}$ and $R = \frac{3+k}{2+k}\beta c t \propto t^{\frac{2+k}{3+k}}$. Accordingly, $F_{\nu,{\rm max}} \propto t^{-\frac{1}{3+k}}$, $\nu_{\rm m} \propto t^{-\frac{7+k}{3+k}}$, and $\nu_{\rm c} \propto t$, respectively. The light curves are

$$
F_\nu \propto
\begin{cases}
t^{\frac{4+k}{3(3+k)}} & \text{for}\ \ \nu < \nu_{\rm m} < \nu_{\rm c}, \\
t^{-\frac{1}{3+k}[1+\frac{(p-1)(7+k)}{2}]} & \text{for}\ \ \nu_{\rm m} < \nu < \nu_{\rm c}, \\
t^{-\frac{1}{3+k}[1+\frac{(p-1)(7+k)}{2}]+\frac{1}{2}} & \text{for}\ \ \nu > \max\{\nu_{\rm c}, \nu_{\rm m}\}.
\end{cases}
\tag{6.11}
$$

So the early X-ray afterglow decline $F_{\nu_{\mathrm{X}}} \propto t^{-1.1}$ suggests a $k \sim (1,\ 0)$ for $p \sim (2.5,\ 2.2)$, implying that after the prompt emission, the XT remnant outflow has a shallow energy distribution. So we assume $E_{\mathrm{tran}} \approx 4\pi\beta^2 R^3 n m_{\mathrm{p}} c^2$ (corresponding to $p \sim 2.2$), which yields

$$\beta \sim 0.23\ E_{\mathrm{tran},46.5}^{1/3} A_*^{-1/3} t_4^{-1/3}. \tag{6.12}$$

Eq. (6.10) thus reduces to

$$F_{\nu_{\mathrm{X}}} \sim 0.04\ \mu\mathrm{Jy}\ \epsilon_{\mathrm{e},-1}^{1.2} E_{\mathrm{tran},46.5}^{1.1} t_4^{-1.2}, \tag{6.13}$$

which is consistent with the XRT flux $\sim 0.06\ \mu\mathrm{Jy}$ at 10^{17} Hz at $t \sim 10^4$ sec (see Fig. 6.1). The outflow energy inferred above is $E_{\mathrm{tran}} \sim 3 \times 10^{46}$ erg, which is comparable to the isotropic energy of the XT.

Within this scenario, the forward shock UV/optical emission should drop with time as $\sim 200\ t_3^{-1.1}\ \mu\mathrm{Jy}$ for $t > 800$ sec, i.e., after the cease of the prompt emission. Such a emission component is consistent with the upper limit of the V-band flux ~ 0.5 mJy at $t \sim 10^3$ sec.

6.4.4   The late X-ray afterglow ($\gtrsim 2 \times 10^4$ sec) and radio afterglow powered by the SN shock

As shown in Eq. (6.12), the XT outflow has been decelerated significantly at a time $\sim 10^4$ sec and should be caught up with by the fast part of SN 2008D's ejecta. As a result, the late time X-ray and radio afterglow emission should be relevant to the SN shock. The late X-ray afterglow data is very limited and may be attributed to the inverse Compton of the SN UV/optical photons by the forward shock electrons (Soderberg et al. 2008). We do not discuss it further and just focus on the radio afterglow emission.

Radio emission below the self-absorption frequency, ν_{a}, would be suppressed significantly. Through the standard treatment (Rybicki & Lightman 1979), in the case of $\nu_{\mathrm{m}} < \nu_{\mathrm{a}} < \nu_{\mathrm{c}}$, we have

$$\nu_{\mathrm{a}} \approx 3.5 \times 10^{11}\ \mathrm{Hz}\ \beta^{\frac{4p-6}{p+4}} t_5^{-1} \epsilon_{\mathrm{e},-1}^{\frac{2(p-1)}{p+4}} \epsilon_{\mathrm{B},-1}^{\frac{p+2}{2(p+4)}} A_{*,-1}^{\frac{p+6}{2(p+4)}}. \tag{6.14}$$

The radio afterglow thus will peak when ν_{a} crosses the observational frequency, ν_{obs} (see also Chevalier 1998), at

$$t_{\mathrm{peak}} \sim 50\ \mathrm{day}\ \left(\frac{\nu_{\mathrm{a}}}{8.5\ \mathrm{GHz}}\right)^{-1} \beta^{\frac{4p-6}{p+4}} \epsilon_{\mathrm{e},-1}^{\frac{2(p-1)}{p+4}} \epsilon_{\mathrm{B},-1}^{\frac{p+2}{2(p+4)}} A_{*,-1}^{\frac{p+6}{2(p+4)}}. \tag{6.15}$$

For parameters $\epsilon_{\mathrm{e},-1} \sim 2$, $\epsilon_{\mathrm{B},-1} \sim 0.02$, $\beta \sim 0.2$, $A_* \sim 1$ and $p \sim 2.5$, SN 2008D's radio afterglow peaks at ~ 15 days with a flux $F_{\nu_{\mathrm{radio,peak}}} \sim 4$ mJy at 8.5 GHz. For $\nu_{\mathrm{m}} < \nu_{\mathrm{radio}} < \nu_{\mathrm{a}} < \nu_c$, $F_{\nu_{\mathrm{radio}}} \propto \beta^2 t^{5/2}$. For $\beta \sim$ const., we have $F_{\nu_{\mathrm{radio}}} \propto t^{5/2}$, which is consistent with the radio

observations.

Therefore, the total energy of the SN fastest component is no less than

$$E_{\mathrm{SN}}(\beta \geq 0.2) \sim 3 \times 10^{48} \ \mathrm{erg} \ A_*^{\frac{5(p-2)}{4(2p-1)}} \epsilon_{\mathrm{e},-1}^{\frac{3(1-p)}{2p-1}} t_6, \tag{6.16}$$

.

For $\nu_{\mathrm{m}} < \nu_{\mathrm{radio}} < \nu_{\mathrm{a}} < \nu_c$, $F_{\nu_{\mathrm{radio}}} \propto \beta^2 t^{5/2}$. For $\beta \sim (\mathrm{const.}, t^{-1/(3+k)})$, we have $F_{\nu_{\mathrm{radio}}} \propto (t^{5/2}, t^{5/2-2/(3+k)})$, respectively. As long as $\nu_{\mathrm{obs}} > \nu_{\mathrm{a}}$ and $\beta \propto t^{-1/(3+k)}$, the light curve is described by Eq. (6.11).

As seen, the peak time and flux are consistent with the radio observation (see Fig. 7 of Soderberg et al. 2008) and the detected $\sim t^{2.5}$ increase implies that $\beta \sim \mathrm{const} \sim 0.2$. The total energy of the SN fastest component is no less than

$$E_{\mathrm{SN}}(\beta \geq 0.2) \sim 3 \times 10^{48} \ \mathrm{erg} \ A_*^{\frac{5(p-2)}{4(2p-1)}} \epsilon_{\mathrm{e},-1}^{\frac{3(1-p)}{2p-1}} t_6, \tag{6.17}$$

which is consistent with the estimate of Soderberg et al. (2008).

In Fig. 6.3 we plot the identified energy distribution of the outflows associated with XT 080109/SN 2008D, in the context of ordinary SNe Ibc, XRF/HN, and GRB/HN. As seen, XT/SN marks the transition between ordinary SN Ibc and XRF/HN.

6.5 Conclusion and Discussion

We have shown that the prompt and the early X-ray afterglow of XT 080109 can be interpreted as the emission powered by a mildly relativistic outflow expanding into a stellar wind medium. XT 080109/SN 2008D then presents a possible evidence for a mildly relativistic outflow, with $\sim 10^{46} - 10^{47}$ erg, preceding the outburst of a normal SN Ibc, which supports the previous speculation on SN 2005bf (Folatelli et al. 2006). In the XT 080109/SN 2008D event, such a weak mildly-relativistic outflow has been decelerated significantly by the dense stellar wind medium in a timescale of $10^2 - 10^3$ sec. So continuous observations since the very beginning of the explosion of a massive star, as in XT 080109/SN 2008D, is crucially important to constrain the existence of a weak but mildly-relativistic outflow component.

A detection of XT 080109/SN 2008D in a 3-years performance of Swift/XRT gives a local rate of its kind as $1/3\mathrm{yr}/(0.0276\mathrm{Gpc})^3 \sim 1.6 \times 10^4 \mathrm{yr}^{-1}\mathrm{Gpc}^{-3}$. This rate, based on a unique event, is uncertain from statistical point of view. First, *Swift*/XRT does not have a very wide view of field to look at the sky; Second, usually *Swift*/XRT doesn't do the X-ray transient trigger as *Swift*/BAT to the γ-ray transients. To get better estimate of the event rate, we make statistics by combining this event with other similar events. Putting XT 080109 and nearby GRB 980425
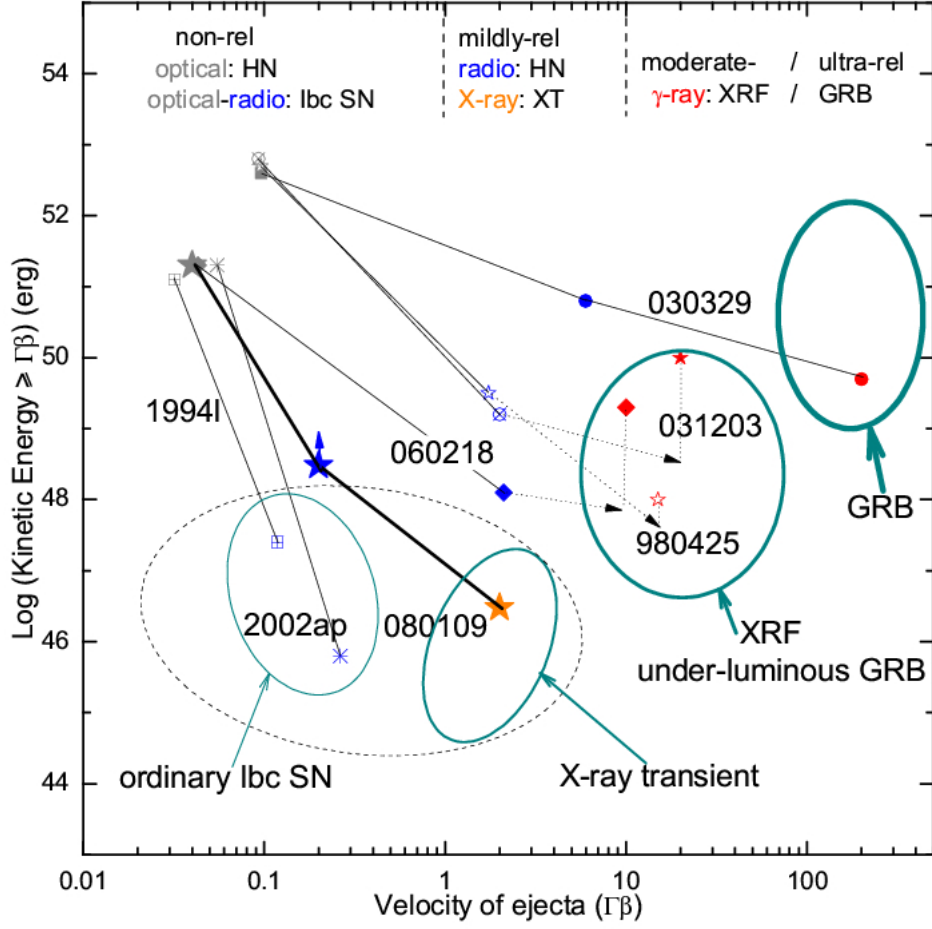
Figure 6.3: The kinetic energy VS. ejecta velocity for GRB-HN, under-luminous GRB-/XRF-HN, X-ray transient-SN, and ordinary SNe Ibc. The dashed ellipse represents the hypothetical case that every SN Ibc has an accompanying X-ray transient. The abbreviations "rel" and "HN" represent "relativistic" and "broad-lined SN Ic", respectively. From left to right, the velocity domain can be roughly divided into non-relativistic, mildly relativistic, and moderate-/ultra-relativistic parts. As seen, γ-ray traces the moderate-/ultra-relativistic material in XRF/GRB (in red); X-ray/radio traces the mildly relativistic material in X-ray transient/broad-lined SN Ic, respectively (in orange and blue); and optical-radio/optical traces the non-relativistic material in ordinary SN Ibc/broad-lined SN Ic, respectively (in grey-blue and grey). The sudden drop of the energy distribution in GRB 031203 and XRF 060218 after the prompt emission (dashed arrow lines) might be due to the geometry correction and/or a high GRB/XRF efficiency. Part of data is from Soderberg et al. (2006a) and Kaneko et al. (2006). XT 080109/SN 2008D marks a potential transition between ordinary SN Ibc and under-luminous GRB-/XRF-HN.

($z = 0.0085$) together, then these two events, detected in 10 years and within a distance 44 Mpc, give a lower limit of the local event rate as $1/10\mathrm{yr}/(0.044\mathrm{Gpc})^3 \sim 4 \times 10^3\,\mathrm{yr}^{-1}\mathrm{Gpc}^{-3}$, accounting for $\sim 10\%$ of the rate of total local SNe Ibc. This rate is a factor of $\sim 10 - 100$ more than, and thus at odds with, that of the classical GRB sample. In view of the high spectroscopic similarity between late SN 2008D and SN 1999ex (Valenti et al. 2008), these two events give a rate lower limit as $\sim 1.7 \times 10^3\,\mathrm{yr}^{-1}\mathrm{Gpc}^{-3}$. In addition, SN 2008D is distinguished for its apparent Ic→Ib

spectroscopic evolution. It was classified as peculiar Type Ic on Jan 11, and then as a Type Ic with possibly some He as seen in NIR spectra on Jan 13-15 (Malesani et al. 2009), and later to a Type Ib on Jan 21 (Modjaz et al. 2008 and reference therein). This evolution is reminiscent of SN 2005bf (Folatelli et al. 2006). A combination of SN 2008D and SN 2005bf would give the rate lower limit as $\sim 1.6 \times 10^3 \, \mathrm{yr}^{-1} \mathrm{Gpc}^{-3}$. From the above statistics, the rate of the XT 080109-like events could be of order $\sim 10^4 \, \mathrm{yr}^{-1} \mathrm{Gpc}^{-3}$, the same order of the total SNe Ibc. Reliable rate estimate needs more very early SN Ibc observations in the future.

The host galaxy, NGC 2770, a star-forming Sc galaxy, stands out from the star-forming dwarf galaxies typically hosting GRBs/XRFs. In terms of the metallicity of the host vicinity, XT 080109, with $12 + \log(\mathrm{O/H}) = 8.9 \pm 0.2$ (Berger & Soderberg 2008b), puts itself more likely in the sample of broad-lined SNe Ic without GRBs than in the sample of nearby broad-lined SNe Ic associated with GRBs/XRFs (Sollerman et al. 2005; Modjaz et al. 2008b; Prieto et al. 2008). But note that there seems no distinct line between these two samples, so the metallicity measurement at the SN 2008D site also seems to be between the above two samples (Modjaz et al. 2008b; Thöene et al. 2008b), making a continuum distribution.

As a result, this event may unveil a continuum from energetic GRB to ordinary SN Ibc.

(1) From ordinary SN Ibc (bottom-left of Fig. 6.3) to energetic GRB (top-right of Fig. 6.3), the capability of their central engines driving a relativistic outburst is becoming stronger and stronger. XT marks the transition between ordinary SN Ibc and under-luminous GRB-/XRF-HN. Meanwhile, whether or not every SN Ibc has an accompanying XT is still uncertain. For this reason in Fig. 6.3 we mark the sum of ordinary SN Ibc and XT using a dashed ellipse.

(2) While Soderberg et al. (2006a) showed that producing GRBs/XRFs needs a mildly relativistic ejecta carrying at least 10^{48} erg, we show here that the X-ray transient population may couple $\sim 10^{46}$ erg to a mildly relativistic, quasi-spherical ejecta.

(3) While under-luminous GRBs/XRFs are likely powered by moderate-relativistic material, X-ray transients are likely powered by mildly relativistic material.

(4) Materials with higher bulk Lorentz factor tend to have a shallower energy-velocity distribution while materials with lower bulk Lorentz factor tend to have a steeper energy-velocity distribution. The decay laws in terms of velocity for each event in Fig. 6.3 (from left to right) matches this principle.

6.6 Acknowledgements

Chapter 7

Conclusion and Outlook

This thesis focuses on GRB afterglows. As is known, nowadays the GRB study not only invokes a range of targets like the GRBs themselves, the afterglow, host galaxies, but also invokes as many bandpasses as possible, such as GeV, MeV, keV, UV, optical, nearinfrared, radio, and so on. When we want to infer something about a GRB, we often need to consider evidence from several different of these aspects to get insight in the underlying GRB physics.

Swift has brought many surprises to the GRB community, one of which is the discovery of the so-called "canonical" X-ray afterglow lightcurve for long GRBs, which shows a significant fraction of long GRBs may have early-time energy injection to their early afterglows, leading to a shallow decay before the normal pre-jetbreak + post-jetbreak decay. The behavior of shallow decay is not witnessed as a norm in short GRB X-ray afterglows, partly because short bursts are relatively fewer and their afterglows are relatively dimmer. However, we do see this shallow decay apparently exist in short GRB 051221A. There could be different interpretations to reproduce this shallow decay, either due to intrinsic effect (e.g., energy injection from the central engine) or extrinsic effects (e.g., two-component model for the afterglow, or inverse Compton scattering of the optical photons by hot electrons). The shallow decay phase even might be an artificial product if the zero time for *Swift*/XRT data is ahead of that for *Swift*/BAT (but the probability of this scenario should be very low).

Meanwhile, we also see X-ray flares take place in both long and short GRB afterglows on a wide range of timescales. This probably requires late-time energy production within the GRB engine. Now that the flaring activity is present in both classes of bursts, its origin may be the same for both classes. For example, considering that the final status for both progenitors could be a black hole + an accretion disk, the flare could come from the instabilities in the accretion process (see Perna, Armitage, & Zhang 2006). As for the shallow decay phase in short GRBs, it might be related to the diversity of short GRBs. In detail, short GRBs may have sub-classes: mergers of NS-NS and mergers of BH-NS. Short GRBs due to the merger of BH-NS may mimic long GRBs in some aspects, such as host environment, presence of energy injection in the afterglow, and so on. For this sub-class of short bursts, they progenitors could first undergo a step of quasi-magnetar and finally evolve to the BH + accretion disk system. That is to say, magnetohydrodynamic

processes may be required to power such bursts instead of neutrino annihilation mechanism. We think GRB 051221A may be a representative of this sub-class.

Swift X-ray afterglow lightcurves are also distinguished by their "weird" behavior relative to optical afterglow lightcurve. If both of them are purely due to the external shock, then they should roughly fit the closure relations predicted by the standard fireball model. As a matter fact, sometimes we see that the X-ray is higher than the inferred value according to optical, sometimes optical is higher than the inferred value according to optical. Since the X-ray excess is shown in a significant fraction of GRBs, this indicates that X-ray afterglows could be dominated by the prolonged activity of the central engine instead of the emission from the external shock. In XRF060218, the multi-wavelength afterglow data cannot be interpreted as from the same physical region, and the X-rays mostly come from the central engine.

Another surprise by *Swift* is the discovery of SN-less nearby GRBs 060505 and 060614. When it comes to the gamma-ray durations of these two bursts, they belong to the conventional long class. It is widely believed that long GRBs are produced by core-collapse of massive stars that have lost their Hydrogen in the outer layer before explosion, and thus should be accompanied with visible SNe Ibc. Therefore there are three possibilities here. The first one is that the two bursts are actually merger bursts even their gamma-ray durations are long; or to be more accurate, their long-duration prompt gamma-ray emission consists of a short-duration hard-spectrum spike similar to conventional short bursts and a long-duration soft-spectrum extended emission as suggested by some people. We found GRB 080503 consists of a short-duration hard-spectrum spike and a strong long-duration hard-spectrum extended emission. This event has very dim optical-to-Xray afterglow and no host galaxy was found down to very deep limit. If one thinks this is a merger burst, then a merger burst could be a burst featuring a short-duration spike and a long-duration extended emission. This is indeed not easy to handle because GRB prompt gamma-ray lightcurves are complicated, containing more or less pulses. The second possibility is that both GRBs 060505 and 060614 are collapsar bursts with little Ni produced so that we cannot see a regular bright SN Ibc. This possibility has been inferred to be plausible by SN simulations. But we are not sure if the scenario which passes the SN simulation would necessarily pass the reality. The third possibility, though seemingly less likely, is that the GRB 060614-like bursts have different origin other than conventional long and short GRBs. There has been speculation that such bursts could be due to the intermediate black hole swallowing a star. If GRB060614-like events never happen again, then this event could just be peculiar burst: it actually occurs at high redshift but overlaps with a nearby galaxy along the line of sight.

In comparison with relativistic GRB 060614 without visible SN Ibc, we propose mildly relativistic X-ray transient 080109 with visible Ic→Ib SN 2008D. This X-ray transient was discovered by accident, but may be a tip of the iceberg. The X-ray spectrum can either be fit with a power-

law or a single blackbody, with the former a bit better than the latter. If the observed emission is interpreted as blackbody emission, the temperature and radiated energy are close to expectations, considering that scattering dominates absorption processes so that spectrum formation occurs deep within the photosphere. This is somewhat fine-tuning. We go for an alternative interpretation, motivated by the gap between ordinary SNe Ibc and energetic hypernovae (HNe). We find the observational data are also close to expectations if the X-ray transient is interpreted as the reverse shock emission of a mildly relativistic wide-angle outflow interacts with the surrounding wind medium. If not every SN Ibc has relativistic ejecta, then such events only account for a fraction of SNe Ibc. To distinguish these two models, we need a wide field-of-view X-ray survey mission together with a wide field-of-view UV/optical telescope because the prompt optical-to-Xray SED plays an important role here.

The outlook for the thesis has two aspects: one is for GRBs, and the other is for myself.

For GRBs, I think *Swift*, *Fermi*, and other telescopes will keep bringing new surprises to the GRB community. Also, a large sample with known redshifts will be established in a few years. On the other hand, new observations bring new problems. In the last few years, GRB classification has become an open question. Even if one takes information from several aspects, it is still difficult to infer whether the given burst is due to a collapsar, a merger or something else. For example, so far the most distant burst is GRB 080913 at $z \approx 6.7$. Its duration in the cosmological rest frame is similar to that of the short population. Presumably this could be a collapsar event, but it seems that the merger origin cannot be reliably ruled out by observational data. Since we even cannot answer the GRB classification question, surely GRB will still be a "hot" branch in astronomy in the foreseeable future.

For me, after I submit the thesis I will try to get my 080109 work accepted as soon as possible. And also submit the GRB 081109A work as soon as possible (Jin, Xu, Fan, & Wei, 2009, to be submitted). In this work, I extracted the X-ray lightcurve and the X-ray spectra at different times (see Fig. 7.1). The X-ray data indicates the afterglow first undergoes the WIND-like medium and then expands into the ISM-like medium at some point where there should be density jump thus accordingly afterglow lightcurve jump.

After these two works, I plan to finish my first purely observational work on the dust properties of the host galaxy of GRB 080605 (Xu et al., in prep). We have found the 2175AA dust extinction feature from its afterglow absorption spectrum taken at VLT/FORS. Shown in Fig. 7.2 below is the 300V spectrum of the afterglow. Our goal is to study the extinction properties of GRB host galaxies. So far, people simply *assume* the extinction properties of a GRB host galaxy are similar to those of the Small Magellanic Cloud, the Large Magellanic Cloud, or the Milky Way. But this assumption has not been reliably tested yet. GRB hosts may have their own dust extinction curve other than any of the above three. We need to have a GRB sample covering a wide redshift
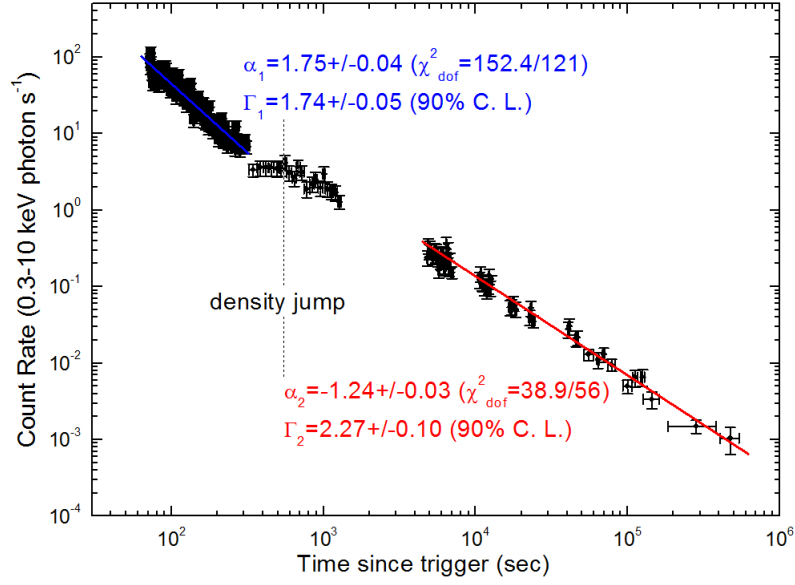
Figure 7.1: The 0.3-10 keV afterglow lightcurve of GRB 081109A. Also shown are the temporal and spectral indexes at early and late times.
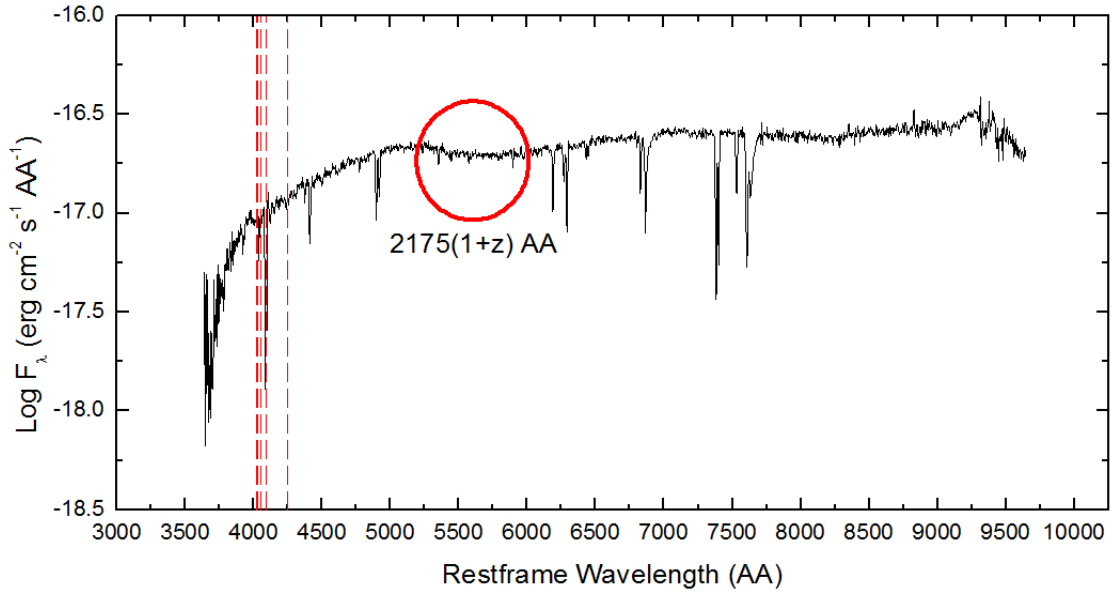

Figure 7.2: The 300V spectrum taken from VLT/FORS2 for GRB 080605 (GCN, Circ. 7832). The 2175 Å absorption feature of the host galaxy is relatively seen in the spectrum. This feature has previously been seen also in the afterglow spectrum of GRB 070802 (Elíasdóttir et al. 2008).

range to investigate what the GRB host extinction behaves and how it evolves with time/redshift.

Overall, I plan to continue with GRB research in the foreseeable future.

Chapter 8

Statement of coauthorship

8.1 Paper I

The Interpretation and Implication of the Afterglow of GRB 060218

by

Y. Z. Fan, T. Piran, & D. Xu

JCAP 0609, 013 (2006)

Chapter 3 is based on this paper. When XRF 060218/SN 2006aj just happened, D. Xu was observing it at the Danish 1.5m telescope in La Silla, Chile. D. Xu and Y. Z. Fan started to discuss this event while following this event at the same time. Y. Z. Fan and T. Piran led the discussion to the final model adopted in the paper. This event led us to conclude that its X-ray afterglow should be attributed to the continued activity of the central engine (within the collapsar scenario could arise from fall-back accretion onto the nascent black hole) while the radio afterglow can be interpreted as the regular external forward shock emission.

Dong Xu   Yi-Zhong Fan

8.2 Paper II

The X-ray afterglow flat segment in short GRB 051221A: Energy injection from a
millisecond magnetar?

by

Y. Z. Fan & D. Xu

MNRAS 372, 19 (2006)

Chapter 4 is based on this paper. D. Xu and Y. Z. Fan fitted the afterglow lightcurves
independently. Y. Z. Fan had the idea first. In Soderberg et al. (2006, ApJ, 650, 261) and
Burrows et al. (2006, ApJ, 653, 468), the authors found an episode of almost constant energy
injection in the afterglow lightcurves of short GRB 051221A. For the first time we showed that,
for a short burst, this energy injection can be accounted for if the central engine is a millisecond
magnetar.

Dong Xu   Yi-Zhong Fan

8.3   Paper III

In search of progenitors for supernova-less GRBs 060505 and 060614:
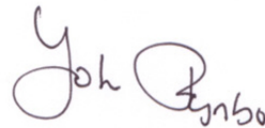re-examination of their afterglows

by

D. Xu, R. L. C. Starling, J. P. U. Fynbo, et al.

ApJ in press (2009)

Chapter 5 is based on this paper. D. Xu wrote the paper and had the idea of this work together with J. P. U. Fynbo. J. P. U. Fynbo did the photometry of the afterglow of GRB 060505. D. Watson provided the Watcher photometry of the afterglow of GRB 060614. R. L. C. Starling did the SEDs of GRB 060505 and GRB 060614, and D. Xu double checked the SEDs. D. Xu also did the rest part of this work mostly.

Dong Xu   Johan Fynbo

8.4   Paper IV

Mildly relativistic X-ray transient 080109 and SN2008D: Towards a continuum
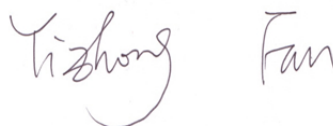from energetic GRB/XRF to ordinary SN Ibc

by

D. Xu, Y. C. Zou, & Y. Z. Fan

ApJ under the second review (2008)

Chapter 6 is based on this paper. D. Xu wrote the paper and had the idea of this work together with Y. Z. Fan, and discussed continuously since the discovery of this event. D. Xu was also responsible for the *Swift* data reduction. In this work we argue that XT 080109/SN 2008D fills in the gap between the energetic GRB/XRF-HN and the ordinary SN Ibc.

Dong Xu   Yi-Zhong Fan

Chapter 9

Publication list during my PhD

This Appendix lists all works I have been involved in during my PhD period.

On referred journal:

(15). **D. Xu**, R. L. C. Starling, J. P. U. Fynbo, J. Sollerman, S. Yost, D. Watson, S. Foley, P. T. O'Brien, J. Hjorth, D. Malesani "In search of progenitors for supernova-less GRBs 060505 and 060614: re-examination of their afterglows", 2009, **ApJ in press**

(14). J. Gorosabel, A. de Ugarte Postigo, A. J. Castro-Tirado, I. Agudo, M. Jelinek, S. Leon, T. Augusteijn, J.P.U. Fynbo, J. Hjorth, M. J. Michalowski, **D. Xu**, P. Ferrero, D. A. Kann, S. Klose, A. Rossi, J. P. Madrid, A. LLorente, M. Bremer, J.-M. Winters, "Simultaneous polarization monitoring of SN2007uy and the axisymmetric SN2008D/XRF080109: isolating geometry from dust", 2008, **ApJL submitted**, arXiv:0810.4333

(13). D. Malesani, J. P. U. Fynbo, J. Hjorth, G. Leloudas, J. Sollerman, M. D. Stritzinger, P. M. Vreeswijk, D. J. Watson, J. Gorosabel, M. J. Michalowski, C. C. Thöne, T. Augusteijn, D. Bersier, P. Jakobsson, A. O. Jaunsen, C. Ledoux, A. J. Levan, B. Milvang-Jensen, E. Rol, N. R. Tanvir, K. Wiersema, **D. Xu**, et al. " Early spectroscopic identification of SN 2008D", 2008, **ApJ**, 692, L84

(12). **D. Xu**, Y. C. Zou, & Y. Z. Fan "Mildly relativistic X-ray transient 080109 and SN2008D: Towards a continuum from energetic GRB/XRF to ordinary SN Ibc", 2008, **ApJ under review**, arXiv:0801.4325

(11). Y. Z. Fan, **D. Xu**, & D. M. Wei "Polarization evolution accompanying the very early sharp decline of GRB X-ray afterglows", 2008, **MNRAS**, 387, 92

(10). Martin Feix, **Dong Xu**, HuanYuan Shan, Benoit Famaey, Marceau Limousin, Hong-Sheng Zhao, Andy Taylor, " Is Gravitational Lensing by Intercluster Filaments Always Negligible?", 2008, **ApJ**, 682, 711

(9). A. E. Ruiz-Velasco, H. Swan, E. Troja, D. Malesani, J. P. U. Fynbo, R. L. C. Starling, **D. Xu**, et al. "Detection of GRB 060927 at z = 5.47: Implications for the Use of Gamma-Ray Bursts as Probes of the End of the Dark Ages", 2007, **ApJ**, 669, 1

(8). J.-E. Ovaldsen, A. O. Jaunsen, J. P. U. Fynbo, J. Hjorth, C. C. Thöene, C. Feron, **D. Xu**, J. H. Selj, J. Teuber "A Search for Host Galaxies of 24 Gamma-Ray Bursts", 2007, **ApJ**, 662, 294

(7). Y. Z. Fan, D. M. Wei, & **D. Xu** "Gamma-ray Burst UV/optical afterglow polarimetry as a probe of Quantum Gravity ", 2006, **MNRAS**, 376, 1857

(6). J. Sollerman, J. P. U. Fynbo, J. Gorosabel, J. P. Halpern, J. Hjorth, P. Jakobsson, N. Mirabal, D. Watson, **D. Xu**, et al. " The nature of the X-Ray Flash of August 24 2005", 2006, **A&A**, 466, 839

(5). Johan P. U. Fynbo, Darach Watson, Christina C. Thoene, Jesper Sollerman, Joshua S. Bloom, Tamara M. Davis, Jens Hjorth, Pall Jakobsson, Uffe G. Joergensen, John F. Graham, Andrew S. Fruchter, David Bersier, Lisa Kewley, Arnaud Cassan, Jos Mara Castro Cern, Suzanne Foley, Javier Gorosabel, Tobias C. Hinse, Keith D. Horne, Brian L. Jensen, Sylvio Klose, Daniel Kocevski, Jean-Baptiste Marquette, Daniel Perley, Enrico Ramirez-Ruiz, Maximilian D. Stritzinger, Paul Vreeswijk, Ralph A. M. Wijers, Kristian G. Woller, **Dong Xu**, Marta Zub "No supernovae associated with two long-duration gamma ray bursts", 2006, **Nature**, 444, 1047

(4). Y. Z. Fan, & **D. Xu** "The X-ray afterglow flat segment in short GRB 051221A: Energy injection from a millisecond magnetar?", 2006, **MNRAS**, 372, L19

(3). D. Watson, J. Hjorth, P. Jakobsson, **D. Xu**, J. P. U. Fynbo, J. Sollerman, C. C. Thöne, K. Pedersen "Are short gamma-ray bursts collimated? GRB050709, a flare but no break", 2006, **A&A**, 454, L123

(2). Y. Z. Fan, T. Piran & **D. Xu** "The Interpretation and Implication of the Afterglow of GRB 060218", 2006, **JCAP**, 0609, 013

(1). J. Sollerman, A. O. Jaunsen, J. P. U. Fynbo, J. Hjorth, P. Jakobsson, M. Stritzinger, C. Feron, P. Laursen, J.-E. Ovaldsen, J. Selj, C. C. Thöne, **D. Xu**, et al. "Supernova 2006aj and the

associated X-Ray Flash 060218", 2006, **A&A**, 454, 503

On non-referred journal (including GCN Circ.):

(14). **D. Xu**; D. Watson; J. P. U. Fynbo; Y. Z. Fan; Y. C. Zou; J. Hjorth. "Mildly relativistic X-ray transient 080109 and SN 2008D: Towards a continuum from energetic GRB/XRF to ordinary SN Ibc", 2008, Nanjing GRB conference, proceeding

(13). **D. Xu** "GRB080913: Swift-BAT spectral lag.", 2008, GCN Circ. 8267

(12). Jakobsson, P.; Vreeswijk, P. M.; **Xu, D.**; Thöene, C. C. "GRB 080605: VLT redshift.", 2008, GCN Circ. 7832

(11). Malesani, D.; Sollerman, J.; Fynbo, J. P. U.; Thoene, C. C.; **Xu, D.**; Hjorth, J.; Leloudas, G.; Vreeswijk, P. M.; Watson, D. J.; Jakobsson, P.; Augusteijn, T.; Villforth, C.; Niemi, S.-M.. "XRF 080109 / SN 2008D: spectroscopic evolution.", 2008, GCN Circ. 7184

(10). Fynbo, Johan; Vreeswijk, Paul; Jakobsson, Pall; Jaunsen, Andreas; Ledoux, Cedric; Malesani, Daniele; Thöene, Christina; Ellison, Sara; Gorosabel, Javier; Hjorth, Jens; Jensen, Brian; Kouveliotou, Chryssa; Levan, Andrew; Møller, Palle; Rol, Evert; Smette, Alain; Sollerman, Jesper; Starling, Rhaana; Tanvir, Nial; Watson, Darach; Wiersema, Klaas; Wijers, Ralph; **Xu, Dong** "Gamma-Ray Bursts as Cosmological Probes: from Concept to Reality", 2007, The Messenger, 130, 43

(9). P. Jakobsson; J. P. U. Fynbo; D. Malesani; P. M. Vreeswijk; J. Hjorth; **D. Xu**; J. Sollerman. "GRB 071112C: emission lines and refined VLT redshift.", 2007, GCN Circ. 7088

(8). P. Jakobsson; D. Malesani; **D. Xu**; J. P. U. Fynbo; J. Hjorth; C. C. Thöene. "GRB 070611: VLT observations", 2007, GCN Circ. 6601

(7) J.-E. Ovaldsen; A. O. Jaunsen; J. P. U. Fynbo; C. Thöene; C. Feron; J. Hjorth; **D. Xu**; J. H. Selj; J. Teuber. "A search for host galaxies of 24 GRBs using the Danish 1.54m", 2006, Nuovo Cimento B, vol. 121, Issue 12, p.1551

(6). J. Hjorth; A. Levan; N. Tanvir; R. Starling; S. Klose; C. Kouveliotou; C. Feron; P. Ferrero; A. Fruchter; J. P. U. Fynbo; J. Gorosabel; P. Jakobsson; D. A. Kann; K. Pedersen; E. Ramirez-Ruiz; J. Sollerman; C. Thöene; D. Watson; K. Wiersema; **D. Xu**. "The Short Gamma-Ray Burst Revolution", 2006, The Messenger, 126, 16

(5). D. Malesani; J. Hjorth; **D. Xu**; M. D. Stritzinger; D. Watson; J. P. U. Fynbo; C. Henriksen; K. Holjem; T. Pursimo; D. Sharapov; H. Uthas. "GRB 061121: flattening of the decay.", 2006, GCN Circ. 5877

(4). J. P. U. Fynbo; C. C. Thöene; B. L. Jensen; J. Hjorth; J. Sollerman; D. Watson; **D. Xu**; J.-E. Ovaldsen; U. G. Joergensen; T. Hinse; K. Woller. "GRB060614: detection of the host galaxy but no supernova emission.", 2006, GCN Circ. 5277

(3). C. C. Thöene; J. P. U. Fynbo; B. L. Jensen; J. Hjorth; **D. Xu**; U. G. Joergensen; K.

Woller. "GRB 060614: optical observations.", 2006, GCN Circ. 5272

(2). J.-E., Ovaldsen; **D. Xu**; J. H. Selj; A. O. Jaunsen; C. Feron; C. Thöene; J. P. U. Fynbo; J. Hjorth. "GRB 060218: optical brightening in V and r.", 2006, GCN Circ. 4816

(1). Z. G. Dai; E. W. Liang; F. Y. Wang; **D. Xu** "Gamma-Ray Burst Cosmology", 2006, 36th COSPAR Scientific Assembly, Beijing, China

Bibliography

Akerlof, C. et al., 1999, Nature, 398, 400

Alard, C. & Lupton, R. H., 1998, ApJ, 503, 325

Amati, L. et al., 2002, A&A, 390, 81

Amati, L. et al., 2007, A&A, 463, 913

Band, D. et al., 1993, ApJ, 413, 281

Barthelmy, S. D. et al., 2005, ApJ, 635, L133

Barthelmy, S. D. et al., 2005b, Nature, 438, 994

Belczynski, K. et al., 2006, ApJ, 648, 1110

Berger, E. et al., 2003, Nature, 426, 154

Berger, E. et al., 2003b, ApJ, 599, 408

Berger, E., et al., 2005, Nature, 438, 988

Berger, E., et al., 2007, ApJ, 664, 1000

Berger, E. & Soderberg, A. M., 2008a, GCN Circ., 7159

Berger, E. & Soderberg, A. M., 2008b, GCN Circ., 7192

Berger, E., 2009, ApJ, 690, 231

Bhat, P. et al., 1994, ApJ, 426, 604

Björnsson, G., Hjorth, J., Pedersen, K., & Fynbo, J. P. U., 2002, ApJ, 579, L59

Björnsson, G., Gudmundsson, E. H., & Johannesson, G., 2004, ApJ, 615, L77

Blandford, R. & McKee, C., 1976, Phys. Fluids, 19, 1130

Bloom, J. S., et al., 2006, ApJ, 638, 354

Bloom, J. S., Butler, N. R., & Perley, D. A., 2008, arXiv:0804.0965

Blumenthal, G. R. & Gould, R. J., 1970, Rev. Mod. Phys., 42, 237

Briggs et al., 1999, ApJ, 524, 82

Butler, N. R., 2007, ApJ, 656, 1001

Burrows, D. N. et al., 2005, Science, 309, 1833

Burrows, D. N. et al., 2006, ApJ, 653, 468

Burrows, D. N. et al., 2008, GCN Circ. 7179

Campana, S. et al., 2005, ApJ, 625, L23

Campana, S. et al., 2006, Nature, 442, 1008

Cenko, S. B. et al. 2008, arXiv:0802.0874

Chen, L., Lou, Y. Q., Wu, M. et al., 2005, ApJ, 619, 983

Chevalier, R. A., 1998, ApJ, 499, 810

Chevalier, R. A. & Li, Z. Y., 2000, ApJ, 536, 195

Chevalier, R. A. & Fransson, C., 2008, ApJ, 683, L135

Chincarini, G. et al. 2005, preprint, (astro-ph/0506453)

Christensen, L., Hjorth, J., & Gorosabel, J., 2004, 425, 913

Costa, E. et al., 1997, Nature, 387, 783

Cummings, J. et al., 2005, GCN Circ., 4365

Cusumano, G. et al., 2006a, GCN Circ., 4775

Cusumano, G. et al., 2006b, GCN Circ., 4786

Dai, Z. G. & Lu, T., 1998a, PRL, 81, 4301

Dai, Z. G. & Lu, T., 1998b, A&A, 333, L87

Dai, Z. G. & Lu, T., 1998c, MNRAS, 298, 87

Dai Z. G., 2004, ApJ, 606, 1000

Dai, Z. G., Liang, E. W., & Xu, D., 2004, ApJ, 612, L101

Dai, Z. G., Wang, X. Y., Wu, X. F., & Zhang, B., 2006, Science, 311, 1127

Dai, Z. G., Zhang, B., & Liang, E. W., 2006, preprint, (astro-ph/0604510)

Davies, M. B., Ritter, H., & King, A. R., 2002, MNRAS, 335, 369

Davies, M. B., Levan, A. J., & King, A. R., 2005, MNRAS, 356, 54

De Luca, A., 2006, GCN Circ., 4853

De Pasquale, M. et al., 2006, MNRAS, 365, 1031

Della Valle, M. et al., 2006, Nature, 444, 1050

Dingus, B. L. et al., 2001, in *High Energy Gamma Ray Astronomy*, ed. F. A. Aharonian and H. J. Völk (AIP: New York), 383

Duez, M. D. et al., 2006, Phys. Rev. D, 73, 104015

Dyks, J., Zhang, B., & Fan, Y. Z., 2006, ApJ, submitted (astro-ph/0511699)

Eichler, D., Livio, M., Piran, T., & Schramm, D. N., 1989, Nature, 340, 126

Eichler, D. & Granot, J., 2006, ApJ, 641, L5

Elíasdóttir, Á. et al., 2008, ApJ submitted, (arXiv:0810.2897)

Evans, P. A., et al., 2007, A&A, 469, 379

Falcone, A. D. et al., 2006, ApJ, 641, 1010

Fan, Y. Z. & Wei, D. M., 2005, MNRAS, 364, L42

Fan, Y. Z., Zhang, B., & Proga, D., 2005, ApJ, 635, L129

Fan, Y. Z. & Xu, D., 2006, MNRAS, 372, L19

Fan, Y. Z., Piran, T., & Xu, D., 2006, JCAP, 09, 013

Fan, Y. Z. & Piran, T., 2006, MNRAS, 369, 197

Fan, Y. Z. & Piran, T., 2006b, MNRAS, 370, L24

Fenimore, E. E., Madras, C. D., & Nayakshin, S., 1996, ApJ, 473, 998

Folatelli, G. et al., 2006, ApJ, 641, 1039

Fox, D. B. et al., 2005, Nature, 437, 845

Frail, D. A. et al., 2001, ApJ, 562, L155

Frail, D. A. et al., 2003, AJ, 125, 2299

Fruchter, A. S. et al., 2006, Nature, 441, 463

Fryer, C. L. et al., 1999, ApJ, 520, 650

Fryer, C. L., Young, P. A., & Hungerford, A. L., 2006, ApJ, 650, 1028

Fynbo, J. P. U. et al., 2003, A&A, 406, L63

Fynbo, L. P. U. et al., 2005, ApJ, 633, 317

Fynbo, J. P. U. et al., 2006, Nature, 444, 1047

Fynbo, J. P. U. et al., 2008, GCN Circ., 8225

Galama, T. J., et al., 1998, Nature, 395, 670

Gallant, Y. A., 2002, *Lecture Notes in Physics*, 589, 24

Gal-Yam, A. et al., 2006, Nature, 444, 1053

Gehrels, N. et al., 2004, ApJ, 611,1005

Gehrels, N. et al., 2005, Nature, 437, 851

Gehrels, N. et al., 2006, Nature, 444, 1044

Ghirlanda, G., Ghisellini, G., & Lazzati, D., 2004, ApJ, 616, 331

Ghirlanda, G. et al., 2004, ApJ, 613, L13

Ghirlanda, G. et al., 2006, A&A, 452, 839

Ghisellini, G., 2001, preprint, (astro-ph/astro-ph/0111584)

Ghisellini, G., Nardini, M., Ghirlanda, G., & Celotti, A., 2009, MNRAS, 393, 253

Goad, M. R. et al., 2006, A&A, 449, 89

Golenetskii, G., Apteaker, R., Mazets, E., Pal'shin, V., Frederiks, D., & Cline, T., 2005, GCN Circ. 4394

Gonzalez, M. M. et al., 2003, Nature, 424, 751

Granot, J., Königl, A. & Piran, T. 2006, MNRAS, 370, 1946

Granot, J. & Kumar, P. 2006, MNRAS, 366, L13

Greiner, J. et al., 2008, ApJ submitted, (arXiv:0810.2314)

Gunn, J. & Ostriker, J., 1969, Nature, 221, 454

Harris, M. & Share, G., 1998, ApJ, 494, 724

Harrison, F. A. et al., 1999, ApJ, 523, L121

Heise, J. et al., 2001, preprint, (astro-ph/0111246)

Halpern, J. P., Kemp, J., Piran, T., & Bershady, M. A., 1999, ApJ, 517, L105

Hjorth, J. et al., 2003, Nature, 423, 847

Hjorth, J. et al., 2005a, ApJ, 630, L117

Hjorth, J. et al., 2005b, Nature, 437, 859

Huang, Y. F., Dai, Z. G., & Lu, T., 2000, MNRAS, 316, 943

Hullinger, D., et al. 2006, GCN Circ. 5142

Hurley, K. et al., 1994, Nature, 372, 652

Immler, S. et al., 2008, GCN Circ. 7168

Ioka, K., Toma, K., Yamazaki, R. & Nakamura, T., 2006, A&A, 458, 7

Jakobsson, P. et al., 2004, ApJ, 617, L21

Jin, Z. P., Yan, T., Fan, Y. Z., & Wei, D. M., 2007, ApJ, 656, L57

Kalberla, P. M. W. et al., 2005, A&A, 440, 775

Kann, D. A. et al., 2007, ApJ submitted, (arXiv:0712.2186)

Kaneko, Y. et al., 2006, ApJ, 654, 385

Katz, J. I. & Piran, T., 1997, ApJ, 490, 772

Katz, J. I., Piran, T., & Sari, R., 1998, PRL, 80, 1580

King, A. R., Olsson, E., & Davies, M. B., 2007, 374, L34

Kippen, M. et al., 2002, preprint, (astro-ph/0203114)

Klebesadel, R., Strong, I., & Olson, R., 1973, ApJ, 182, L85

Kluźniak, W. & Ruderman, M., 1998, ApJ, 505, L113

Kobayashi, S. & Sari, R., 2000, ApJ, 542, 819

Kochanek, C. S. et al., 2008, ApJ, 684, 1336

Kong, A. K. H. & Maccarone T. J., 2008, ATel, 1355

Kouveliotou, C., Meegan, C. A., Fishman, G. J., et al., 1993, ApJ, 413, L101

Kulkarni, S. R. et al., 1998a, Nature, 393, 35

Kulkarni, S. R. et al., 1998b, Nature, 395, 663

Kulkarni, S. R. et al., 1999a, Nature, 522, L97

Kulkarni, S. R. et al., 1999b, Nature, 398, 389

Kumar, P., 1999, ApJ, 523, L113

Kumar, P. & Panaitescu, A., 2000, ApJ, 541, L51

Kumar, P. & Piran, T., 2000, ApJ, 535, 152

Kumar, P., et al., 2007, MNRAS, 376, L57

Lazzati, D., Ghisellini, G., & Celotti, A., 1999, MNRAS, 309, L13

Lazzati, D. & Begelman, M. C., 2006, ApJ, 641, 972

Le Floc'h, E. et al., 2003, A&A, 400, 499

Lee, W. H. & Kluźniak, W., 1995, Acta Astronomica, 45, 705

Lee, W. H. & Kluźniak, W., 1999a, ApJ, 526, 178

Lee, W. H. & Kluźniak, W., 1999b, MNRAS, 308, 780

Lee, W. H. & Ramirez-Ruiz, E., 2007, New Journal of Physics, 9, 17

Li, Z. Y. & Chevalier, R. A., 1999, ApJ, 526, 716

Li, L. X., 2007, MNRAS, 375, 240

Li, L. X., 2008, MNRAS, 388, 603

Lyutikov, M. & Blandford, R., 2003, preprint, (astro-ph/0312347)

MacFadyen, A. I., Woosley, S. E., & Heger, A. 2001, ApJ, 550, 410

Malesani, D. et al., 2004, ApJ, 609, L5

Malesani, D. et al., 2007, A&A, 473, 77

Malesani, D. et al., 2009, ApJ, 692, L84

Mangano, M. et al., 2007, A&A, 470, 105

Mao, J. et al., 2008, GCN Rep., 138, 1

Matzner, C. D. & McKee, C. F., 1999, ApJ, 510, 379

Mazzali, P. A. et al., 2006, Nature, 442, 1018

Mazets, E. P., Golenetskii, S. V., & Ilinskii, V. N., 1974, JETP Lett., 19, 77

McBreen, S., Foley, S., Watson, D., et al., 2008, ApJ, 677, L85

Meegan, C. et al., 1992, Nature, 355, 143

Mészáros, P., Rees, M. J., & Wijers, R. A. M. J., 1998, ApJ, 499, 301

Mészáros, P. & Rees, M. J. 1999, MNRAS, 306, L39

Mészáros, P., 2002, ARA&A, 40, 137

Metzger, M. R. et al., 1997, Nature, 387, 878

Mirabal, N. & Halpern, J. P., 2006, GCN Circ., 4792

Mirabal, N. et al., 2006, ApJ, 643, L99

Modjaz, M. et al., 2006, ApJ, 645, L21

Modjaz, M. et al., 2008, AJ, 135, 1136

Modjaz, M. et al., 2008b, AJ, 135, 1156

Moderski, R., Sikora, M., & Bulik, T., 2000, ApJ, 529, 151

Nagataki, S. et al., 2003, ApJ, 596, 401

Nagataki, S., 2009, ApJ submitted, (arXiv:0902.1908)

Nakazato, K., 2008, PRD, 78, 083014

Nomoto, K., Tanaka, M., Tominaga, N., et al., 2007, New Astronomy Review, (arXiv:0707.2219)

Narayan, R., Paczyński, B., & Piran, T., 1992, ApJ, 395, L83

Nakar, E. & Piran, T., 2004, MNRAS, 353, 647

Nava, L. et al, 2006, A&A, 450, 471

Norris, J. P. et al., 1986, ApJ, 301, 213

Norris, J. P. et al., 2000, ApJ, 534, 248

Norris, J. P. & Bonnell, J. T., 2006, ApJ, 643, 266

Nousek, J. A. et al., 2006, ApJ, 642, 389

Nysewander, M., Fruchter, A. S., & Pe'er, A., 2008, ApJ submitted, (arXiv:0806.3607)

O'Brien, P. T. et al., 2006, ApJ, 647, 1213

Ofek, E. O., Cenko, S. B., Gal-Yam, A., et al., 2007, ApJ, 662, 1129

Pacini, F., 1967, Nature, 216, 567

Paczyǹski, B., 1986, ApJ, 308, L43

Paczyǹski, B., 1986, AIPCS, 428, 783

Paczyǹski, B., 1991, Acta Astronomica, 41, 257

Panaitescu, A., Spada, M., & Mészáros, P., 1999, ApJ, 522, L105

Panaitescu, A., 2005, MNRAS, 363, 1409

Panaitescu, A. et al., 2006, MNRAS, 369, 2059

Panaitescu, A., 2007, MNRAS, 379, 331

Parsons, A. et al., 2005, GCN Circ., 4365

Pe'er, A. & Zhang, B., 2006, ApJ, 653, 454

Pei, Y. C., 1992, ApJ, 395, 130

Perna, R. & Belczynski, K., 2002, ApJ, 570, 252

Perna, R., Armitage, P. J., & Zhang, B., 2006, ApJ, 636, L29

Price, P. A., Berger, E., & Fox, D. B., 2006, GCN Circ., 5275

Price, D. & Rosswog, S., 2006, Science, 312, 719

Perley, D. A., et al., 2008, ApJ submitted, (arXiv:0811.1044)

Pian, E. et al., 2006, Nature, 442, 1011

Piran, T., Shemi, A., & Narayan, R., 1993, MNRAS, 263, 861

Piran, T., 1999, Phys. Rep., 314, 575

Piran, T., 2005, Reviews of Modern Physics, 76, 1143

Piranomonte, S., D'Avanzo, P., Covino, S., et al., 2007, A&A, 491, 183

Preece, R. D. et al., 2000, ApJS, 126, 19

Prieto, J. L., Stanek, K. Z., & Beacom, J. F., 2008, ApJ, 673, 999

Ramirez-Ruiz, E., Celotti, A., & Rees, M. J., 2002, MNRAS, 337, 1349

Rees, M. J. & Mészáros, P., 1994, ApJ, 430, L93

Rees, M. J. & Mészáros, P., 1998, ApJ, 496, L1

Rhoads, J. E., 1999, ApJ, 525, 737

Racusin, J. L. et al., 2008, Nature, 455, 183

Ramirez-Ruiz, E., 2004, MNRAS, 349, L38

Rosswog, S. et al., 1999, A&A, 341, 499

Rosswog, S., Ramirez-Ruiz, E., & Davis, M., 2003, MNRAS, 345, 1077

Rosswog, S., 2005, ApJ, 634, 1202

Rosswog, S., 2007, MNRAS, 376, L48

Rybicki, G. B. & Lightman, A. P., Radiative Processes in Astrophysics (Wiley, New York. 1979)

Ruderman, M., Ann. NY Acad. Sci, 1975, 262, 164

Ruffert, M. & Janka, H. T., 2001, A&A, 380, 544

Ryde, F. & Pe'er, A., 2008, ApJ submitted, (arXiv:0811.4135)

Sakamoto, T. et al., 2006, GCN Circ., 4822

Sari, R. & Piran, T., 1995, ApJ, 455, L143

Sari, R., Narayan, R., & Piran, T., 1996, ApJ, 473, 204

Sari, R., Piran, T., & Narayan, R., 1998, ApJ, 497, L17

Sari, R. & Piran, T., 1999, ApJ, 517, L109

Sari, R., Piran, T., & Halpern, J. P., 1999, ApJ, 519, L17

Sari, R. & Esin, A. A., 2001, ApJ, 548, 787

Savaglio, S., 2006, New Journal of Physics, 8, 195

Savaglio, S., Glazebrook, K., & Le Borgne, D., AIPC, 836, 540, (arXiv:astro-ph/0601528)

Schlegel, D. J., Finkbeiner, D. P., & Davis, M., 1998, ApJ, 500, 525

Schmidt, B., Peterson, B., & Lewis, K., 2006, GCN Circ., 5258

Shapiro, S. L. & Teukolsky, S. A., 1983, Black Holes, White Dwarfs, and Neutron Stars: The Physics of Compact Objects (New York: Wiley)

Shao, L. & Dai, Z. G., 2007, ApJ, 660, 1319

Shemi, A. & Piran, T., 1990, ApJ, 365, L55

Shen, R. F. et al., 2009, MNRAS, 393, 598

Shibata, M. et al., 2006, PRL, 96, 031102

Soderberg, A. M. et al., 2006a, ApJ, 650, 261

Soderberg, A. M. et al., 2006b, ApJ, 638, 930

Soderberg, A. M. et al., 2008, Nature, 453, 469

Sokolov, V. V. et al., 2001, A&A, 372, 438

Sollerman, J. et al., 2005, New Astronomy, 11, 103

Sollerman, J. et al., 2006, A&A, 454, 503

Sollerman, J. et al., 2007, A&A, 466, 839

Stanek, K. Z. et al., 2003, ApJ, 591, L17

Stanek, K. Z. et al., 2006, Acta Astronomica, 56, 333

Stanek, K. Z. et al., 2006b, ApJ, 654, L21

Starling, R. L. C. et al., 2007, ApJ, 661, 787

Stetson, P. B., 1987, PASP, 99, 191

Sumiyoshi, K. et al., 2006, PRL, 97, 1101

Tagliferri, G. et al. 2005, Nature, 436, 985

Thöene, C. C. et al., 2008, ApJ, 676, 1151

Thöene, C. C. et al., 2008, ApJ submitted, (arXiv: 0807.0473)

Troja, E. et al., 2007, ApJ, 665, 599

Uhm, A. L. & Beloborodov, A. M., 2007, ApJ, 665, L93

Usov, V. V., 1992, Nature, 357, 472

Valenti, S. et al., 2008, GCN Circ., 7221

Vaughan, S. et al., 2006, ApJ, 638, 920

Vietri, M. & Stella, L., 1998, ApJ, 507, L45

Wang, W. & Dai, Z. G., 2001, Chin. Phys. Lett., 18, 1153

Watson, D., Hjorth, J., Jakobsson, P., et al., 2006, A&A, 454, L123

Waxman, E., 2004, ApJ, 605, L97

Wei, D. M. & Lu, T., 1998, ApJ, 505, 252

Wei, D. M. & Lu, T., 2000, A&A, 360, L13

Wijers, R. A. M. J. & Galama, T. J., 1999, ApJ, 523, 177

Wolf, C. & Podsiadlowski, P., 2007, MNRAS, 375, 1049

Woosley, S. E., 1993, ApJ, 405, 273

Woosley, S. E., Zhang, W. Q., & Heger, A., 2003, AIPC, 662, 185

Woosley, S. E., & Bloom, J. S., 2006, ARA&A, 44, 507

Wu, X. F., Dai, Z. G., Huang, Y. F., & Lu, T., 2003, MNRAS, 342, 1131

Xu, D., Dai, Z. G., & Liang, E. W., 2005, ApJ, 633, 603

Xu, D. et al., 2008, ApJ, in press, (arXiv:0812.0979)

Xu, D., Zou, Y. C., & Fan, Y. Z., 2008, ApJ submitted, (arXiv:0801.4325)

Yamazaki, R., Ioka, K., & Nakamura, T., 2004, ApJ, 607, L103

Yost, S. A., Harrison, F. A., Sari, R., & Frail, D. A., 2003, ApJ, 597, 459

Zhang, B. & Mészáros, P., 2001, ApJ, 552, L35

Zhang, B. & Mészáros, P., 2004, Int. J. Mod. Phys. A, 19, 2385

Zhang, B. et al., 2006, ApJ, 642, 354

Zhang, B. et al., 2007, ApJ, 655, L25

Zhang, W. Q., Woosley, S. E., & Heger, A., 2004, ApJ, 608, 305